Investigation of Particle Size Increase of Micronized Copper Azole Preservative and the Effectiveness of Mixing Systems for Storage Tanks

By

Alexander Murray

Submitted in partial fulfilment of the requirements

for the degree of Master of Applied Science

at

Dalhousie University

Halifax, Nova Scotia

March 2024

Table of Contents

List of Tables

List of Figures

Abstract

Sedimentation in the holding tanks of the wood preservative micronized copper azole (MCA) is a key concern to the wood preservation industry. MCA is in suspension unlike other traditional preservative treating solutions. This project evaluates the effects of the current wood treating conditions on the size of micronized copper particles, the chemical composition of particles over 1 µm, and the potential of implementing a recirculation system for minimizing sedimentation in full scale operations. Experimental results demonstrated elevated temperatures led to an increase in size of MCA, while other parameters exhibited negligible effects. Analysis of particles over 1 µm showed malachite and copper oxides were among the particles identified. Computational Fluid Dynamics (CFD) simulation showed several fluid recirculating retrofits, namely improved inlet configuration could minimize settling, and such modifications would be a simple and inexpensive option for the wood preservation industry, Stella-Jones Inc.

List of Abbreviations Used

AWPA	American Wood Protection Association
CCA	Chromated Copper Arsenate
CFD	Computational Fluid Dynamics
CSA	Canadian Standard Association
DDPM	Dense Discrete Phase Modeling
DPM	Discrete Phase Modeling
EDXRF	Energy Dispersive X-Ray Florescence
ICDD	International Centre for Diffraction Data
MCA	Micronized Copper Azole
Mold 14	Acticide 14
Mold 45	Acticide 45
MP200	Micronized Copper Concentrate
MSNB	MicroShades Natural Brown
MTZ	Tebuconazole
NPS	Nominal Pipe Size
PDF	Powder Diffraction File
PTFE	Polytetrafluoroethylene
SDS	Safety Data Sheet
SEM	Scanning Electron Microscope
EDS	Energy Dispersive Spectroscopy
WDXRF	Wavelength Dispersive X-Ray Florescence
XRD	X-Ray Diffraction
XRF	X-Ray Fluorescence

Acknowledgements

I wish to thank my supervisor, Dr. Sophia He and the rest of my committee, Dr. Haibo Niu and Dr. Azadeh Kermanshahi pour for their assistance with my project.

I would also like to thank Kathleen Walker for her invaluable assistance with designing and conducting these experiments. The staff of the Truro, Stella-Jones facility and Erin Sullivan were also of great assistance during the long days of pilot plant testing.

I also wish to thank my family for their support throughout this process, both moral and editorial.

I also wish to thank Stella-Jones Inc. for funding this project and the use of their facilities and equipment.

1.0 Introduction

1.1 Background

Pressure treated wood is a widely used building material for industrial and residential construction. Residential treated lumber is usually treated with water borne solutions, with up to 95% being treated with Chromated Copper Arsenate (CCA) prior to 2003 (Shultz & Nicholas, 2011). A regulation change in 2003 prohibited the use of CCA for the residential market, due to concerns of arsenic and chromium leaching into residential properties (Gerstein & Zaccaria, 2004). Chronic and acute effects of arsenic and chromium exposure may negatively affect many organs (Morais et al., 2021). As these concerns were mainly in residential settings, CCA is still permitted for industrial applications (Schultz & Nicholas, 2011). Due to this amended regulation, a safer preservative was required to replace the residential demand previously filled by CCA. As a replacement, Micronized Copper Azole (MCA) was introduced to the industry as an alternative metallic based preservative with similar protection to CCA.

MCA differs from many other wood preservatives in that the main active ingredient, micronized copper, is present as a suspension while most other wood preservatives are solutions. These copper particles are present in the form of basic copper carbonate, $Cu_2CO_3(OH)_2$, at sizes under 1 micron as specified by AWPA (AWPA, 2022). Henceforth, copper carbonate will be used to refer to basic copper carbonate. The MCA treating solution commonly used in practice consists of micronized copper particles in suspension in water, plus a dye for aesthetics and fungicide to protect wood from copper resistance fungi. Wood is treated with MCA under fluid pressure to ensure that the preservative penetrates the structure of the wood.

The pressure treating process involves loading lumber into a pressure treating vessel, pulling an initial vacuum, filling the vessel with preservative under vacuum, pressurizing the vessel until the cycle is complete, pumping the preservative back into storage tanks for reuse, then pulling a vacuum to remove any excess preservative (Brashaw & Bergman, 2021). After treatment, excess preservative solution is pumped back to the mixing cylinder, along with some impurities collected during treatment including wood fragments and other debris as well as sugars and/or extractives leached from the wood (King, 2014). The preservative which is pumped back is then topped up with fresh preservative concentrate and/or diluted with water to maintain sufficient volume and solution strength for subsequent charges. As a result of significant portions of this solution being reused through several charges, it is referred to as a stressed solution.

Stressed MCA solution is known to result in the deposition of sludge in the bottom of storage tanks and treating cylinders, with particle size increases being a suspected cause. These precipitates result in a decrease in solution strength as active ingredients settle out, increase maintenance expenses, additional cost of lost active ingredients, and increased disposal fees for sludge. These are the issues that Stella-Jones Inc. is now facing in its current operations.

Stella-Jones is a large wood preservation company operating in the United States and Canada. The company treats wood for a variety of applications including commercial lumber, railway ties, guardrail posts and telephone poles. The wood is treated using a variety of water and oil borne wood preservatives, including the recent addition of MCA. Therefore, Stella-Jones is interested in supporting this project to investigate what

contributes to particle clumping, what the larger particles consist of, and how to improve holding tank agitation to minimize settling.

The American Wood Protection Association (AWPA) stipulates that 95% of micronized particles must be under 1 micron in the solution, as an increased particle size would prevent copper particles from properly penetrating the wood during treatment. In addition, larger particles also settle faster which may cause greater sedimentation within the storage tanks. However, the causes of particle size increase remain unclear and there is no relevant studies identified in the literature.

In this research work, the treating solution was subject to external stressors of pressure, temperature, vacuum and combinations of the three to examine the effects of these stressors in a pilot scale plant, specifically the effect on copper concentration and particle size increase in stressed solutions. MCA treating solution was re-used for several treating cycles as an additional stressor. Particles over 1 micron were filtered out and analyzed to determine their composition. In addition to physical experiments, agitation retrofits to holding tanks were modelled using Computational Fluid Dynamics (CFD) software to evaluate the impact on settling.

1.2 Objectives

The purpose of this study was to reduce the occurrence of sedimentation in Micronized Copper Azole preservative holding tanks. The three objectives are outlined as follows:

- Investigate the effects of wood treating conditions (temperature, pressure, and vacuum) on the properties (predominantly particle size) of the stressed MCA treating solution in a pilot scale plant.
- Identify the composition of particles over 1 μm that formed in treating solution.
- Conduct a CFD simulation of several fluid recirculating retrofit methods for a representative MCA storage tank to determine which best reduces settling.

1.3 Significance of the Current Work

Current work found that the temperature was the leading stressor causing an increase in particle size of MCA. The influence of other parameters was negligible as demonstrated by insignificant changes in copper concentration between treatment cycles. The particles over 1 μm constituted mainly malachite and copper oxides, and some transitional forms of copper. The full reason for MCA particle size increase during the treating processes escaped the current work. Future research is needed. However, the Computational Fluid Dynamics (CFD) simulation did show several fluid recirculating retrofits could minimize settling in the storage tanks and could be a simple and cost-effective solution. The outcomes of this project provided Stella-Jones Inc. with possible process optimization to prevent larger particle formation, as well as insights into how to best retrofit solution storage tanks for better recirculation. This will reduce costs and environmental impact from the loss of active ingredients in the solution as well as costs of tank cleaning and sludge disposal.

2.0 Literature Review

2.1 Wood Preservative Micronized Copper Azole (MCA)

2.1.1 Composition

Micronized Copper Azole has been used to treat consumer lumber in North America since its introduction in 2006 (PR Newswire Association LLC, 2009). This water borne preservative formulation is applied to wood through a pressure treating process. The main active ingredient in MCA is the micronized copper particles, which are made by mechanically grinding water insoluble copper compounds (Freeman & McIntyre, 2008). The two AWPA approved MCA formulations specify that the copper compound is basic copper carbonate (AWPA, 2022).

A polymeric dispersant is typically added during the copper particle grinding process to improve efficiency. The dispersant attaches to the surface of the particles to keep them apart which avoids clumping to help the micronized copper particles remain stable in water during storage and treatment (Freeman & McIntyre, 2008). Larger micronized particles are easier to prepare but achieve worse penetration and retention when treating wood. Freeman & McIntyre, (2008) identify this as being caused by particles greater than the diameter of window pits (10,000 nm) or membranes in bordered pits (400 to 600 nm) clogging pathways in the wood structure, preventing further preservative uptake. Keeping particles smaller than these openings results in more uniform preservative penetration. Unlike soluble copper treatments where chemical fixation binds copper into the wood, micronized copper particles are deposited in the wood structure, with the polymeric dispersants theorized to help the particles adhere to the wood (Freeman & McIntyre, 2008).

Copper resistant fungal species are capable of degrading copper treated wood and so an azole is incorporated in MCA treating solutions (Civardi, Schubert, Fey, Wick & Schwarze, 2015). The AWPA, (2022) specifies this to be Tebuconazole in Standard P61-16. Other compounds are also incorporated into MCA wood treating solutions such as additional fungicides depending on chemical supplier and a wood dye. The wood dye is added for appearances to give the treated wood color and the composition is company specific.

2.1.2 American Wood Protection Association Standards

Wood treatment and preservatives used must align with standards specified in The American Wood Protection Association (AWPA) which is an organization founded in 1904 as a forum for industry, researchers, government and consumers to share information. The AWPA is the principal standards writing organization for wood preservative technologies in the United States of America (AWPA, 2022).

To ensure consistency across the industry, preservatives must conform to the relevant AWPA standard. For MCA, this is Standard P61-16, which governs the composition of treating solutions (AWPA, 2022). This specifies that the active components of the treating solution must have copper (Cu) present as basic copper carbonate at 95.4-96.8%, and Azole as Tebuconazole present at 3.2-4.6% in water (AWPA, 2022). The micronized components are to be made with a particle size distribution where 95% of particles are smaller than one micron. The basic copper carbonate and tebuconazole used to prepare treating solution should be in excess of 95% purity on an anhydrous basis. Deviation

outside of these treating standards is permitted if preservative retention in treated material meets requirements and immediate adjustments to preservative composition are taken. Minimum retentions in kg of active preservative ingredients per cubic meter of wood ranging from 1.0 kg/m^3 to 6.6 kg/m^3 are required, depending on the specific use case of wood being treated (AWPA, 2022).

2.1.3 Canadian Standards Association

The Canadian Standards Association (CSA) is a Canadian standards development and certifying organization. CSA O80 is the wood preservative standard, which covers all aspects of wood treatment. MCA was added to the CSA O80 standard in 2012, incorporating requirements from the AWPA, which are modified where needed for Canadian conditions (CSA, 2021). Requirements on the purity of ingredients, composition and other parameters are the same as the equivalent AWPA standard. One difference is in the deviation outside of listed treating standards. The CSA O80 standard is more descriptive, stating that for a specified retention the minimum sum of active ingredients must equal this retention, and providing minimums of Copper as Cu metal and Azole active that must be present in treated product. Active preservative retentions of 0.9 kg/m^3 to 3.3 kg/m^3 are required, depending on the specific use case of wood being treated (CSA, 2021). These retention requirements differ from the AWPA equivalent standards (AWPA, 2022).

2.1.4 Treatment Process

MCA preservative solution is mixed on site at facilities to the appropriate concentration using concentrate of each ingredient including micronized copper (MP200), azole (tebuconazole), dyes (MSNB), fungicides (mold14 and mold45), and water. Wood is treated according to the Bethell process, also known as the Full Cell process (Environment Canada, 2013). The treating procedure specified in AWPA, 2022 is as follows: the wood to be treated is placed in a pressure cylinder, and a vacuum is applied to remove air from the wood cells. The cylinder is filled with preservative under vacuum, then pressurized. The preservative is held under pressure until a set amount of time has elapsed, or to the point that no more preservative can be added, indicating maximum retention has been reached. The pressure is removed, and the preservative is pumped out of the cylinder and back into holding tanks. A vacuum is then applied to the wood in the cylinder to remove any excess preservative to minimize dripping and future leaching (Environment Canada, 2013).

2.1.5 MCA Particle Settling Behavior

Particles of copper carbonate present in MCA solutions are subject to the same forces as any other particle in a solution such as gravitational force, buoyancy, drag and interparticle forces. Stokes law of settling governs the settling behavior of a spherical object contained within a fluid, specifically the drag force experienced. The formula for Stokes' Law is as follows:

$$F_d = 6\pi\mu r v$$

Where F_d is frictional force (Stokes's drag), μ is dynamic viscosity of the liquid, r is the radius of the spherical object, and v is flow velocity relative to the object (Dey, Ali & Padhi, 2019). A given object in a volume of still liquid will experience the force of gravity pulling downwards, buoyancy upwards, and drag force will also act upwards to slow descent through the liquid. The forces of buoyancy and gravity on an object are given by:

$$F_g = \frac{4}{3}\pi r^3(\rho_s - \rho_f)g$$

Where Fg is the force acting downward (gravity less buoyancy) ρ_s and ρ_f are density of solid and fluid respectively, and g is gravitational acceleration.

The terminal settling velocity of a particle will occur when Fg, the force acting downwards equals the drag force Fd acting on the particle. By setting F_d equal to F_g, the equations may be rearranged to get the settling velocity of an object of known size, as given by:

$$v = \frac{2(\rho_s - \rho_f)gr^2}{9\mu}$$

Where v is settling velocity. The use of Stokes law of settling relies on the assumptions that liquid flow is laminar, particles are spherical, particles are of homogenous composition with smooth surfaces, and there are no interactions between particles. These assumptions limit the direct usefulness of the law to some systems, however there are correction factors available, or practices such as using the equivalent spherical diameter of different particle geometries (Dey, Ali & Padhi, 2019).

Small particles on the order of 1 micron may coagulate due to attraction by van Der Waals forces, resulting in larger equivalent particle size and increased sedimentation rate (Chhabra & Basavaraj, 2019). The stability of particles depends on the repulsive effect of an electrical double layer surrounding particles along with other contributing factors such as solution density, presence of other molecules, and solution pH (Chhabra & Basavaraj, 2019). As per AWPA standard P61-16, a proprietary surfactant is incorporated within the treating solution to improve solution stability (AWPA, 2022). As the surfactant is confidential and thus unknown, the exact influence on the behavior of particles in suspension is unknown. However, it can be seen from equations governing Stokes law that factors such as particle size, particle density, treating solution density and viscosity will have an impact on the rate of particle settling. These properties are also required inputs for CFD simulations to predict particle behavior as well, so quantification is essential (Anderson, 1995).

2.1.6 Measuring Viscosity

Viscosity may be broadly described as opposition to flow of a fluid. Dynamic viscosity refers to the shear stress for a given area required before a fluid sample begins to deform (Hibbeler, 2018). Kinematic viscosity refers to the resistive flow of a fluid under a gravitational field and can be obtained by dividing the dynamic viscosity by fluid density. Dynamic viscosity has metric units of (Pa·s), while kinematic viscosity is given in (m^2/s). Essentially, dynamic viscosity relates to force applied to a fluid, while kinematic viscosity relates to velocity applied.

There are several ways to determine the viscosity of a fluid. Dynamic viscosity was originally calculated by George Stokes using Stokes law as covered in Section 2.1.5. The original method was to take a tube of liquid, drop a sphere of known density into the top and measure the time taken for the object to fall a given distance after terminal velocity had been achieved (Biswas, Saha & Bandyopadhyay, 2021). Knowing distance, time taken, density and size of the sphere, the dynamic viscosity could be calculated (Hibbeler, 2018). Equipment relying on this principle is known as a falling ball viscometer. Orifice viscometers rely on filling a container with a known amount of a liquid and using the time for the container to empty through an orifice of a known size to measure the kinematic viscosity. Capillary viscometers involve timing the travel of a liquid sample through a length of capillary tube of known dimensions to determine kinematic viscosity (Sariyerli, Sakarya, & Akcadag, 2018). Rotational viscometers, which immerse a cylinder in a cup filled with liquid and measure the torque required to rotate the cylinder, are also commonly used (Hibbeler, 2018).

2.2 Analytical Methods for Particle Composition

2.2.1 X-Ray Fluorescence

X-Ray Fluorescence is a non-destructive analytical method capable of detecting the elemental composition of a sample. It can provide qualitative and quantitative data on a liquid sample with minimal preparation required (Rouessac & Rouessac, 2007).

To analyze a sample, the sample is excited by a primary X-ray source. The excited sample emits secondary X-rays, known as fluorescent X-rays (Rouessac & Rouessac, 2007). These X-ray wavelengths are characteristic to an element, which allows for

qualitative analysis on elements present in a given sample. With an appropriate calibration curve, the intensity of a given X-ray wavelength allows for quantitative data to be obtained from the sample. Detection limits as low as 0.002 wt% for copper are found with XRF units used by Stella-Jones (Hitachi, 2017).

There are 2 primary types of XRF detectors, Energy Dispersive X-ray Fluorescence (EDXRF), and Wavelength Dispersive X-ray Fluorescence (WDXRF). EDXRF is set up to measure all elements in the detectable range simultaneously, while WDXRF measures elements sequentially (Rouessac & Rouessac, 2007). With an EDXRF, the primary X-ray source is directed at the sample. The fluorescent X-rays emitted by the sample pass through a collimator before contacting a semiconductor detector. This detector converts X-rays into energy pulses and counts their quantity. The pulse energy gives the wavelengths which allows for elemental determination, while the count of the pulses gives quantitative information (Rouessac & Rouessac, 2007). EDXRF analyzers have the advantage of quick analysis as they scan all elements simultaneously. They are also cheaper and simpler than other options as they have fewer components. The disadvantage is that they tend to have poor resolution compared to other models, less accuracy at low concentrations and poor sensitivity for low weight atomic elements (Rouessac & Rouessac, 2007).

For an WDXRF, the primary X-ray is directed at the sample, with a portion of the fluorescent X-rays passed through a collimator. These X-rays impact a dispersive crystal which is designed so that the signal is amplified by constructive interference as per Braggs Law (Rouessac & Rouessac, 2007). Braggs Law is stated as $n\lambda=2d\sin\theta$, where n is the diffraction order, λ is the fluorescent X-ray wavelength, d is the wavelength

between the lattice planes of the dispersive crystal and θ is the angle of incidence. By changing the angle of incidence by means of moving the dispersive crystal and detector, only one amplified wavelength at a time is reaching the detector. This allows for a higher resolution, sensitivity to low atomic number elements, and higher sensitivity to trace element concentrations due to the amplifying effect (Rouessac & Rouessac, 2007). The disadvantage of this equipment is that it is more complex and thus expensive, as well as taking longer to analyze a sample for several elements.

AWPA Standard Method A9-21 outlines how to analyze treated wood and treating solutions using XRF analysis (AWPA, 2022). This method is specifically for the detection of elements phosphorous, sulfur, chlorine, chromium, copper, zinc, arsenic and iodine, which range from atomic number 15 to 53. Using liquid sample cups lined with mylar film, method A9-21 covers how to determine solution concentrations using WDXRF or EDXRF equipment (AWPA, 2022).

2.2.2 Scanning Electron Microscopy- Energy Dispersive Spectroscopy

Scanning Electron Microscopy-Energy Dispersive Spectroscopy (SEM-EDS) is an analytical method used to analyze solid samples. SEM-EDS analysis provides very detailed images of samples as fine as the nanometer scale, while also giving elemental composition information of a sample. Scanning electron microscopes function by directing a magnetically focused beam of very low energy electrons at a sample. The impact by the electron beam on the sample results in backscattered electrons and secondary electrons which are detected by the SEM-EDS equipment (Rouessac &

Rouessac, 2007). The position of the detector and signal intensity are used to generate an image.

Backscattered electrons are electrons from the beam which are reflected after elastically interacting with the sample. Larger atoms in a sample are more likely to scatter electrons than smaller atoms (Goldstein, Newbury, Michael, Ritchie, Scott & Joy, 2017). Thus, a detector therefore gets a stronger signal from heavier atoms as more are reflected back out of the sample, proportional to the atomic number. This allows an image to be formed which also conveys information on the sample composition in the form of elemental distribution, but not identity. Secondary electrons result from inelastic interactions between the electron beam and the sample (Goldstein et al. 2017). They have lower energies than backscattered electrons, and provide topographical information to the SEM.

EDS detectors gain qualitative and quantitative information from characteristic X-rays. When the primary electron beam of the SEM impacts the inner shell of an atom, it can displace this electron creating an electron hole, which an outer shell electron will move to replace (Goldstein et al. 2017). This jump from one valance energy to another releases a characteristic X-ray, unique to each element. A silicon drift detector picks up these X-rays with the energy of detections identifying specific elements while the frequency of detections of a given energy quantifies the amount present. This detection process is very similar to EDXRF analysis (Rouessac & Rouessac, 2007).

2.2.3 X-Ray Diffraction

X-Ray Diffraction (XRD) analysis allows for detailed information to be collected on materials with a crystalline structure. Samples are exposed to X-rays, with the angle between the X-ray source and detector varied over a given range. The wavelength of the X-rays directed at the sample is comparable to the distance between atoms in crystalline compounds. This results in constructive interference according to Braggs law (described in Section 2.2.1) at certain angles unique to each crystalline structure (Rouessac & Rouessac, 2007). As the angle between the X-ray source and the detector changes, a diffraction pattern is obtained which can be compared to reference diffraction patterns for known compounds.

X-Ray diffraction of powdered materials can be compared to the Powder Diffraction File (PDF) database maintained by the International Centre for Diffraction Data (ICDD) (Gates-Rector & Blanton, 2019). This method is capable of distinguishing between different phases and crystalline structures of similar compounds as crystalline structure differences less than 1 Angstrom can be identified by their unique diffraction angles. XRD analysis can even identify strain in samples through the effect of strain on the crystal structure. It is, however, limited to only being able to analyze crystalline or semi-crystalline structures).

2.3 Storage Tank Recirculating Modelling

2.3.1 Computational Fluid Dynamics Background

Computational Fluid Dynamics involves the use of computer simulations to solve and analyze solutions to complex fluid flow problems. The main set of equations which govern fluid flow, and thus computer simulated fluid flow, are the Navier-Stokes equations (Anderson, 1995). Original programs developed would focus on two-dimensional analysis of systems due to limited available computing power, before progressing to panel methods which used simplifications to model surfaces. With increased computing power, models were developed which could accurately model three-dimensional bodies (Anderson, 1995). Recent developments have focused on including an increasing number of parameters which were previously not modellable, such as the behavior of small particles in liquids, turbulent eddies and better approximations of boundary conditions.

The basis of the finite volume method of CFD modelling is that a large object is subdivided into smaller sections over which calculations can be performed. The initial run occurs with an initial assumption on what the program may expect to find. After this initial run is completed, the impact of the results of one section is applied to adjacent sections, and another run is completed factoring this in. The simulation will be repeated many times until the numbers converge on a final value (Anderson, 1995). The process of sectioning up the model is referred to as meshing, with the size of meshes specified by the user, depending on the desired precision. Software is typically used to generate a consistent mesh. Meshing functions generally involve finer meshing around flow boundaries (Ochieng & Onyango, 2010). This may be to account for geometry that does

not conform to the larger cells, or to account for the more complicated flow generally seen at the boundary of fluids. A mesh refinement study is often done, where increasingly fine meshes are run up until the point where the values of interest no longer change. At this point, the mesh size no longer has an impact on the final results, this is known as mesh independence (Anderson, 1995).

Once the physical geometry of a simulation is set up, the user must define several parameters. These include the density and viscosity of a fluid, boundary conditions, and the inputs/outputs of the system (Anderson, 1995). Once the process is completed, the user may generate usable plots from the simulation, such as section views of fluid velocities, temperatures, mixing ratios, or perform other processes such as particle injection studies.

2.3.2 Particle Modelling Approaches

There are several available methods to simulate modelling of multiple phases of material. The two most commonly used methods of modelling are Euler-Euler and Euler-Lagrange modelling, also known as Multiphase modelling and Discrete Phase Models (DPM) respectively. The following discussion will focus on the modelling of solid particles in a liquid medium, although these models may also apply to other interactions of multiple phases.

The Euler-Lagrange discrete phase model treats the fluid as continuous, and the dispersed phase is considered as a large number of discrete particles (Shi & Rzehak, 2020). The fluid phase is solved using the Navier-Stokes equations, while the dispersed phase is

modelled by calculating the motion of a large number of individual particles through the flow using a Lagrangian frame of reference (Adamczyk et al., 2014). The trajectory of the calculated particles is influenced by force of gravity, particle inertia and hydrodynamic drag (Saidi, Rismanian, Monjuezi, Zendehbad & Fatehiboroujeni, 2014). Other factors such as the effects of turbulent flow in the fluid phase, particle collisions, rotational effects, various drag laws and other parameters may be enabled in CFD simulation where applicable (ANSYS Inc., 2023). The continuous phase always has an impact on the discrete phase, as the motion of the fluid influences the motion of particles. Whether or not the discrete phase particles exchange momentum, mass and energy with the fluid phase depends on if two-way coupling is enabled (Tarpagkou, & Pantokratoras, 2013). With two-way coupling enabled, the discrete phase and continuous phase equations are alternatively solved until the solutions converge for each iteration. As two-way coupling is more computationally demanding, it is omitted when the impact of the discrete phase on the continuous phase is minimal, such as low volume fractions of small and light particles (ANSYS Inc., 2023). Steady particle tracking is used for cases where a particle will reach a final destination by coming into contact with a boundary layer within a period of time, while unsteady tracking settings are used for cases where particles may never reach a steady state final destination prior to flow solution being updated, such as settling simulations (ANSYS Inc., 2023).

In Euler-Euler modelling, both phases being modelled are treated as interpenetrating and continuous. In the case of solid particles present in a liquid, both phases are treated as a fluid. The solid phase is treated as a continuum with properties analogous to a fluid (Shi & Rzehak, 2020). Continuity and mass equations are solved for each phase for every cell

in the simulation, and then multiplied by the volume fraction α of a given cell (Hamdan, Sebastia-Saez, Hamdan, Arellano-Garcia, 2020). The volume fraction represents the fraction of a cell composed of a given phase and may range from 0 to 1. A cell with a volume fraction of 0 is fully comprised of the primary phase, while a cell with a volume fraction of 1 is fully comprised of the secondary phase with any value in between representing the ratio between them (Hamdan et al., 2020). A separate continuity equation is solved to keep track of the volume fraction of each cell. As more particles enter a given cell, the volume fraction of this cell would increase (Hamdan et al., 2020). The Eulerian method of modelling particles can be understood as dealing with overall concentrations of particles compared to the Lagrangian method modelling each individual particle (Saidi et al., 2014).

The choice of which model to use depends on the details of the system being modelled as well as what sort of data is to be collected. Euler-Lagrange modelling is better suited to observing particle scale behavior such as collisions and interactions between particles than Euler-Euler models (Shi & Rzehak, 2020). This also allows for more detailed modelling of particle deposition; however, the Euler-Lagrange model is only applicable when the particle volume fraction is low (Andrews & O'Rourke, 1996). The Ansys Fluent DPM model is only applicable when the volume fraction of particles is below 10-12% (ANSYS Inc., 2023). Euler-Euler models are capable of handling higher particle volume fractions than Euler-Lagrange methods and are well suited to monitoring particle concentrations (Saidi et al., 2014). The Euler-Euler approach tends to be more computationally efficient for larger systems (Shi & Rzehak, 2020). This is because the Eulerian method of modelling the second phase focuses on average behavior of particles

rather than the Lagrangian method of accounting for individual particles (Saidi et al., 2014).

Modified versions of both general frameworks are also available within Ansys Fluent to reduce computational cost or expand the applicability of a given model. One example is the Dense Discrete Phase Model (DDPM) which can handle higher particle loadings than the regular DPM (Adamczyk et al., 2014). The Mixture Model is a simplified version of the full Eulerian model which sacrifices accuracy for greater computational stability and lower computing cost (ANSYS Inc., 2023). Modelling of behaviors such as flocculation cannot currently be accounted for by general CFD modelling.

2.3.3 Quantifying Particle Settling

The behavior by which particles settle in liquids may be subdivided into four different classes of settling. Class 1 settling covers unhindered settling of discrete particles. Class 2 settling addresses cases where dilute suspensions of particles flocculate as they settle. Class 3 settling is hindered and zone settling behavior, where particle concentrations increase to the point where particles no longer settle independently as fluid displaced by adjacent particles moves upward, reducing settling velocity. Class 4 settling is compression settling, where high particle concentrations are compressed under gravity, forcing out fluid within the settled particle mass (Scholz, 2016). As flocculation cannot currently be simulated with CFD and project intent is to avoid sedimentation from occurring, class 1 settling is the focal point of the following discussion.

Recirculatory mixing in a tank involves removing liquid from one spot in a tank and reinjecting it in a different location. This can be accomplished with a pump and a piping loop to recirculate the fluid and can be an effective method to prevent settling. In a simulation to compare the relative benefits of different recirculatory mixing systems, a method to compare success must be established. Ansys Fluent simulations is a powerful tool which allows for the collection, processing, and analysis of many different forms of data. Within the DPM simulation this includes coordinates and velocity of each simulated particle (ANSYS Inc., 2023). Visual data on particle paths and location can also be generated. The deposition and resuspension of particles can also be accounted for, including mapping places where particles have settled out completely along the bottom surface of a tank (Muttenthaler & Manhartsgruber, 2020). A volume particle injection allows for a statistically significant number of particles to be generated interspersed through the fluid medium (ANSYS Inc., 2023).

By using a volume injection of particles and allowing the simulation to run for a set period of time with no agitation and several methods of recirculatory mixing, the previously described data allows for several types of comparison. The average change in height of all particles can be compared, with less decrease indicating better mixing. Secondly, the number of particles with zero velocity can be compared, with fewer unmoving particles indicating better mixing. Finally, the number of particles settled along the bottom of the tank that cannot be resuspended can be compared, with fewer stuck particles indicating less settling (ANSYS Inc., 2023). Comparing these relative terms may allow for less time to be simulated and thus less time steps, reducing the time per simulation run.

3.0 Experimental Methods and Materials

3.1 Materials

Wood preservative concentrates used in this study were sourced from Timber Specialties Limited, specifically from a shipment sent to the Gormley, Ontario Stella-Jones treating facility. The five concentrates are MicroPro 200C-TS, MicroShades Natural Brown (MSNB), Tebuconazole (MTZ), Acticide 14 (Mold 14) and Acticide 45 (Mold 45). The treating solution follows AWPA Standard 61-16, having a composition on an active basis of copper as Cu of 96.1% and azole as tebuconazole of 3.9%. Copper particles are composed of basic copper carbonate dispersed in water with proprietary surfactants. Bottled distilled water procured from local Wal-Mart (Great Value brand) was used to prepare all solutions except where otherwise stated. Treating solutions from working solution tanks and water samples from the Gormley, Ontario treating facility well and storm water collection system were collected by plant staff. Kiln dried 14 mm wood cubes were prepared from decking boards of spruce, pine and fir collected from three separate Home Depot locations. Non-kiln dried cubes were prepared from spruce, pine and fir boards collected from different trees from a local sawmill (Miller Company, Truro N.S.). 50 ml Luer lock syringes made by Becton Dickson (BD) were used with Whatman #6884-2510 1 µm GD/X syringe filters with built in prefilter for the syringe filtration process. 1 µm PTFE membrane filters were sourced from Whatman for vacuum filtration process.

3.2 MCA Solution Stressing Testing

3.2.1 Solution Preparation

MCA solution is comprised of six ingredients including water, MP200, tebuconazole, MSNB, mold 14, and mold 45. Solutions were prepared for experiments by weight, with components individually weighed and added to a large container. Containers were then rinsed out with distilled water, and the total solution brought up to weight using calculated value of distilled water. The solutions were agitated with a paint mixer drill attachment and copper concentration confirmed using XRF procedure outlined in Section 3.2.2. A separate batch was prepared to be used for each series of experiments, not for each specific trial and was kept agitating with the paint mixer attachment to avoid settling and rechecked prior to each use.

All solutions except where otherwise indicated used a 2% MCA treating solution, where 2% of the solution by weight is copper. The other ingredients were added as per Timber Specialties treatment guidelines with instruction by Stella-Jones. Table 3.1 indicates the quantity of each component added to prepare 1000 g of solution, as well as the specified concentrations in the units provided.

Table 3.1. Solution component specifications and grams required to prepare 1000 g MCA solution.

	Specified Solution Strength	Amount of Each Component (g)
MicroPro 200C-TS	2% Cu by Weight	71.43
MTZ	4% of mass of Cu by Weight	2.4
MSNB	2% Dye Concentrate by Weight	20
Mold 14	45 PPM	0.3235
Mold 45	160 PPM	0.3475
Distilled Water	N/A	905.5

3.2.2 Monitoring Copper Content by X-Ray Fluorescence (XRF)

AWPA A9-21, Standard Method for Analysis of Treated Wood and Treating Solutions by X-Ray Spectroscopy, was followed for the analysis of all liquid preservative samples using a Hitachi LAB-X5000 EDXRF (AWPA, 2022). The EDXRF is calibrated annually by a technician and re-standardized monthly with a standard sample to account for possible drift as per equipment instructions. Solutions were prepared by weight to contain all compounds present at the levels found in the treating solutions analyzed but with varying levels of copper. These solutions were used to prepare a copper calibration curve for analysis.

20 mL liquid samples were placed in Mylar film lined sample cells for analysis using the LAB-X5000 curve mentioned above for determining levels of copper in this specific wood preservative solution. This specific curve was prepared to avoid matrix effects with the analysis. The analysis program using this curve has been set up to analyze each sample three times consecutively, providing the average of the three repetitions as the result.

3.2.3 Filtering of Solution

In each of the solution stressing trials, samples collected were agitated then run through XRF analysis as per Section 3.2.2 to determine the weight percent of copper in solution. The samples were then reagitated, passed through a 1 µm filter and then the level of copper in the solution was measured in the XRF again. This allowed for calculation of the percentage of copper contained in particles over 1 µm in size.

A syringe was used to draw up 50 mL of sample, a syringe filter attached and then the sample passed through this syringe filter. The filtered solution was then resuspended prior to XRF analysis. As per AWPA Standard P61-16, micronized components are to be made with a particle size distribution d95 of less than 1 µm so a syringe filter with a pore size of 1 µm was used. Due to the high particle loading with 2% copper solutions, a syringe with a built in prefilter was used to avoid clogging. Each aliquot was analyzed for copper concentration pre filtration and post filtration. All unstressed and stressed solutions mentioned were analyzed in this way.

3.2.4 MCA Solution Stressing Procedure

2% MCA treating solutions were prepared as per Section 3.2.1, with solution copper concentrations confirmed using the XRF procedure described in Section 3.2.2. Preservative solutions were subjected to different stressors including pressure (150 psi), temperature (50 °C), and vacuum (25 inHg) independently. This corresponds to maximum possible values observed in production environments. Except where otherwise clarified, solutions are at room temperature (~20 °C). Stressor combinations of pressure with temperature and pressure with temperature then vacuum were also tested. All stressors were applied for 30 minutes in accordance with usual preservative cycle times, using the Truro, Stella-Jones pilot plant mimicking the actual production environment used for wood treatment. The pilot plant consists of a chemical storage tank, pressure vessel, heating jackets, pressure pump, vacuum pump and gauges as shown in Figure 3.1.

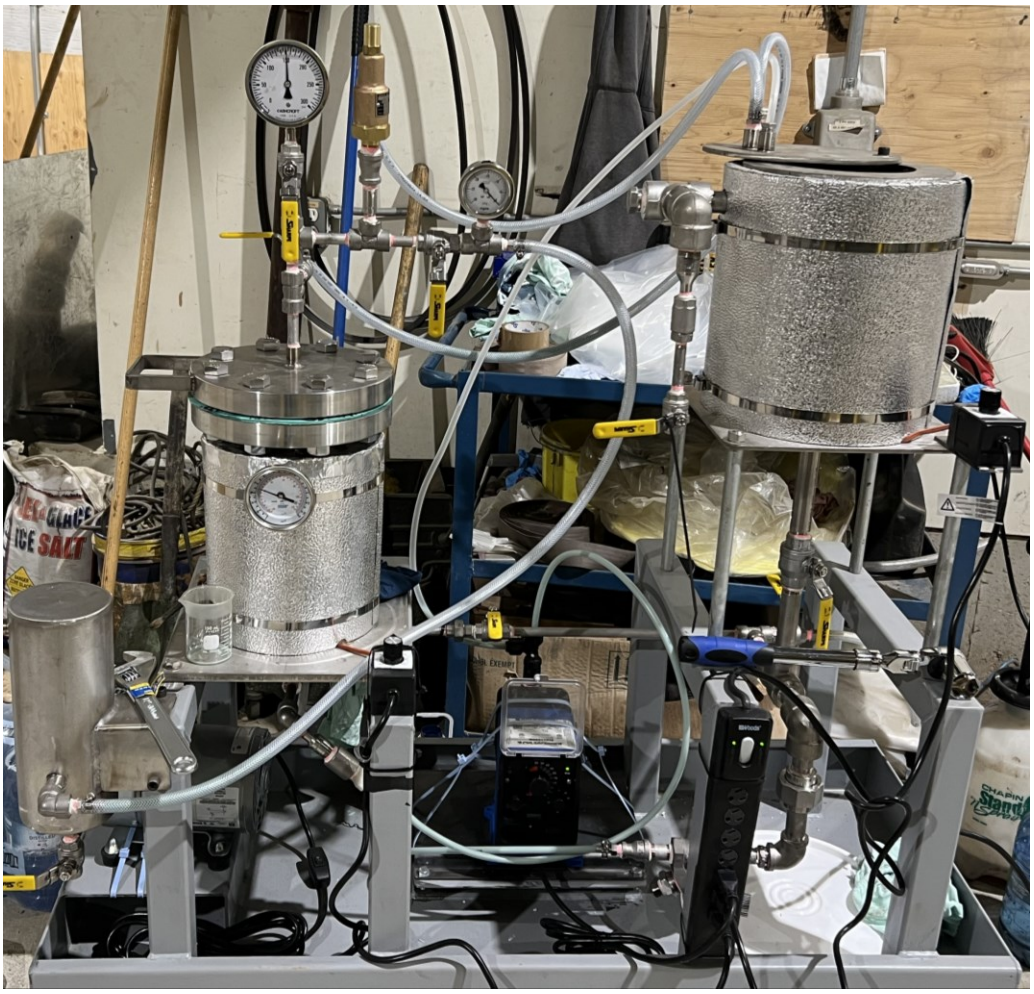

Figure 3.1. Pilot scale treating plant used for solution stressing trials.

Trials were conducted with the pressure vessel bolted shut, as seen on the left in Figure 3.1. With the chemical storage tank (right) filled, the pressure cylinder was filled under vacuum or gravity filled if open to atmosphere. Once the pressure cylinder has been filled, a valve was closed so that the fluid must go through a backflow prevention valve into the pressure pump to build pressure. This pump was a diaphragm pump with a low but highly adjustable flowrate, allowing pressure to be precisely controlled by adding fluid to compensate for preservative take up by wood samples if present. A heating jacket was used for temperature trials and a vacuum pump connected at the top allowed for a

vacuum to be applied and the unit to be filled under vacuum where applicable, or alternatively filled under gravity without vacuum. A block flow diagram is shown below in Figure 3.2.

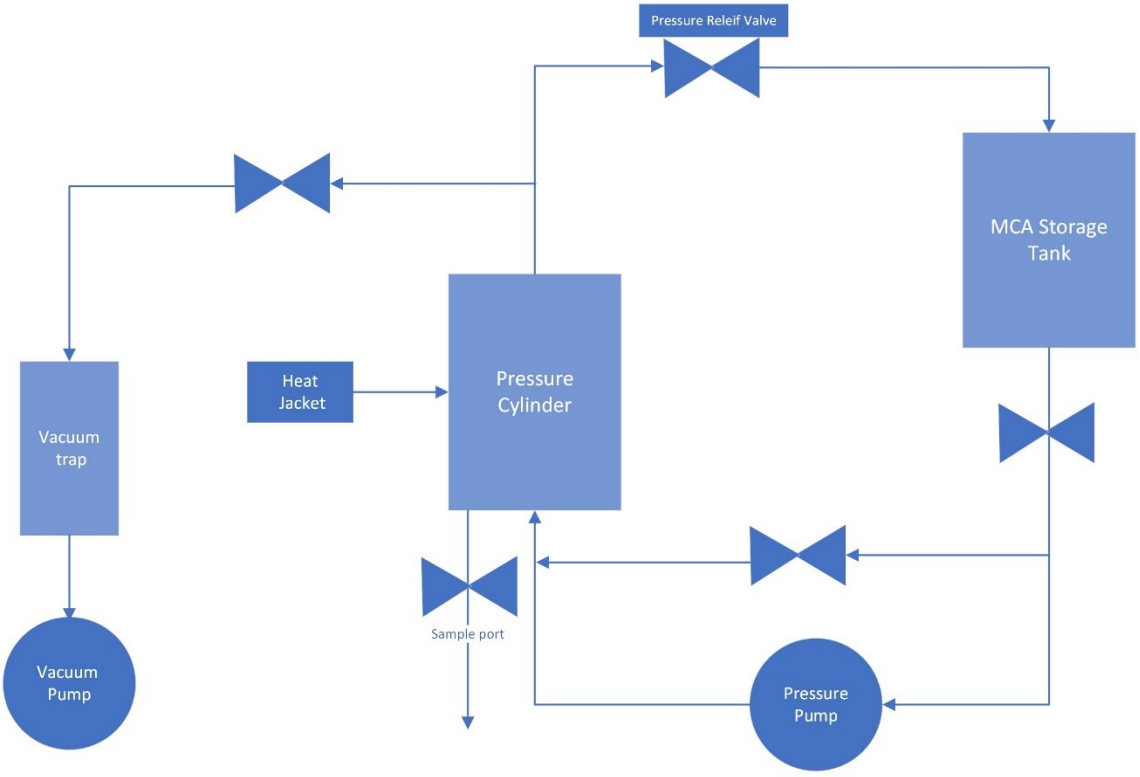

Figure 3.2. Pilot plant schematic.

Table 3.2. Description of stressors applied to 2% MCA treating solutions.

Solution	Description
Pressure	150 psi for 30 minutes
Temperature	50 °C for 30 minutes
Vacuum	25 inHg for 30 minutes
Pressure & Temperature	150 psi at 50 °C for 30 minutes
Pressure & Temperature then Vacuum	150 psi at 50 °C for 30 minutes then 25 inHg for 30 minutes

A summary table of trials is presented in Table 3.2. Samples were drawn from a port beneath the pressure treating cylinder. After a small amount of flow passed through the port, a 50 mL sample was collected for the first aliquot. 5 aliquots were taken in this way

from the sample port as the pilot plant is drained. A small amount of fluid was drained between the collection of each aliquot to better capture fluid from different regions of the pressure vessel. A minimum of 2 separate containers with 500 mL of stressed solution was preserved for future use.

Each aliquot collected was tested for copper concentration using the XRF method from Section 3.2.2, passed through a 1 µm syringe filter as described in Section 3.1.3 before being tested again in the XRF. In this way, copper concentrations in solution pre and post-filtration were recorded.

3.2.5 Treating Charges of Wood to Stress MCA Solution

MCA solutions were also stressed by completing treating cycles with wood blocks loaded in the pilot plant to examine the influence of wood on the treating solution. A mix of 300 blocks of Spruce, Pine and Fir were used per treating charge, with trials done on kiln dried and non-kiln dried wood separately.

The treating cycle consisted of sealing the wood in the pressure vessel and applying a 25 inHg initial vacuum for 30 minutes, then filling the pressure cylinder with preservative while under vacuum. The preservative was maintained at 37.8 °C as per Timber Specialties guidelines. 150 psi of pressure was applied for 30 minutes, at which point the pressure cylinder was drained and the 5 aliquots collected from the sampling port. All the preservative solutions were saved to be used in the second treating charge. A final vacuum of 25 inHg was applied for 30 minutes before the treated wood was removed, fresh untreated wood added, and the stressed solution reused for the second trial. This

process was repeated for a third treating cycle with the same preservative mixture. Aliquot analysis process is as described in Section 3.2.4.

3.2.6 Gormley Work Solution and Water Testing

Samples of well used stressed treating solutions from a production environment were obtained from the Gormely, Ontario treating facility. Two different strengths, 0.5% and 0.8% MCA solution were sourced. These solutions were well agitated to ensure resuspension before the pre- and post-filtration copper levels were obtained.

Well water and storm water (from the system for collecting runoff from the plants containment areas) instead of distilled water used in stressing test were used to prepare a 2% MCA treating solution as per the process outlined in Section 3.1.1. These solutions were kept agitating for 48 hours before being tested pre- and post-filtration as with the other solutions.

3.3 Particle Characterization

3.3.1 Sample Filtering Procedure

A portion of preserved stressed solution as well as unstressed stock solutions from selected trials were resuspended through vigorous shaking of sample containers. These solutions were then vacuum filtered through 1 µm PTFE membrane filter using a Buchner funnel system. When a small amount of material was collected on the membrane filter, it would be replaced, and a new filter added to avoid capturing smaller particles in a clogged filter. The filters were then allowed to fully dry on weigh dishes. The filtered

material was dried into flakes as seen in Figure 3.3. The material was then broken down into a powder by taking the filter paper and lightly crushing it against the weigh dish. This method was used to get the powder for SEM and XRD analysis.

Figure 3.3. Example of particles over 1 µm filtered from solution dried on filter paper prior to being broken down into powder.

3.3.2 SEM-EDS Analysis of Filtered Particles

SEM sample holders had double sided graphite sticky tape applied to them. The powdered samples prepared in Section 3.3.1 were then sprinkled over the sticky tape surface to try to coat as much of the area as possible with the sample. The samples were then sputter coated with a 15-nanometer layer of a gold-palladium to improve sample conductivity to reduce charging.

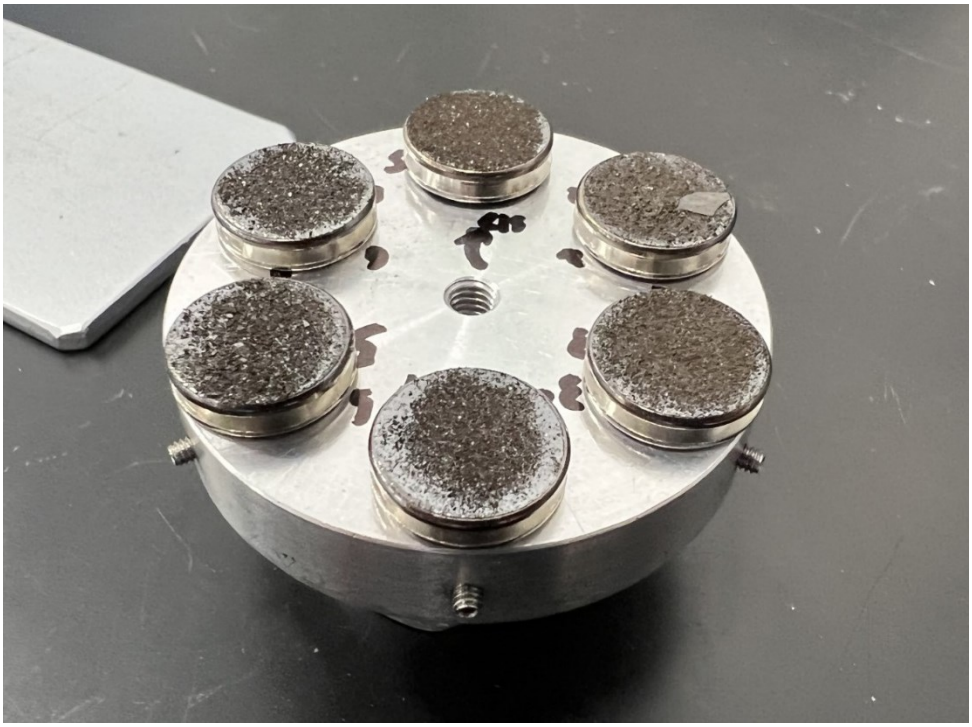

Figure 3.4. Coated samples prepared for SEM-EDS analysis.

These samples were then analyzed by SEM-EDS (Thermo Scientific Axia ChemiSEM Scanning Electron Microscope, Dalhousie Mechanical Engineering Department) to determine the elemental composition of the particles collected. Multiple box EDS scans of each sample were done to account for possible variation in the composition of particles in the sample. Three different areas of each sample stub were focused in on at 1000 times magnification using the SEM. With the sample in view, five separate areas were selected for a box scan to ensure EDS data was of the particles on the sample holder, not the sample holder itself. This provided 15 datapoints of the elemental composition for each sample. Magnified images of each region scanned were also collected.

3.3.3 X-Ray Diffraction Analysis

X-ray powder diffraction was conducted on all samples analyzed by SEM-EDS in Section 3.3.2. A Bruker D8 Advance High Speed X-ray Diffractometer in the Dalhousie Mechanical Engineering Department was used for the analysis. The powdered sample material collected by filtration in Section 3.3.1 was placed in sample holders and levelled for analysis. A Cu anode with 40 kV, 40 mA was used as the source of Kα radiation with a silicon strip (LynxEye^{TM}) detector. The samples were analyzed over a 2θ range of 5° to 90°, with a step size of 0.002628°. The diffraction data patterns obtained from samples were filtered to account for background and Kα radiation signals, then analyzed against ICDD Powder Diffraction Files (PDF) database to match patterns and identify compounds.

3.4 CFD Analysis of Storage Tank Mixing

3.4.1 CFD Analysis Model Generation, Mesh Independence Study

Tank geometries were modelled in Ansys SpaceClaim 3D modelling software (Ansys Fluent, ANSYS Inc.) and imported into Ansys Fluent to generate meshes. Several meshes of each tank design were generated with poly-hexcore mesh elements. Mesh independence was verified by solving for the steady-state flow field with the same inlet mass flow rate and pressure outlet conditions enabled. The value of area averaged inlet pressure at convergence was determined for each mesh. The mass flow inlet used results in pressure over the inlet to be able to drive fluid flow, with the amount of pressure required affected by all regions of the mesh, not just elements near the inlet. By plotting the area averaged inlet flow at convergence for progressively finer meshes, the point at

which this value levels off represents the point where the flow being studied was considered independent of the mesh and no further refinement desired. The mesh chosen for each tank geometry is the coarsest mesh which shows less than a 1% deviation in area averaged inlet pressure, as at this coarseness the simulation is not affected by the mesh coarseness.

A mass flow inlet boundary condition was applied at the inlet position and a pressure outlet boundary condition was used at the outlet of the tank. A fluid with the viscosity of the MCA treating solution was assigned to the fluid domain. The SST k-omega turbulence model was used as regions of laminar and turbulent flow exist (ANSYS Inc., 2023). The SIMPLE method of pressure-velocity coupling with second order discretization was used for the analysis. The convergence criteria for residuals were set to 1×10^{-4} for continuity, momentum, and turbulence equations. Standard initialization was used, and each mesh was run until convergence.

3.4.2 CFD Analysis Modelling Information

The converged steady state flow simulated in the mesh independence study was used as the starting point for the transient simulation. This was done so that the particles positions would begin being tracked as they are generated in an already resolved flow field, rather than an unknown amount of the initial transient simulation time being taken up by the flow field attempting to be stabilized. As the purpose is to determine the behavior of a continuously operating recirculating system, this allows for the behavior of the particles to be observed from the initial moment (time = 0) rather than having to wait and

determine when the flow field has stabilized as time is progressing. The time settings were changed from steady state to transient time. The Discrete Phase Model was then enabled for particle modelling as the particle volume fraction is low. Unsteady particle tracking was enabled, with the applicable physical models of virtual mass force and pressure gradient force also applied to the particles (ANSYS Inc., 2023).

A volume injection was used to introduce 1000 particles of the correct density at the start of the simulation (time = 0) interspersed throughout the full fluid volume to approximate an initially well mixed particle dispersion. Boundary conditions were adjusted so that any particle leaving the outflow boundary would reappear at the tank inlet at the initial inlet velocity so that the number of particles being tracked did not change.

The initial timestep size was 0.05 seconds per timestep for 20 timesteps, then 0.1 seconds per timestep for 40 timesteps before increasing to 0.5 seconds per timestep for 50 timesteps. The timestep size was then increased to 1 second per timestep for all remaining timesteps. The gradual increase in timestep was done to improve stability at the beginning of the particle tracking (ANSYS Inc., 2023).

3.4.3 CFD Data Collection

Ansys Fluent software can produce xy files where the x column is the particle ID number (1 to 1000 in this case), and the y column is data on each particle (ANSYS Inc., 2023). Data files on the particle height from the tank floor, as well as the velocity magnitude of each particle were collected at set intervals. The initial datapoint was collected at 5 seconds of simulated flow time rather than time = 0 to give particles a few iterations to

establish their behavior and avoid possible initialization related errors (ANSYS Inc., 2023). After the initial data collection at 5 seconds, position data was collected every hour of simulated flow time. This data was collected for each tank geometry and flow condition modelled.

Data on the heights of all particles at each time step allowed for the average height of particles to be determined and compared as time progresses. To determine how many particles have settled, the datasets were analyzed to determine which particles were within 1 mm of the floor of the tank. Particles with a velocity magnitude near zero were also sorted. If a particle is within 1 mm of the tank floor and has a velocity magnitude of less than 0.0001 m/s, it is considered settled. Both criteria need to be met as a particle at the base of the tank but still moving should not be considered settled as it may resuspend, while a particle with no velocity several meters from the bottom is also not settled. The height criteria of 1 mm and velocity magnitude near zero were used to account for residual errors in the particle tracking often resulting in values approaching zero but not quite reaching zero (ANSYS Inc., 2023). Simulations were run for the amount of time it took half of the particles to settle out in the tank with no agitation as a reference point.

4.0 Results and Discussion

The three subsections herein correspond to the three specific objectives outlined in the introduction. The results of investigating the impacts of treating parameters (stressors) on increased copper containing particle size are presented in Section 4.1. The second objective of identifying particles over 1 µm filtered out of solution was investigated using SEM-EDS analysis as well as XRD analysis and is presented in Section 4.2. Lastly, Section 4.3 provides the results of CFD simulations evaluating several possible tank recirculating retrofits for storage tanks.

4.1 MCA Solution Stressing Tests

In order to understand which wood treating conditions impact the copper containing particle size of MCA solutions, pilot-scale solution stressing trials were conducted. All solutions were prepared by weight according to the procedure described in Section 3.1.1. Solutions were stressed according to the procedure outlined in Section 3.1.5, with continual checks that stressor parameters and times were maintained. All 5 sample aliquots were filtered and analyzed as soon as possible after the completion of the experiment. Each aliquot had its pre-filtration copper concentration determined by the XRF method and calibration curve described in Section 3.1.3 before being passed through the 1 µm syringe filters using the process outlined in Section 3.1.4. The filtered solution was then measured through the XRF to get the post-filtration copper concentrations. The percent reduction of copper, indicating the percentage of copper containing particles over 1 µm, was calculated as follows:

$$Percent\ Change\ in\ Cu\ concentration$$

$$= \frac{(Filtered\ Cu\ wt\% - Unfiltered\ Cu\ wt\%)}{Unfiltered\ Cu\ wt\%} \times 100$$

Stressing parameter values of pressure, temperature and vacuum were chosen based on values used in production environments. The pressure parameter value of 150 PSI corresponds to the maximum treating pressure which may be applied in most treating facilities (CSA, 2021). The vacuum parameter value of 25 inHg corresponds to the highest vacuum which treating facilities may apply. Temperature stressing parameters of a maximum of 50 °C were used as this is the maximum temperature at which the preservative solution is considered stable, and so any possible elevated treating temperatures in the future would not exceed this value.

4.1.1 Pressure, Temperature, Vacuum, Combination of Stressors

2 % MCA solution was prepared and used to test the effects of a variety of stressors such as pressure, temperature, vacuum and the combination of these stressors on the copper concentration in the stressed solutions. The resulting copper concentrations in solutions pre and post filtration as well as percent reduction are summarized in Table 4.1.

Table 4.1. Cu concentrations in MCA solution stress tests.

	Cu Concentration in Solution Pre-Filtration (wt.%)	Cu Concentration in Solution Post-Filtration (wt.%)	Percent Change in Cu Concentration (%)
Unstressed Solution	2.019	2.014	-0.284
Pressure Test 1	2.023	2.016	-0.313
Pressure Test 2	2.024	2.017	-0.333
Pressure Test 3	2.023	2.018	-0.272
Temp Test 1	2.039	2.001	-1.864
Temp Test 2	2.050	2.015	-1.697
Temp Test 3	2.043	2.016	-1.337
Vacuum Test 1	2.037	2.031	-0.304
Vacuum Test 2	2.037	2.032	-0.419
Vacuum Test 3	2.021	2.016	-0.264
Unstressed Solution	2.026	2.022	-0.197
Pressure Temp Test 1	2.051	2.012	-1.875
Pressure Temp Test 2	2.044	2.004	-1.959
Pressure Temp Test 3	2.043	1.998	-2.186
Press, Temp & Vac Test 1	2.041	2.005	-1.803
Press, Temp & Vac Test 2	2.042	2.006	-1.756
Press, Temp & Vac Test 3	2.042	2.006	-1.775

Note: 5 aliquots were taken for each test and averaged values are presented.

This initial test shows that the unstressed stock solutions had a percent change in Cu concentration of approximately -0.25% after filtration. This is considered to be the baseline quantity of copper containing particles in solution over 1 μm in size. Table 4.1 shows the Cu concentration changes in the trials subject to stressors of pressure and vacuum are in the range of 0.264% to 0.419%, indicating changes were not significant as they did not show any apparent deviation from the baseline. However, all trials which involved stressing at elevated temperatures of 50 °C showed an appreciably greater reduction in copper concentration post-filtration. This indicates that temperature as a stressor has led to an increase in copper containing particle size, resulting in a greater quantity of particles over 1 μm being filtered out. This may be due to the higher

temperature solution leading to more energetic particles, increasing the likelihood of particles combining in a collision.

These trials spurred further temperature testing, with another 3 trials being conducted at 75 °C. This data is presented in Table 4.2 along with the 50 °C trial data from Table 4.2 for comparison.

Table 4.2. Cu concentrations in MCA solution 50 °C and 75 °C stress tests.

	Cu Concentration in Solution Pre-Filtration (wt.%)	Cu Concentration in Solution Post-Filtration (wt.%)	Percent Change in Cu Concentration (%)
Unstressed Solution	2.071	2.064	-0.338
Temp 50 °C Test 1	2.039	2.001	-1.864
Temp 50 °C Test 2	2.050	2.015	-1.697
Temp 50 °C Test 3	2.043	2.016	-1.337
Unstressed Solution	2.072	2.065	-0.338
Temp 75 °C Test 1	1.620	1.470	-22.04
Temp 75 °C Test 2	2.370	2.040	-25.37
Temp 75 °C Test 3	2.300	2.210	-10.41

The 75 °C trials had a far greater reduction in copper levels in the solution than any other stressors that have been tested. In most other trials, the stressed but pre-filtration copper concentration in solution did not differ much from the copper concentration seen in the unstressed stock, however, it should be noted that for the 75 °C trials there was a notable change. In Table 4.2, as with other tables in this section, the test data presented is the average of the 5 aliquots taken as part of the sampling procedure. Where the sampling port is at the bottom of the pressure vessel, the first aliquot of liquid sampled is from near the bottom of the cylinder and the fifth from near the top. In all other trials, the difference in copper concentrations and percent reductions was not observable between these 5 datapoints. In this trial of temperature 75 °C, the amount of copper in the aliquots from

near the bottom of the pressure vessel was higher than those near the top of the pressure vessel, showing a very clear separation and rapid settling of the copper containing particles in solution. This can be observed visually, as in Figure 4.1 where the collected aliquots on the left from the bottom of the tank are substantially lighter than those on the right from near the top of the fluid volume. The lighter indicates a higher presence of micronized copper particles, which as a concentrate has a light bluish color.

Figure 4.1. Image showing aliquots 1 through 5 from 75 °C solution stressing trial.

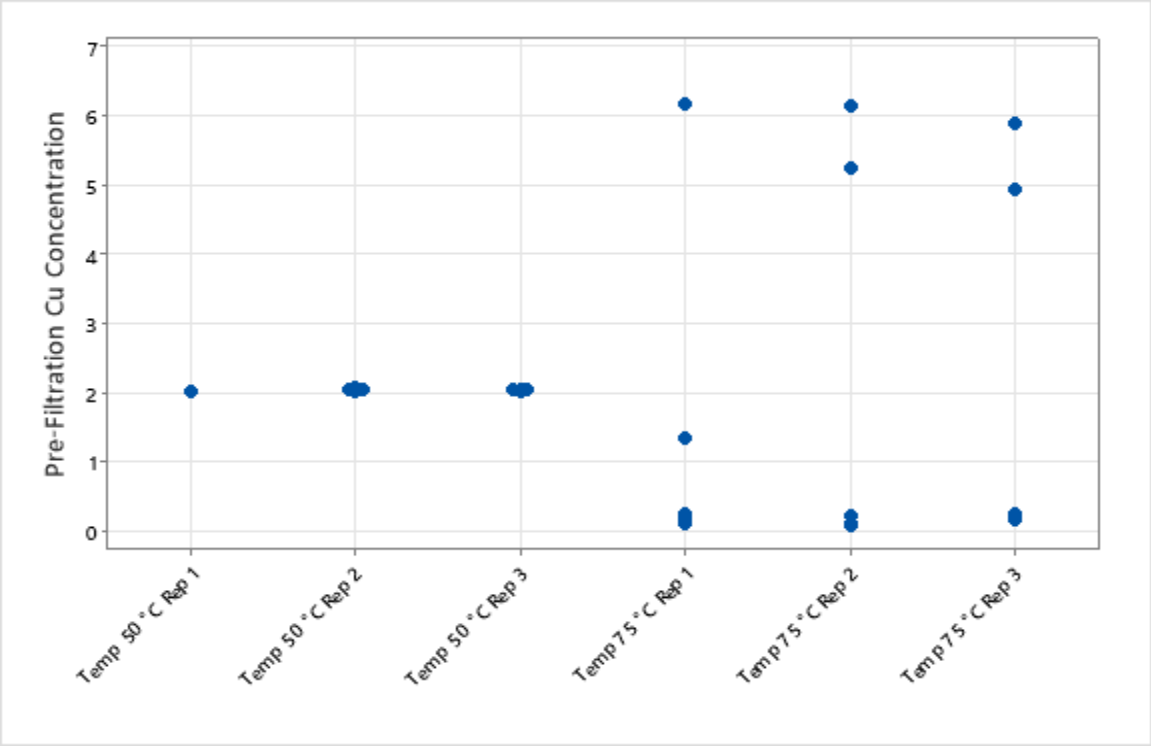

Figure 4.2. Individual value plot of pre-filtration copper concentrations for 50 °C and 75 °C trials.

Figure 4.2 highlights the extreme spread seen in the copper concentrations in the 75 °C unfiltered stressed stock solutions compared to the 50 °C solutions. The results indicate that the treating solution degraded significantly at the higher temperatures with the active ingredient settling out of solution. The particles were no longer well suspended. The aliquots taken from near the top of the pressure vessel had very little copper concentration, while those near the bottom had extremely high copper concentrations. A substantially greater portion of the copper particles were filtered out as evidenced by the percent difference post-filtration. The greater reduction in copper containing particles post-filtration indicates that the higher heat trial led to larger particle formation causing this settling. It should be noted that the XRF calibration curve prepared for this experiment ranged from 0 to 2.5% Cu concentration by weight, and some data from the

75 °C temperature trial exceeded this range. This, as well as the substantially greater reduction in copper concentration post-filtration implies that the 75 °C trial data should not be included in statistical analysis against other trials. However, it still is appropriate for illustrating trends.

In summary, temperature was the only observed factor which had an appreciable impact on the formation of larger copper containing particles. Pressure or vacuum stressors applied to the solution alone did not show a substantial deviation from the baseline stock solution values. With an additional 75 °C temperature trial, the influence of temperature is even more apparent, with an even greater increase in copper containing particles over 1 µm identified as well as visual degradation of the solution. A further statistical analysis is presented in Section 4.1.4.

4.1.2 Pressure treating Kiln Dried and Non-Kiln Dried Wood

The above stressing tests were conducted without the presence of wood, solely aiming to identify the impact of process parameters. It is also important to investigate the impact of the presence of wood during a treating cycle on the solution. Trials on the treatment of wood blocks corresponded to the procedure outlined in Section 3.2.5. The treating cycle parameters were those specified by Timber Specialties, with 3 charges tested as this is the maximum number of sequential charges treated before solutions would require topping up with additional components. A mix of 300 blocks of Spruce, Pine and Fir were used per treating charge to ensure that each had a mixture of all three tree species to replicate the currently treated mix of lumber at Stella-Jones facilities. Two types of wood blocks were used, kiln dried (moisture content 12%) and non-kiln dried (moisture content 7.5%).

The moisture content of the kiln dried wood was greater than the non-kiln dried wood, possibly due to storage conditions prior to purchase, but any impact on wood chemistry related to the rate of drying difference would still be captured. Both moisture contents are also below the recommended 20-30% moisture content of wood being treated (Timber Specialties, 2019). Data on the change in copper concentration pre- and post-filtration for each charge of the kiln dried and non-kiln dried wood can be seen in Table 4.3.

Table 4.3. 2% MCA solution used to treat multiple charges of wood blocks.

	Cu Concentration in Solution Pre-Filtration (wt.%)	Cu Concentration in Solution Post-Filtration (wt.%)	Percent Change in Cu Concentration (%)
Unstressed Solutions	2.031	2.026	-0.246
Kiln Dried Soln Charge 1	2.036	2.016	-0.995
Kiln Dried Soln Charge 2	2.060	2.037	-1.119
Kiln Dried Soln Charge 3	2.065	2.041	-1.153
Undried Soln Charge 1	2.055	2.044	-0.557
Undried Soln Charge 2	2.069	2.050	-0.936
Undried Soln Charge 3	2.085	2.065	-0.960

Note: Average of 3 charges of each type are presented in table.

All values of copper reduction are clearly greater than the baseline level of reduction shown by the stock solutions here. A large amount of variation between individual trial runs is present. The large volume of 300 small blocks was chosen to maximize surface area in contact with the preservative solution to better simulate bundles of treated lumber used in full scale treating cycles, with a total volume of wood chosen to be 40% of the volume of the treating cycle in line with what many larger scale charges use. Given the number of small sawn blocks, factors such as the amount of sawdust on blocks to be treated may have led to some of the variation.

Despite the individual variations between tests, solutions used to treat wood showed a greater reduction in copper concentration post-filtration, implying an increase in copper containing particle size. This reduction in copper concentration post-filtration is less than that seen in the stressing trials which involved exposure to elevated temperatures as noted in Section 4.1.1. Where the solution temperature used in the treating cycle with wood blocks was 37.8 °C and the temperature stressing tests in Section 4.1.1 were done at 50 °C, this lower reduction of copper may well be related more to the heating of the solution than anything to do with the presence of wood for the treating cycles. This is further evidenced by there not being a consistently increasing reduction in copper concentration post-filtration as the solution was reused to treat further charges. Further statistical analysis is presented in Section 4.1.4.

4.1.3 Production Plant Work Solution and Influence of Water Comparison

Given the results of the pilot scale solution stressing trials observed in previous sections, an experiment was conducted to see how the observed reduction in copper concentration post-filtration from these trials compares to samples of stressed work solutions from a full-scale treating facility. This knowledge would also provide an important link between research and real life to determine how the problem compares. Therefore, 0.5% and 0.8% MCA work solution samples from a treating cylinder charging tank from the Gormley, Ontario Stella-Jones facility were obtained and evaluated. Well water and storm water used in operation in Gormely were also sent to Truro, and a 2% MCA copper solution was made with these water samples. The purpose of preparing this solution was to determine if there was a significant difference in copper reduction based on the water

used for mixing. The samples in this analysis included an 0.8% MCA solution with distilled water, a 2% MCA solution with storm water (from runoff water recovery system), and a 2% MCA solution with well water. In addition to these samples, the 0.5% MCA and 0.8% MCA working solution provided by Gormley were tested for copper reduction of copper particles greater than 1 micron after filtration. A summary table of the various percent copper reductions per commodity may be observed in Table 4.4.

Table 4.4. Cu Concentrations in MCA solutions related to Gormley facility.

	Cu Concentration in Solution Pre-Filtration (wt.%)	Cu Concentration in Solution Post-Filtration (wt.%)	Percent Change in Cu Concentration (%)
0.5% MCA Gormley Working Solution	0.553	0.529	-4.355
0.8% MCA Gormley Working Solution	0.875	0.851	-2.735
0.8% MCA Unstressed Solution prepared with Distilled water	0.840	0.837	-0.357
2% MCA Unstressed Solution prepared with Gormley Well Water	2.018	2.007	-0.535
2% MCA Unstressed Solution prepared with Gormley Storm Water	1.996	1.987	-0.490

Based on the information provided in Table 4.4, the copper reduction from samples provided by Gormley was higher than the stock solution samples made in Truro NS, with copper reduction percentages of 0.8% MCA being 2.735% and 0.357% respectively. This examination also includes the copper content of work solutions made with Ontario well water and Ontario storm water, which had copper reductions of -0.535 and -0.490 respectively. In production environments, water in the solution comes from a combination of well water from an onsite well, as well as small amounts of storm water.

Data indicates slightly greater quantities of copper particles over 1 µm than the stock solutions prepared with distilled water, but it is not a statistically significant increase, indicating that impurities in the water is not a significant factor. This interpretation of the results is expanded upon in the comparative statistical analysis in Section 4.1.4. Furthermore, the samples of production solution provided from Ontario were significantly stressed because the solutions are generally "topped up" with the required components of MCA to meet specifications, whereas for the pilot scale trials at the Truro facility, a fresh batch of MCA was made for each stressor tested. Finally, the stressed solution provided from Ontario also had a higher chance of chemical inconsistencies. Since the components of micronized copper are made batchwise, there was a higher chance that an error from the manufacturing could negatively impact the overall MCA quality.

In summary, stressed MCA treating solutions provided by the Gormley facility showed a greater reduction in copper concentration post-filtration than any pilot-scale trials, indicating more copper particles over 1 µm. This indicates that the formation of larger copper containing particles is an issue seen in production environments. Unstressed stock solutions prepared with water obtained from the Gormley production facility did not show a significant difference from stock solutions prepared with distilled water. This indicates that the greater presence of copper containing particles over 1 µm in size is caused by factors that might have not been evaluated in the pilot scale testing. The greater presence of copper containing particles over 1 µm in size compared to pilot scale testing is likely influenced by environmental factors not yet identified.

4.1.4 Statistical Analysis of Experimental Results and Comparison of All Trials

A Welch's One-Way Analysis of Variance test was conducted using Minitab 2021 software. This allows for the determination of which means are different from one another, a two-sided 95% confidence level ($\alpha = 0.05$) was used (Corner, 2024). The different datasets in the trial were found to not have equal variance, which is why Welch's ANOVA was used as opposed to a typical One-Way ANOVA test. A Games-Howell method of pairwise comparisons was selected as it allows for multiple pairwise comparisons between groups to be conducted in order to determine which means differ significantly from each other, using different degrees of freedom for each comparison to account for the unequal variance (West, 2021). Datasets with the same letter are not significantly different from one another at $\alpha = 0.05$.

Table 4.5 Multiple means comparison with Games-Howell method of pairwise comparison on all solution stressing trials, $\alpha = 0.05$.

Averages of Trials	Percent Change in Cu Concentration Pre- and Post-Filtration (%)	Games-Howell Pairwise Comparisons Grouping
Unstressed Solutions	-0.255	A
Pressure Test 1-3	-0.322	A
Vac Test 1-3	-0.376	A B
Stormwater Solution	-0.490	A B C
Well Water Solution	-0.535	A B C
Undried Wood Charge 1	-0.557	A B C
Undried Wood Charge 2	-0.936	C
Undried Wood Charge 3	-0.960	C
Kiln Dried Wood Charge 1	-0.995	B C
Kiln Dried Wood Charge 2	-1.119	B C D
Kiln Dried Wood Charge 3	-1.153	C D
Temp 50 °C Test 1-3	-1.727	D E
Press Temp & Vac Test 1-3	-1.839	D E
Press Temp Test 1-3	-2.021	E

The Games-Howell method multiple means comparison groupings shown in Table 4.5 provide statistical validation to the discussion in previous sections. Many trials in the dataset have large coefficients of variance, indicating that individual data points have a large variance from the mean. This results in the grouping information from an ANOVA multiple means comparison will have greater overlap than otherwise might have been observed. One notable example of this overlapping occurs between kiln dried wood charge 2 sharing a grouping with unheated solutions such as the vacuum trials. It also

shares a separate statistical grouping with some of the trials heated to 50 °C which showed far greater reductions in copper. In spite of the variance, general trends can still be observed and statistically validated.

The only solution stressing trials which did not show a statistically significant reduction in copper solution strength post-filtration were the stressing trials which did not have temperature applied. They share the same grouping letter A with stock solution. This indicates pressure is not a significant stressor causing particle size increase. Temperature is undoubtedly the most significant stressor (grouping D and E) which drives the formation of larger copper containing particles, as all solutions with elevated temperatures resulted in more copper in solution being filtered out by the 1 μm filter. While pressure as a stressor on its own shows no appreciable effect, when coupled with temperature it may lead to the formation of larger particles of copper as seen by grouping E, where the trials at 50 °C and under pressure showed slightly higher reductions than the trial at 50 °C with no other factors.

As per Timber Specialties guidelines, all wood treating trials were conducted at a temperature of 37.8 °C. These fell mostly into groupings B and C, showing a greater reduction in copper concentration post-filtration than the unstressed stock solutions or solutions stressed at room temperature. These wood treating trials also generally showed lower percent reductions than the solution stressing trials conducted at 50 °C, as is to be expected due to the slightly lower treating temperature.

One other significant finding is that the solutions made with water from the Gormley, Ontario treating facility was not significantly different from the stock solution (both in grouping A) but showed a slightly greater reduction in copper than the distilled water

stock solution post-filtration. This may be an avenue for further investigation as part of why the production plant stressed solutions from the Gormley facility discussed in Section 4.1.3 showed a substantially greater reduction in copper concentration post-filtration than any of the pilot-scale trials. These factors could include stressor combinations not listed here which were not investigated due to time constraints, such as more treating charges at higher temperatures, or quality of solution concentrates being supplied. The greater reduction observed in Gormley solutions could also be caused by environmental factors unique to that system not considered here such as dirt and dust coating the wood used in production or yet unconsidered factors.

In summary, temperature as a stressor appears to be the primary cause of increased copper containing particle size, resulting in a greater quantity of particles over 1 µm being filtered out. Solutions which were not heated were not statistically different from stock solutions. Using the same treating solution for multiple wood charges did not result in significantly greater copper reduction in solution. Temperatures of 50 °C coupled with pressure did lead to lower copper levels in filtered solution than temperature on its own. Lastly, none of these trials resulted in post-filtration copper value reductions comparable to the actual production solutions sourced from the Gormley facility, indicating other factors may be present in the production facilities which have not yet been identified.

4.2 Identifying Particle Composition

To identify the composition of particles over 1 µm filtered out of stressed solutions, characterization of these particles was conducted. This may allow for better insight into

what is occurring and what process may be causing the particle clumping. Due to the unknown composition of the particles in question, non-destructive analytical methods were chosen. Samples of particles over 1 μm filtered out of solution were obtained by filtering selected stressed and stock solutions using the filtration procedure described in Section 3.3.1. Due to time and cost constraints not all solution stressing trials were filtered for analysis; a representative subset of 9 samples was used. Multiple stock solutions were included as a baseline, while the 50 °C, 75 °C, PTV, kiln dried and non-kiln dried wood were chosen as they showed the largest percent reduction of copper in their trial types and represent several different types of stressors. Gormley 0.5% work solution was included as a sample representative of real-world conditions in a production environment. These are listed in Table 4.6

Table 4.6. Samples selected for particle composition analysis.

Sample Name	Sample ID	Description
Stock Solution	TSD1	Unstressed 2% MCA solution
Temp 50°C	50C2	50 °C for 30 minutes
Temp 75°C	75C2	75 °C for 30 minutes
Stock Solution	SD2	Unstressed 2% MCA solution
Press Temp & Vac	PTV3	150 psi at 50 °C for 30 minutes then 25 inHg for 30 minutes
Stock Solution	SW3	Unstressed 2% MCA solution
Kiln Dried Wood Charge 3	KD3	Kiln dried wood blocks treated with 150 psi at 37.8 °C for 30 minutes then 25 inHg for 30 minutes, third solution stress test.
Undried Wood Charge 3	UD3	Non-kiln dried wood blocks treated with 150 psi at 37.8 °C for 30 minutes then 25 inHg for 30 minutes, third solution stress test.
Gormley 0.5% Work Solution	GRM.5	Used 0.5% MCA treating solutions from Gormley facility working tanks.

4.2.1 SEM-EDS analysis

The samples listed in Table 4.6 were analyzed by SEM according to the procedure detailed in Section 3.2.2. This allowed for the collection of atomic percent data for all the samples. The EDS analysis system was set to display results for elements found in detectable quantities, with gold and palladium from the coating being filtered out. Hydrogen is not detectable with this system, nor are other elements lighter than boron. An example of a sample SEM image showing the areas scanned highlighted by the numbered boxes is shown in Figure 4.3.

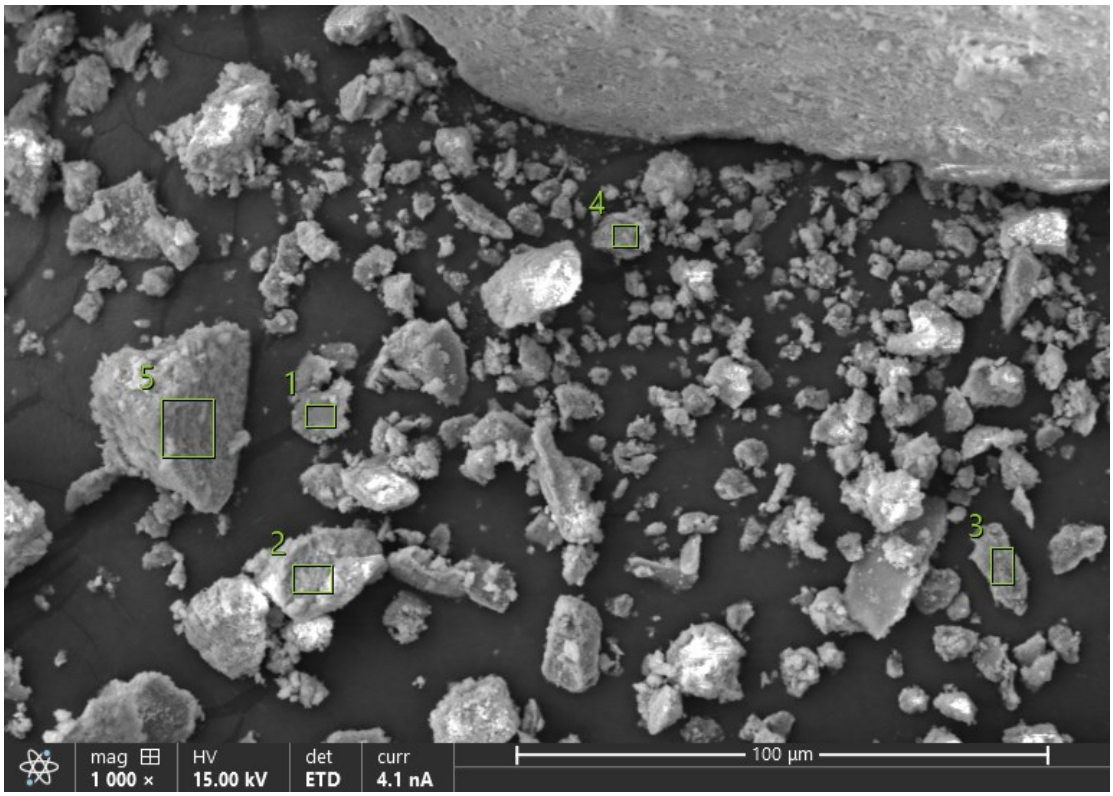

Figure 4.3. SEM image capture of particles filtered from stock solution sample (TSD1) with areas scanned using EDS analysis highlighted in numbered boxes.

The darker background represents the graphite sticky tape on the sample with the raised objects being the filtered particles analyzed. These do not represent the actual size of the

particles as they came from breaking down the flakes which formed from the particles collected on the filter paper. The box scans can be seen to only cover the sample area and not the carbon paper. The lighter, whiter areas on some of the samples come from charging, where there was insufficient conductivity on certain particles in the sample. Table 4.7 shows the atomic percent data collected for this sample. Note: All atomic percent data is out of the elements identified by the EDS analysis software.

Table 4.7. Atomic percent data for stock solution TSD1.

Sample ID	Spectrum	Carbon Atomic%	Oxygen Atomic%	Copper Atomic%	Iron Atomic%
TSD1	1	29.1	43.3	24.4	3.1
	2	22.8	43.8	29.7	3.8
	3	22.8	29.1	42.4	5.7
	4	10.4	6.3	74.6	8.8
	5	28.7	39.1	28.4	3.8

It can be seen in Table 4.7 that there is a large amount of variability between some of the spectral results. Spectrum 4 has triple the amount of copper present in spectrum 1. EDS analysis is highly sensitive to charging as a negative charge buildup on the sample surface can reduce the impact energy of incident electrons to a level where atoms with higher energy electron shells may no longer fluoresce (Newbury, 2004). This also interferes with the background spectrum detected which can affect the detection of lighter elements as well. Charging was reduced by increasing sample conductive coating thickness from 10 nm to 15 nm but was not eliminated. The box shown in spectrum 4 is near a much larger piece of sample and a white spot of charging.

To eliminate anomalous datapoints as mentioned in the previous paragraph, a combination of statistical outlier testing and examination of spectra were used to eliminate some of the datapoints to come up with average values used in the rest of the

section. Images of spectra identified for deletion were inspected to ensure they did not appear visually distinct from other parts of the sample to avoid arbitrarily deleting possible unidentified compounds. No more than 2 out of 15 datapoints were deleted for any type of sample.

Table 4.8. Average atomic percent data for all samples.

Sample Name	Sample ID	Carbon Atomic (%)	Oxygen Atomic (%)	Copper Atomic (%)	Iron Atomic (%)
Stock Solution	TSD1	28.38	44.46	23.94	3.24
Temp 50°C	50C2	28.41	50.14	18.7	2.46
Temp 75°C	75C2	22.48	54.14	21.05	2.34
Stock Solution	SD2	30.97	46.03	19.22	2.82
Press Temp & Vac	PTV3	30.00	44.33	22.02	3.12
Stock Solution	SW3	29.74	45.92	20.95	2.99
Kiln Dried Wood Charge 3	KD3	30.29	44.69	21.60	3.09
Undried Wood Charge 3	UD3	31.35	42.57	21.93	3.22
Gormley 0.5% Work Solution	GRM.5	29.31	41.93	23.62	4.18

The EDS results in Table 4.8 provide several clues about the sample compositions. All of the samples contained carbon, oxygen, copper and iron in similar quantities. This indicates that iron compounds from the MSNB dye are present in addition to the copper from the copper carbonate. Looking at Table 4.9, the atomic percent of several compounds found in the SDS sheets provided by Timber Specialties for MSNB (revised 2021) and MP200 (revised 2019), and similar copper oxides may be seen.

Table 4.9. Atomic percent of EDS detectable atoms (excludes hydrogen) of several compounds of interest which may be present in filtered particles.

	EDS Detectable Atoms	Carbon Atomic %	Oxygen Atomic %	Copper Atomic %	Iron Atomic %
$Cu_2CO_3(OH)_2$ (Malachite)	8	12.5	62.5	25	0
$Cu_3(CO3)_2(OH)_2$ (Azurite)	13	15.4	61.5	23.1	0
CuO (Copper II Oxide) (Tenorite)	2	0	50	50	0
Cu_2O (Copper I Oxide) (Cuprite)	3	0	33.3	66.7	0
Fe_2O_3 (Iron Oxide Red) (Maghemite)	5	0	60	0	40

The SDS datasheet for MSNB indicates that Fe_2O_3 is the only iron containing compound present. By assuming all the iron present in the sample is present in this form, the amount of copper, carbon and oxygen remaining can be considered. The data for Sample ID TSD1 is used to show this calculation process. As each Fe_2O_3 molecule has 3 oxygen atoms for every 2 iron atoms, 1.5 atom of oxygen for every 1 atom of iron is removed. Assuming 100 atoms total (ignoring that they are indivisible for a moment):

$$44.6\ O_2 - \left(\frac{3O_2}{2\ Fe}\right) 3.24Fe = 39.74O_2\ Remaining$$

As converting back to atomic percent remaining would no longer add up to 100, the sum of the atoms is taken. The amount of oxygen, carbon and copper atoms is multiplied by this factor to get the new atomic percent of the sample excluding the part comprised of Fe_2O_3. This adjusted data is shown in Table 4.10.

Table 4.10. Averaged atomic percent data for all samples excluding Fe_2O_3.

Sample Name	Sample ID	Carbon Atomic (%)	Oxygen Atomic (%)	Copper Atomic (%)	Iron Atomic (%)
Stock Solution	TSD1	30.87	43.08	26.04	N/A
Temp 50°C	50C2	30.37	49.65	19.99	N/A
Temp 75°C	75C2	23.87	53.77	22.36	N/A
Stock Solution	SD2	33.67	45.44	20.89	N/A
Press Temp & Vac	PTV3	32.73	43.25	24.02	N/A
Stock Solution	SW3	32.28	44.98	22.74	N/A
Kiln Dried Wood Charge 3	KD3	32.94	43.56	23.49	N/A
Undried Wood Charge 3	UD3	34.44	41.46	24.09	N/A
Gormley 0.5% Work Solution	GRM.5	33.08	40.25	26.66	N/A

The AWPA (2022) states that the copper present in the sample is to be in the form of basic copper carbonate, also known as malachite. This was expected to be the likely form of most of the copper present in the sample, however it is immediately apparent from looking at the atomic percent composition of malachite in Table 4.9, that there is not enough oxygen present in any of these samples for this to be the only form in which copper is present. Given the 20-25% copper concentrations detected, oxygen concentrations of 62.5% would need to be present for this to be possible. Azurite, a similar copper containing carbonate also could not be the only compound present due to insufficient oxygen. As a result, malachite is most likely present, but an unknown portion of the copper is present in another form. This may be copper (I) or copper (II) oxide, as malachite ores often contain quantities of these two mineral forms (Klein, Dutrow & Dana, 2008). This is explored further in Section 4.2.2.

Any ratio of copper oxide or copper carbonate would leave an excess of carbon unaccounted for. The excess carbon present may be from carbon containing compounds

present in the MSNB or one of the fungicides, which would require additional analysis to identify due to the inability of this method to evaluate structure or identify hydrogen.

4.2.2 X-Ray Diffraction

X-Ray diffraction is well suited to the analysis of crystalline structures, allowing for further investigation of what form of copper the filtered particles have taken. As malachite, azurite, copper (I) oxide, copper (II) oxide and iron oxide red all exist in crystalline forms, determining which is present is possible. Table 4.11 lists the characteristic diffraction patterns of several sample substances suspected to be present in the sample using the ICDD PDF-4 Minerals 2023 database (Gates-Rector & Blanton, 2019). The PDF number is the Powder Diffraction File number, allowing the diffraction pattern and further information to be referenced with the ICDD database. The three greatest intensity characteristic diffraction angles are also highlighted in this table, as these indicate the primary angles used for identification.

Table 4.11. List of substances identified in sample diffraction patterns.

	PDF Number	Highest intensity Diffraction Angle 2θ	Second highest intensity Diffraction Angle 2θ	Third highest intensity Diffraction Angle 2θ	Color Used In Sample Patterns
$Cu_2CO_3(OH)_2$ (Malachite)	00-056-0001	31.320	17.572	24.097	Orange
$Cu_3(CO3)_2(OH)_2$ (Azurite)	00-011-0682	25.310	17.204	40.528	Yellow
CuO (Copper II Oxide) (Tenorite)	00-047-0518	38.685	35.494	48.658	Purple
Cu_2O (Copper I Oxide) (Cuprite)	04-007-9767	36.427	42.313	61.382	Green
Fe_2O_3 (Iron Oxide Red) (Maghemite)	00-039-1346	35.630	30.241	62.925	Blue

Figures 4.4 through 4.12 show the individual results for each of the diffraction patterns obtained from filtered samples. The characteristic diffraction patterns of samples listed in Table 4.11 are overlaid.

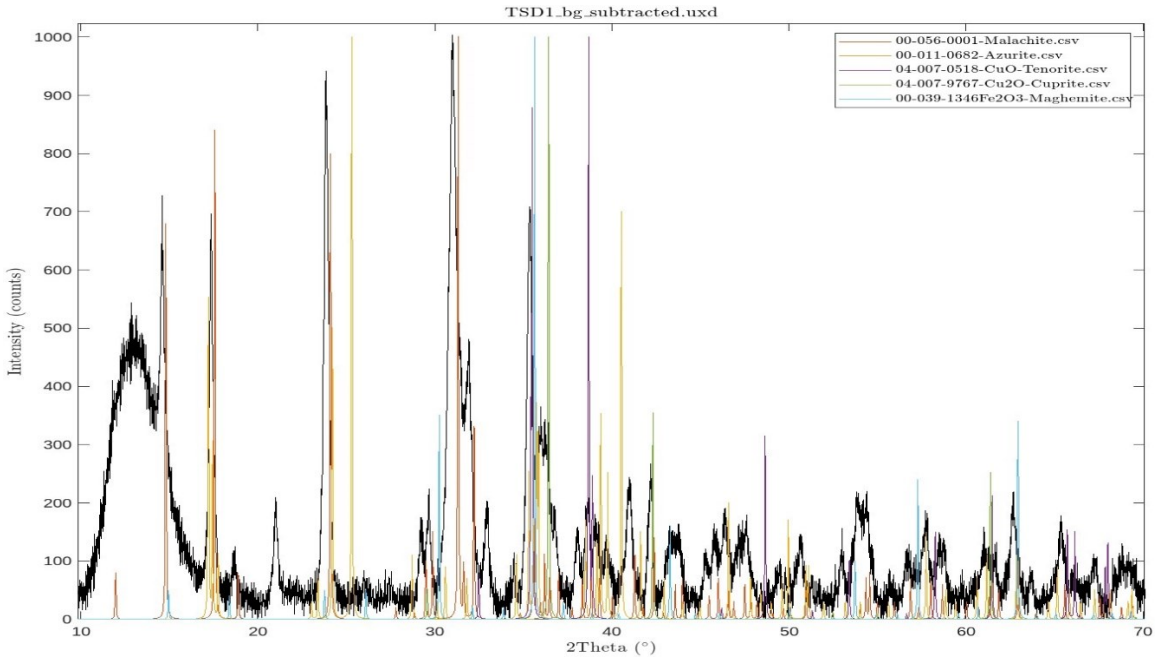

Figure 4.4. X-ray diffraction pattern for sample TSD1 peaks from Table 4.11, highlighted.

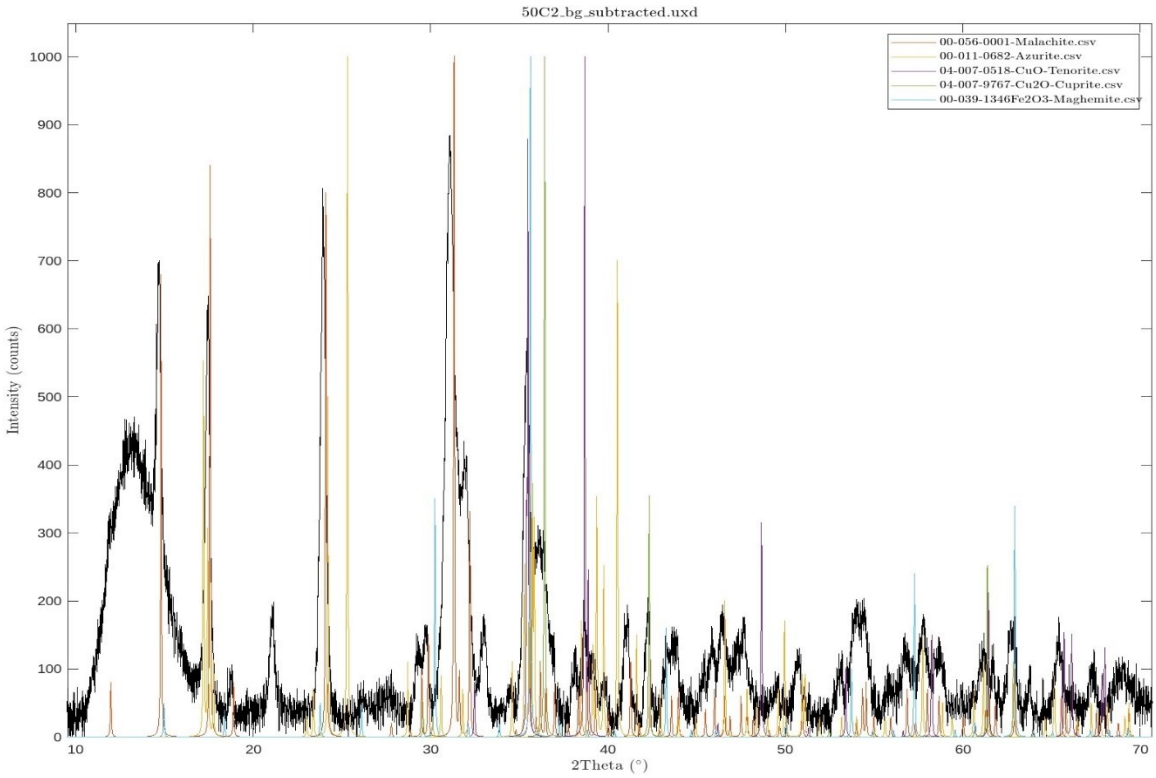

Figure 4.5. X-ray diffraction pattern for sample 50C2 peaks from Table 4.11, highlighted.

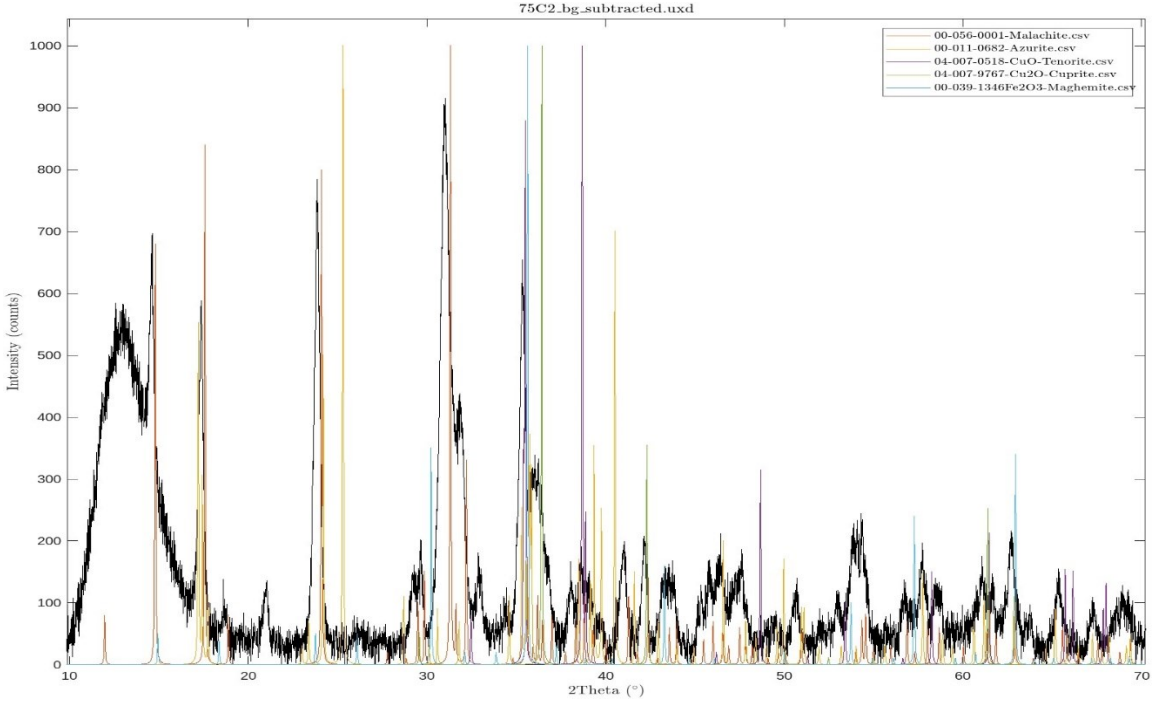

Figure 4.6. X-ray diffraction pattern for sample 75C2 peaks from Table 4.11, highlighted.

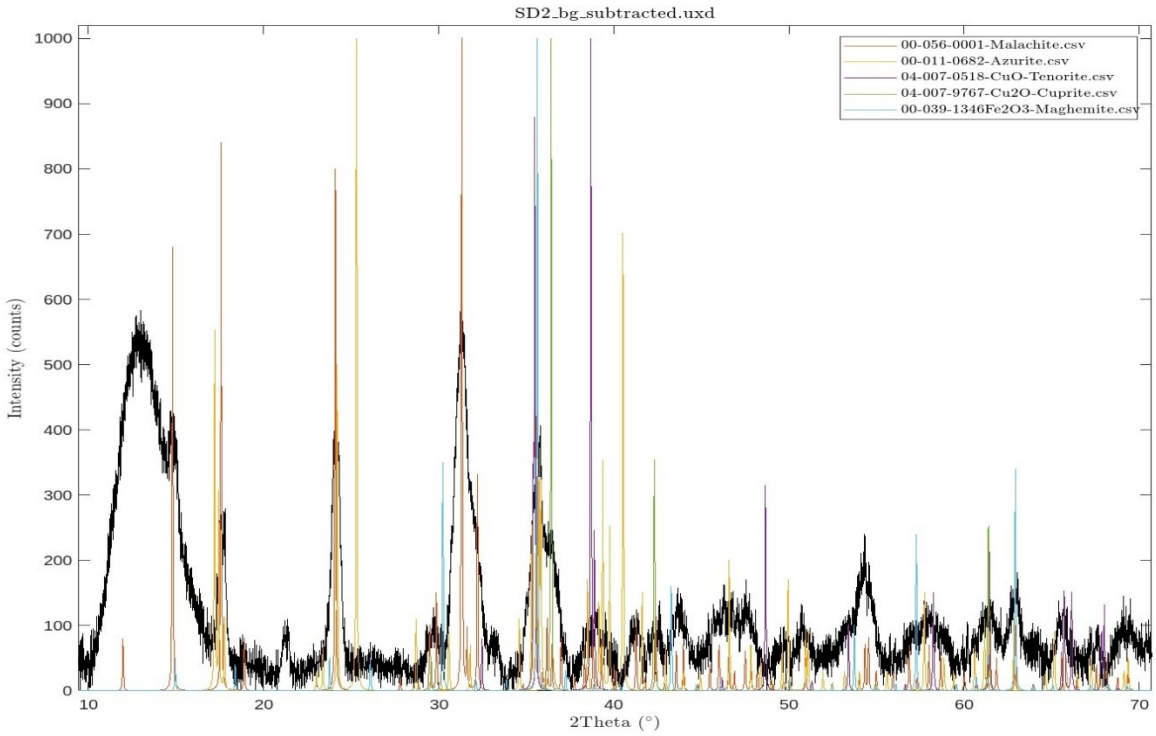

Figure 4.7. X-ray diffraction pattern for sample SD2 peaks from Table 4.11, highlighted.

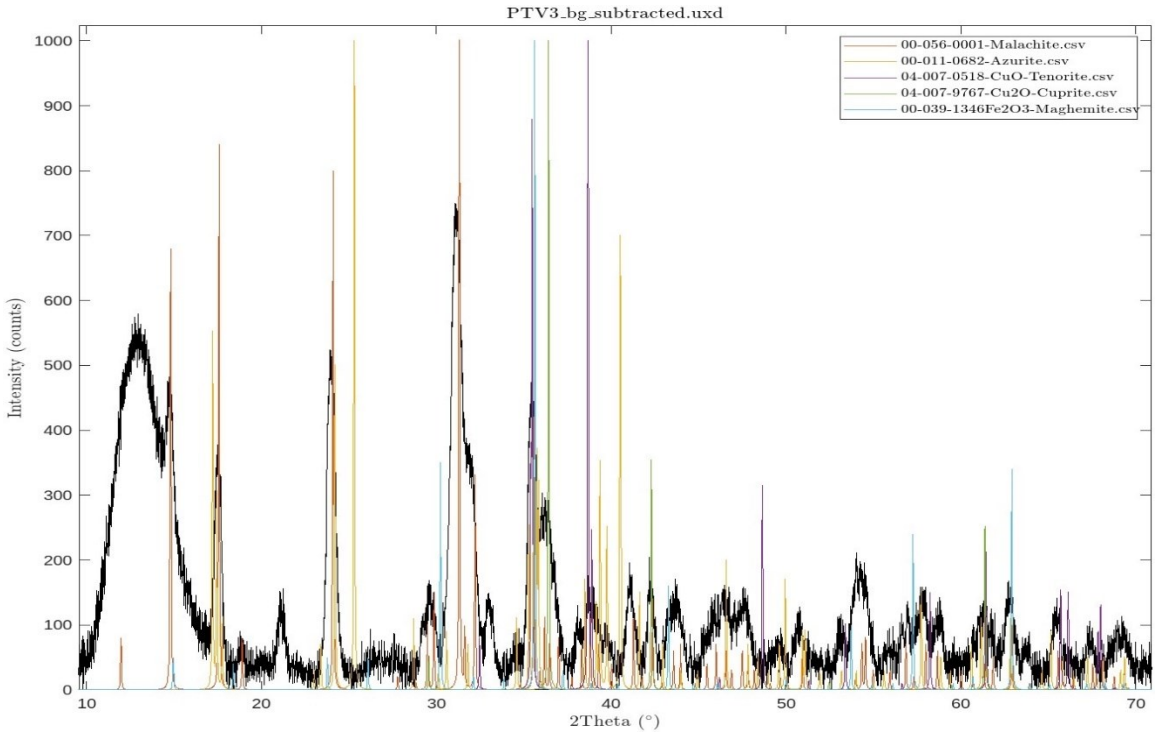

Figure 4.8. X-ray diffraction pattern for sample PTV3 peaks from Table 4.11, highlighted.

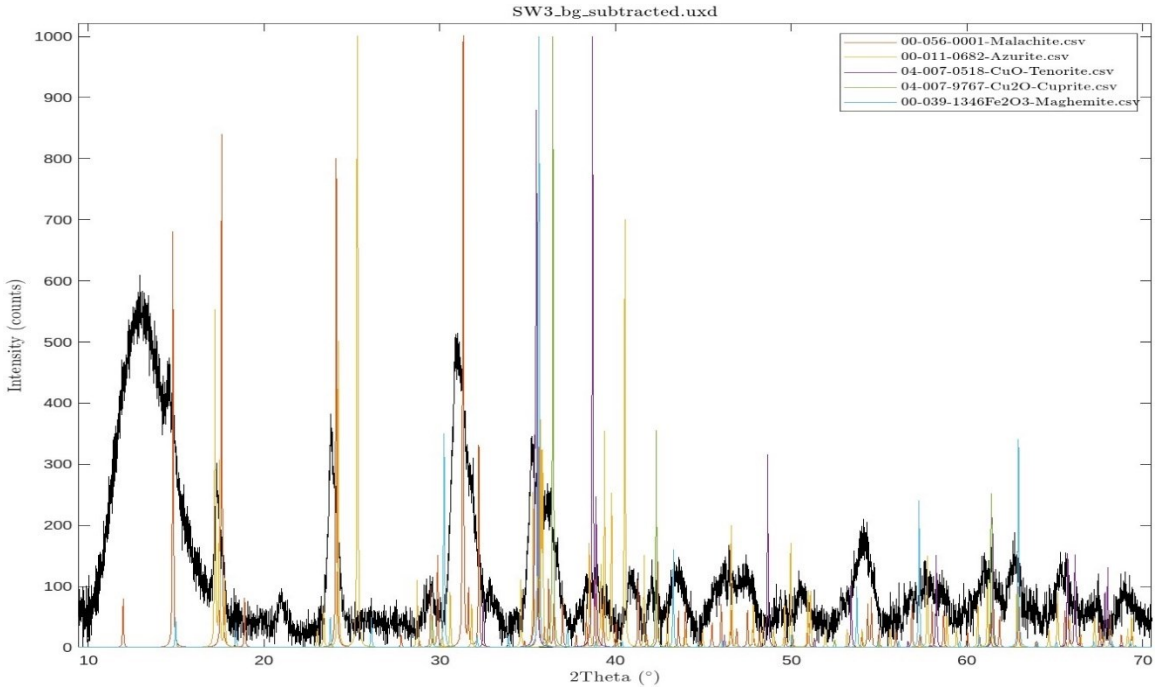

Figure 4.9. X-ray diffraction pattern for sample SW3 peaks from Table 4.11, highlighted.

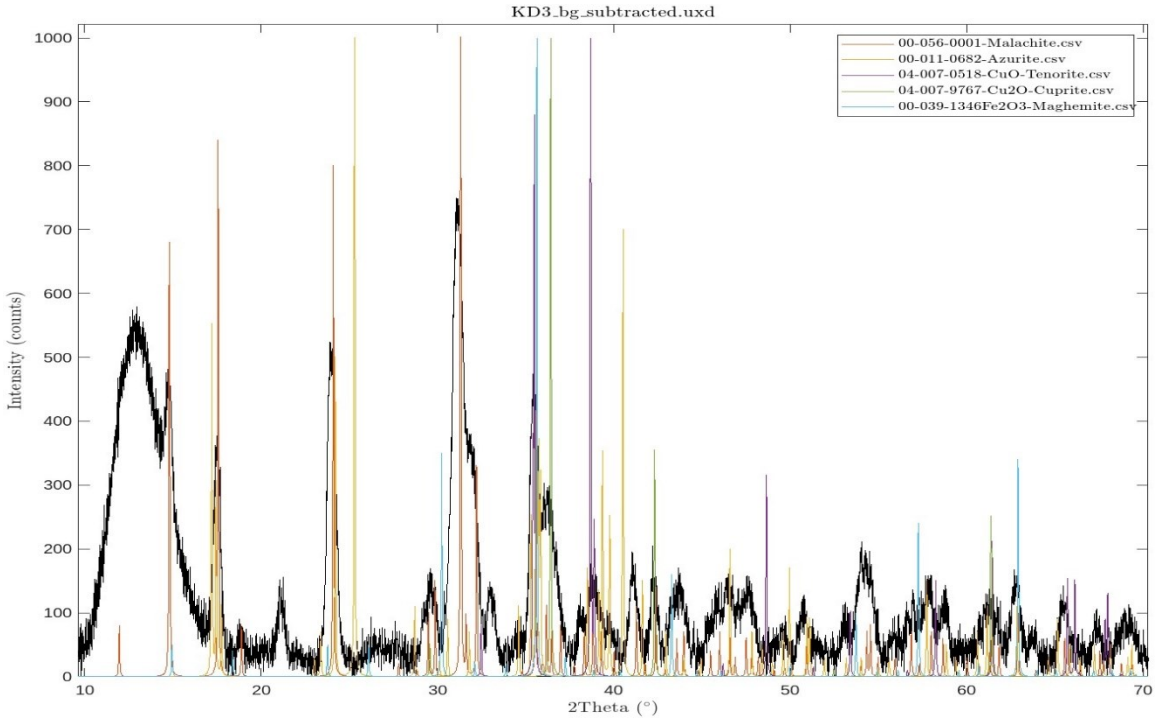

Figure 4.10. X-ray diffraction pattern for sample KD3 peaks from Table 4.11, highlighted.

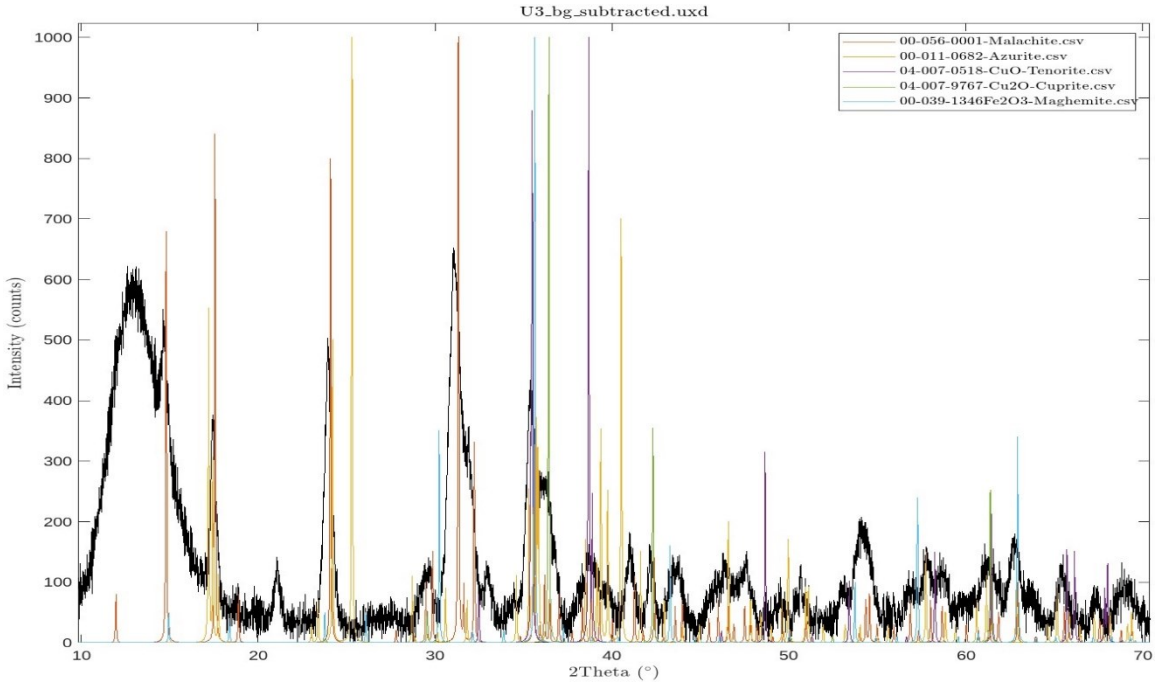

Figure 4.11. X-ray diffraction pattern for sample U3 peaks from Table 4.11, highlighted.

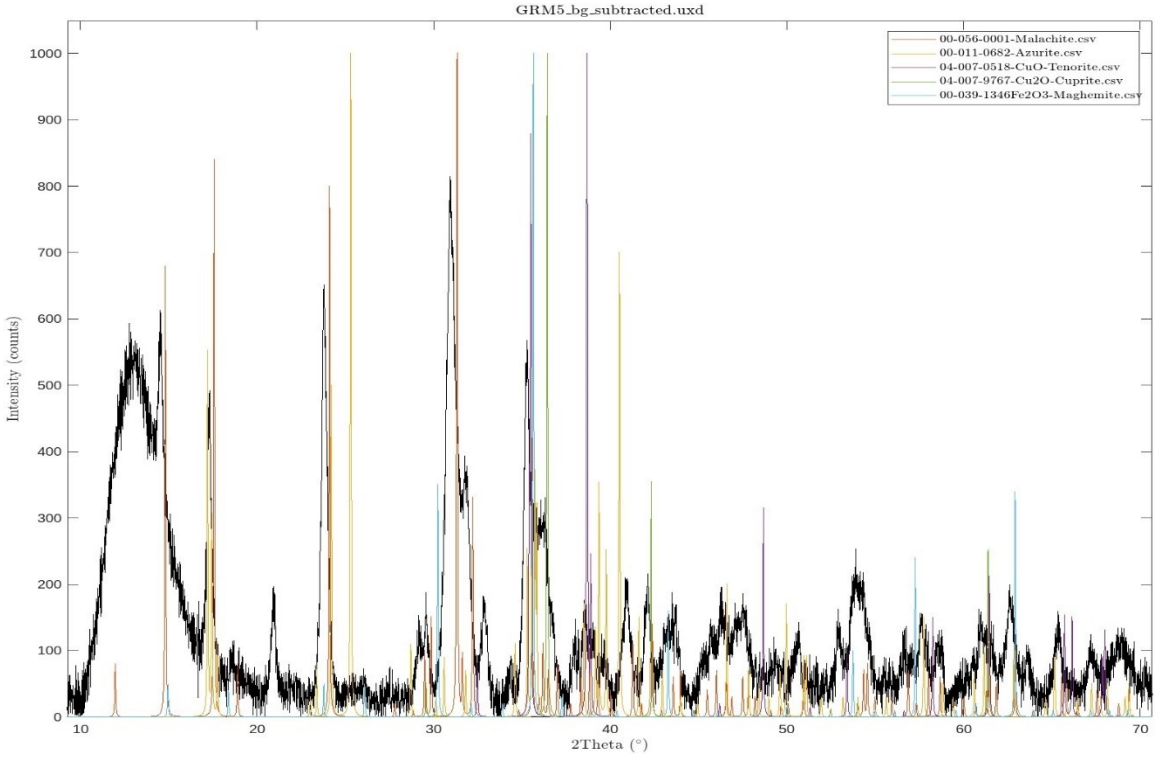

Figure 4.12. X-ray diffraction pattern for sample GRM.5 peaks from Table 4.11, highlighted.

Seeing the characteristic diffraction patterns plotted against the diffraction patterns in the sample, several observations can be made. Principally, all samples analyzed had similar diffraction pattern peaks to one another, indicating all samples had similar compositions in similar ratios. By overlaying the characteristic diffraction patterns over the sample with a relative intensity of 1000 for the greatest peak, the presence or absence of compounds is readily apparent. The characteristic diffraction peak of Azurite as highlighted in yellow has its highest intensity diffraction 2θ angle of 25.310, which does not line up with peaks in any samples of interest. Azurite thus does not appear to be present in quantity in the samples.

The characteristic diffraction peaks of malachite (represented in orange) are at 2θ 31.32, 17.572 and 24.097 corresponding to larger peaks in all analyzed samples. It clearly demonstrated that malachite is present in all of the samples of stressed solutions as well as stock solutions. Looking just at the stressed solution sample from Gormley (Figure 4.12) and stock solution sample TSD1 (Figure 4.6), the malachite peaks fall within the peaks observed in the samples but appear to be shifted a very slight amount to the right from perfectly fitting the peaks. This peak shift may be due to subtly different strain in crystals and different moisture contents.

Looking at the characteristic peaks for tenorite in purple (2θ of 38.685, 35.494 and 48.658) and cuprite in green (2θ of 36.427, 42.313 and 61.382), the diffraction patterns of these copper oxides line up with the diffraction patterns shown in all samples tested. The match in diffraction patterns coupled with the finding in Section 4.2.2 that there is inadequate oxygen relative to copper in samples for all copper to be in the form of malachite strongly supports the presence of tenorite and cuprite. The presence of these

compounds in unstressed stock solutions as well as all other stressed solutions may indicate that these copper oxide compounds did not form due to stressors, but rather were present in the original stock solutions. Lastly, iron in the form Fe_2O_3 (blue) is present in the sample as supported by this form being present on the SDS sheets.

Due to the many similar forms of most iron oxides, copper oxides and copper carbonate coupled with the impure nature of these filtered samples, precise qualification and quantification was not possible. It was, however, evident that malachite is not the only copper containing compound present, with significant but unquantifiable amounts of two copper oxides being found. Further research is needed to definitively determine all types of copper containing compounds in particle form in MCA solutions as well as the causes of particle size increase.

4.3 CFD Tank Recirculating Simulations

The settling behavior of particles in a preservative holding tank was modelled using Ansys fluent CFD software. Four different inlet locations/geometries were simulated but the holding tanks were otherwise identical.

The geometries of the tanks being simulated as well as several parameters of the model are shown and discussed in Section 4.3.1, while Section 4.3.2 contains the mesh independence analysis. Section 4.3.3 examines the settling of particles in a tank with no recirculation and Section 4.3.4 compares settling with recirculation in the 4 different inlet locations.

The decision to use DPM modelling was made as the objective is to compare four inlets and determine which inlet positions are best able to maintain particle suspensions in production environments. This assumes that the surfactant has not degraded, and so flocculant settling is not occurring. As the intent is to model inlet positions where particles are not settling out, the volume fraction should not reach levels where the DPM is not applicable and hindered settling does not apply.

4.3.1 Tank Geometries and Simulation Parameters

The intent of the simulation is to examine possible retrofits to the existing preservative holding tanks. The constraints around tank size, inlet locations and flow rates were based on Stella-Jones requirements. The same basic layout of a 3.048 m (10 ft) diameter and 6.096 m tall (20 ft) cylindrical preservative storage tank was used as this represents the general size of tank used in Stella-Jones. All models have inlet and outlet pipes which are 52.5 mm in diameter, based on the interior diameter of a 2-inch NPS schedule 40 pipe. The outlet pipe modelled in the simulation is 3 pipe diameters long (157.5 mm) to allow for flow to fully resolve. Figure 4.13 shows the first inlet position, which is in to the top of the tank. All geometries have the same outlet position, which is 102.45 mm (approximately 4 inches) from the bottom of the tank represented by L1 in Figure 4.13. Table 4.12 lists the dimensions given in Figures 4.13 and 4.14 below. Figure 4.13 shows the first inlet position, 1/3 of the radius from the tank edge (L3 = 508 mm).

Table 4.12. List of dimensions shown in Figures 4.13 and 4.14.

Dimension	(mm)
L1	102.45
L2	157.5
L3	508
L4	304
L5	52.5

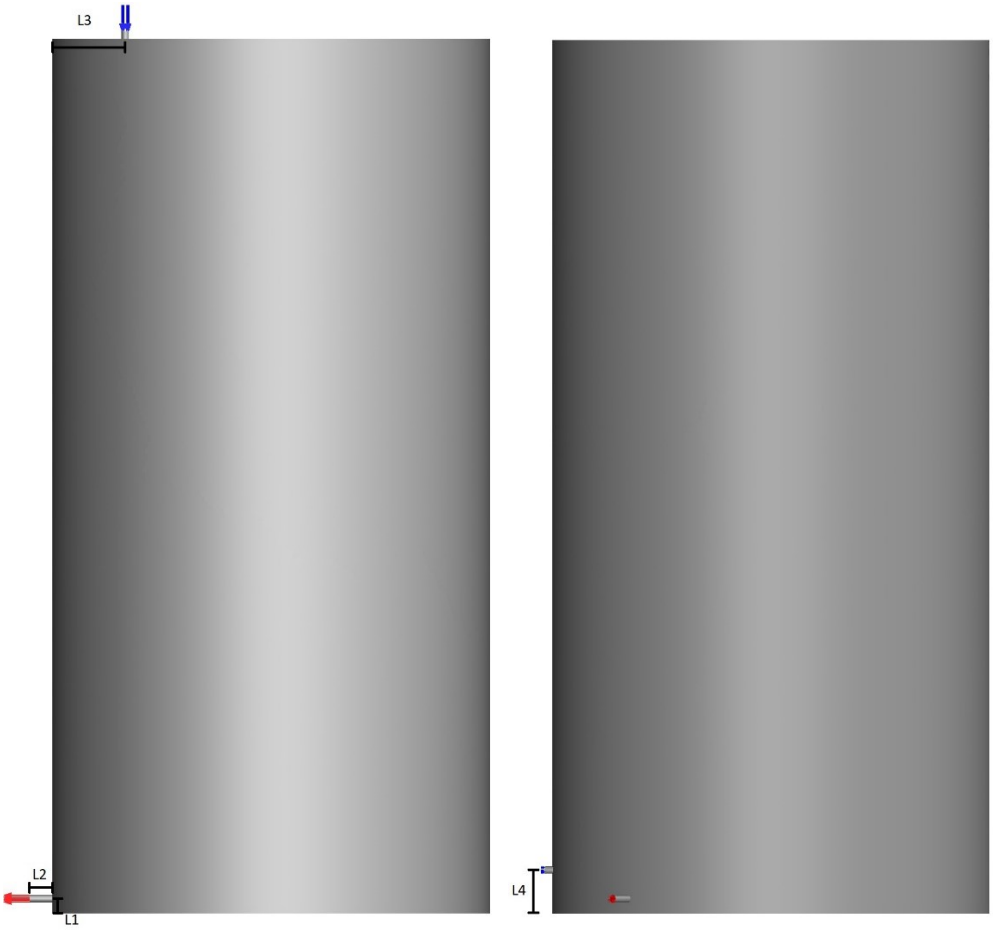

Figure 4.13. Inlet position 1 (Left), inlet position 2, 3, 4 (Right).

The second, third and fourth inlet positions all are 304 mm (12 inches) above the tank floor and 45° offset from the central angle, shown in Figure 4.13 (right). Inlet position 2 is directed straight into the sidewall of the tank as seen, where L4 is the 304 mm height up from the bottom of the tank. Inlet position 3 enters the tank in the same position as

inlet position 2 but protrudes into the tank before angling down at 45° directed toward the center of the tank, as shown in Figure 4.14.

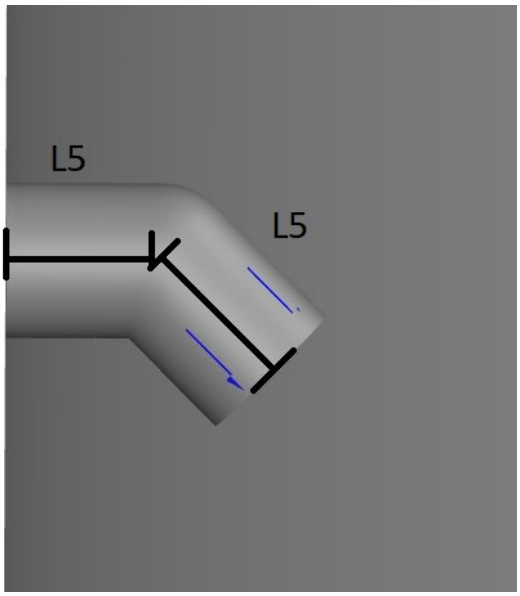

Figure 4.14. Detail of inlet with an angle 45° down (position 3) or angled down and to the left to create clockwise flow (position 4).

Inlet position 4 is similar to inlet position 3, but pipe section L5 shown in Figure 4.14 is angled 45° down and to the left, away from the inlet to potentially create a swirling effect on the tank floor.

The entire recirculatory pump loop was not modelled to reduce complexity and reduce simulation time, as behavior within the pump itself and adjacent piping was not the focus of the study. A flow rate of 10 gallons per minute was modelled using a mass flow inlet of 0.063 kg/s of water. This mass flow rate was suggested by Stella-Jones as a starting point for pump size, with the understanding that if no inlet positions were capable of proper agitation with this flow rate that other flow rates would be considered.

The average viscosity of MCA preservative solution was experimentally determined to be 1.6 centipoise, and this value was used for the fluid simulated. Fluid density was kept the same as water, with the difference in density in real world MCA solutions being accounted for by the total mass of particles in the simulation.

Particles were simulated to have a density of 4000 kg/m^3 to represent malachite (basic copper carbonate). This should reflect the actual situation as malachite was the majority of particles in the treating solution and is a listed component. Other copper oxides identified are not modelled as they are not meant to be in solutions. A particle diameter of 10 μm was used, as opposed to the 1 μm size of particles expected to be in solution. This was done as the terminal settling velocity of a 1 μm particle with the density of malachite falling in a liquid with the density of water and viscosity of 1.6 centipoise is 0.000001021526 m/s would take around 271.9 hours to settle one meter. This would consume a vast of computing capacity and take an extremely long time for this simulation. A 10 μm particle has a terminal velocity of 0.0001021526 m/s, taking approximately 2.719 hours to settle 1 m which would save computing time and equally simulate difference between agitated and non-agitated systems Moreover, any system capable of reducing the settling of 10 μm particles would be capable of suspending 1 μm particles. The velocity magnitude cutoff to be considered settled was thus chosen to be 0.0001 m/s, as this is slightly below the terminal settling velocity of 10 μm particles in the solution.

4.3.2 Mesh Independence Analysis

A mesh independence analysis was conducted as outlined in Section 3.4.2 in order to ensure the mesh size used had no effect on the simulated results. All mesh independence testing was conducted on the top inlet tank geometry mesh layout, with the settings used to generate this mesh being used for the other tank geometries. All meshes generated have a body of influence around the inlet with a more refined mesh, with a finer mesh and several boundary layers near the interface between the fluid and the tank. What differs is the max cell size and number of boundary layers, with finer meshes having tighter constraints. The number of mesh cells, area-averaged inlet pressure as well as the percent difference from the finest mesh run are shown in Table 4.13

Table 4.13. Results of mesh independence study.

	Mesh Cells	Area Average Inlet Pressure (Pa)	Difference from the Finest Mesh (%)
1 (Coarsest Mesh)	177396	78.570	1.651
2	1038891	76.700	-0.769
3 (Chosen Mesh)	1111472	77.538	0.316
4	1999845	77.501	0.268
5 (Finest Mesh)	4339681	77.294	0

Mesh 3 showed a very slight difference in area averaged inlet pressure at convergence with a quarter of the mesh cells used compared to the finest mesh considered (mesh 5). Mesh 3 showed a very slight difference in area averaged inlet pressure from meshes 4 and 5, demonstrating the solution obtained is independent of the mesh. As mesh 3 has a quarter of the cells, using this mesh will also be much more computationally efficient.

4.3.3 Settling in Uncirculated Tank

To establish a baseline rate of settling, determine the length of time to run simulations and compare to theoretical Stokes law values, a transient particle settling simulation was conducted with no recirculatory flow. Given that the 1000 particles modeled will have random positions at time = 0 in the simulation, the average particle height would be half the tank height of 6.096 m. So, approximately 500 particles would be over 3.048 m and 500 particles would be below this line. Based on the 2.719 m/hr predicted rate of settling for a 10 µm particle, it would take 8.15 hours for half of the particles to settle out. Therefore, 8 hours of settling were simulated. Table 4.14 shows the average height of all 1000 particles modelled, the number of particles within 1 mm of the tank floor, the number of particles with a velocity magnitude of 0.0001 m/s or less and the number of particles considered settled.

Table 4.14. Uncirculated tank particle settling data (1000 particles total).

Tank Layout	Average Particle Height (m)	Particles within 1 mm of tank floor	Particles with 0.0001 m/s or less Velocity Magnitude	Particles settled
Initial	2.9954	0	0	0
1 Hour	2.6405	66	66	66
2 Hours	2.3083	133	133	133
3 Hours	2.0003	192	192	192
4 Hours	1.7126	249	249	249
5 Hours	1.4465	310	310	310
6 Hours	1.2029	364	364	364
7 Hours	0.9846	440	440	440
8 Hours	0.7875	494	494	494

Initially, the average particle height is near the middle of the tank with no particles at the tank floor or with a velocity magnitude below 0.0001 m/s as expected, therefore no particles are settled. As time progresses, more and more particles settle out, leading to

494 particles being at rest at 8 hours, as expected. The increase in the number of particles settled and the decrease in average particle height over time can be seen in Figures 4.15 and 4.16 respectively. Figure 4.17 shows the final position of particles at the end of 8 hours of simulated settling.

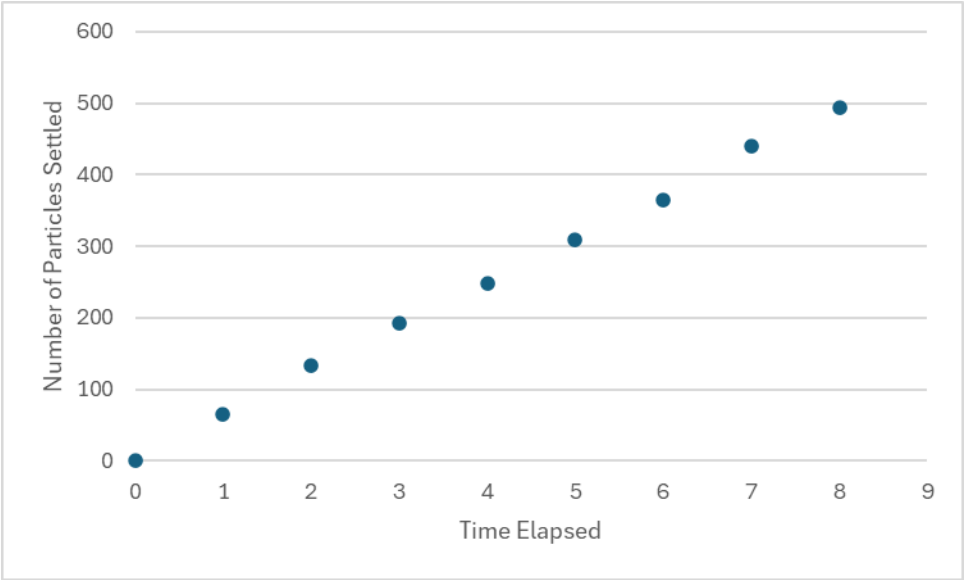

Figure 4.15. Number of particles settled with time in the uncirculated tank.

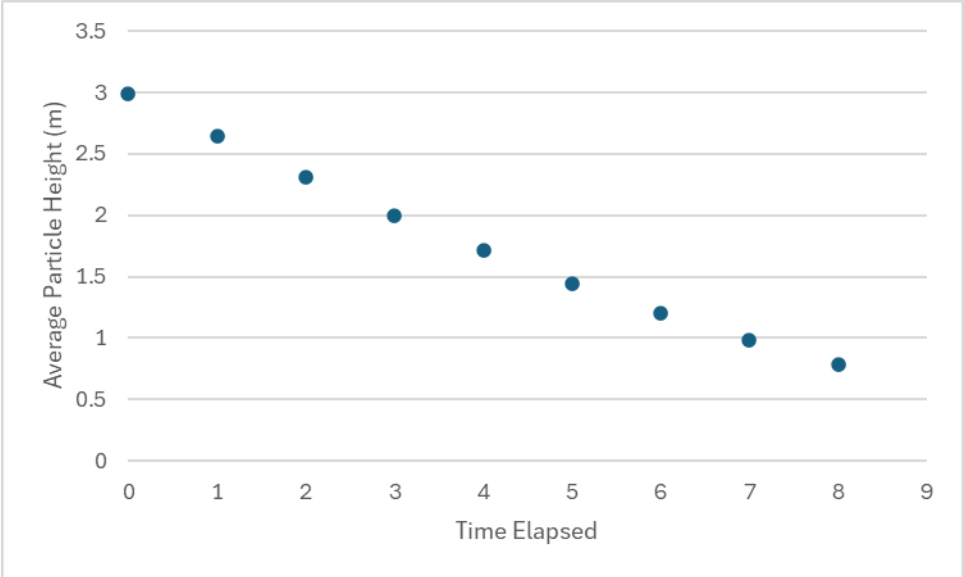

Figure 4.16. Average particle height with time in the uncirculated tank.

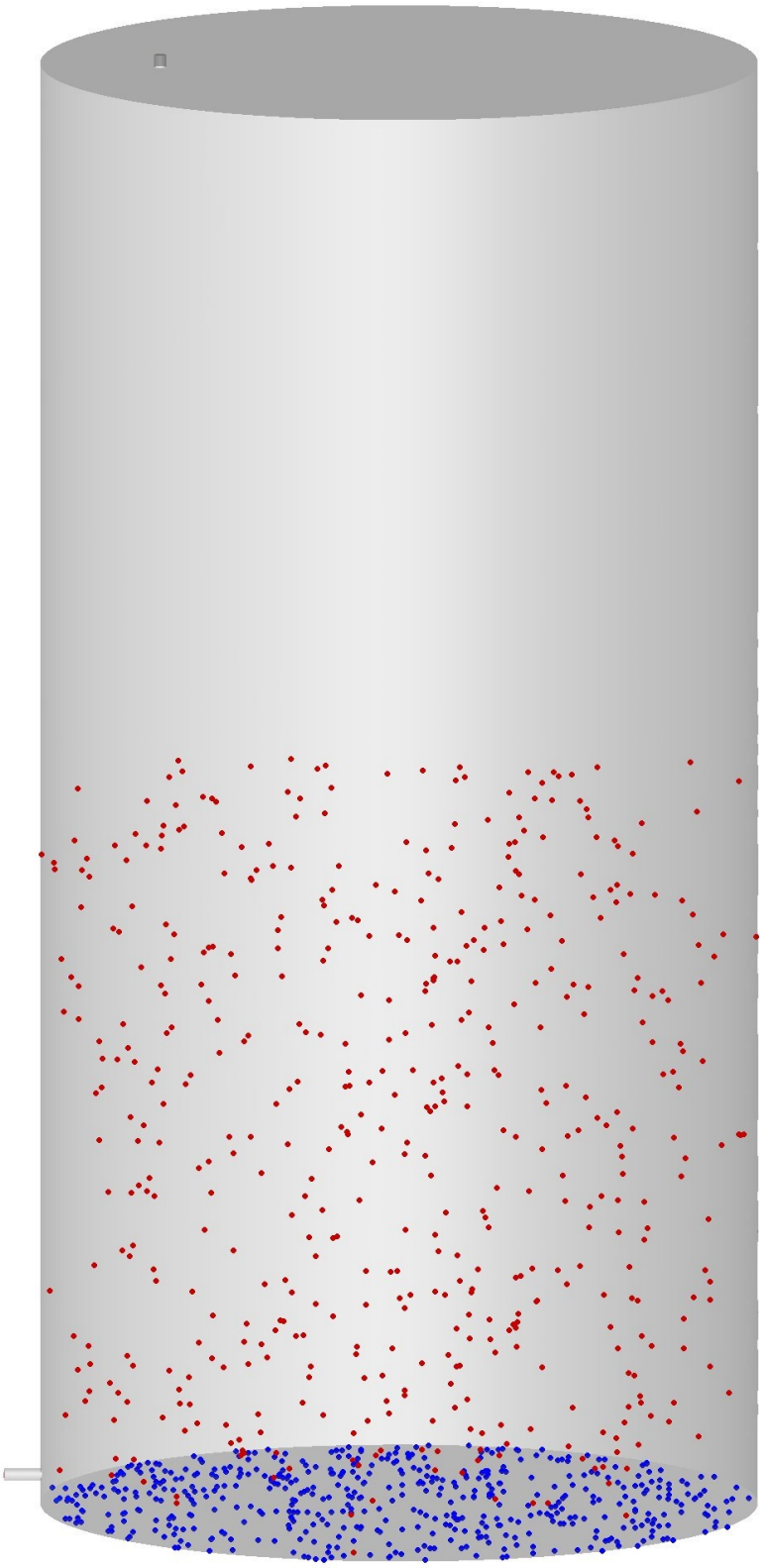

Figure 4.17. Final particle positions after 8 hours of settling in the uncirculated tank.

As mentioned in Section 4.3.1, the terminal settling velocity of a 10 µm particle is estimated to be 0.0001021526 m/s, according to Stokes Law of settling. The velocity of particles which were settling in the simulation was found to be 0.000102274 m/s. The simulated value is 0.116% higher than the theoretical but is considered acceptably close.

In summary, the settling model without recirculation was found to have a starting particle height and terminal settling velocities in line with expectations. The rate of settling and total number of particles settled per hour is also in line with expectations. It was verified that in 8 hours of simulated particle behaviour, approximately half of the particles settled out. Taking this as a benchmark, all simulations with recirculation will be run for 8 hours to allow a comparison of how particle settling rates differ from the baseline over this period.

4.3.4 Settling Comparison of Different Inlet Geometries

Each of the four inlet positions were modelled with a recirculatory flow rate of 10 GPM (6.3 kg/s) for 8 hours to observe the differences in particle settling. Tables 4.15 to 4.18 show the average height of all 1000 particles modelled, the number of particles within 1 mm of the tank floor, the number of particles with a velocity magnitude of 0.0001 m/s or less and the number of particles considered settled.

Table 4.15. Inlet Position 1 particle settling data (1000 particles total).

	Average Particle Height (m)	Particles within 1 mm of tank floor	Particles with 0.0001 m/s or less Velocity Magnitude	Particles settled
Initial	3.0587	0	0	0
1 Hour	2.7647	67	54	50
2 Hours	2.6797	130	87	84
3 Hours	2.5498	189	67	62
4 Hours	2.2157	242	171	165
5 Hours	2.1448	281	245	244
6 Hours	1.9615	317	299	299
7 Hours	1.9846	362	354	351
8 Hours	1.8554	392	384	381

Note: Particles slightly over the velocity magnitude were included if the particles had 0 y-velocity.

Table 4.16. Inlet Position 2 particle settling data (1000 particles total).

	Average Particle Height (m)	Particles within 1 mm of tank floor	Particles with 0.0001 m/s or less Velocity Magnitude	Particles settled
Initial	3.0713	0	0	0
1 Hour	2.8941	8	1	1
2 Hours	2.8178	21	0	0
3 Hours	2.5679	15	1	0
4 Hours	2.6520	15	0	0
5 Hours	2.7898	6	2	0
6 Hours	2.9603	13	1	0
7 Hours	3.0021	6	2	0
8 Hours	3.0196	21	0	0

Table 4.17. Inlet Position 3 Particle Settling Data (1000 particles total).

	Average Particle Height (m)	Particles within 1 mm of tank floor	Particles with 0.0001 m/s or less Velocity Magnitude	Particles settled
Initial	2.9882	0	1	0
1 Hour	3.0109	1	2	0
2 Hours	2.8537	1	1	0
3 Hours	3.0722	0	1	0
4 Hours	3.0507	1	0	0
5 Hours	3.0050	0	1	0
6 Hours	2.9882	0	0	0
7 Hours	2.9047	0	0	0
8 Hours	2.9865	1	1	0

Table 4.18. Inlet Position 4 particle settling data (1000 particles total).

	Average Particle Height (m)	Particles within 1 mm of tank floor	Particles with 0.0001 m/s or less Velocity Magnitude	Particles settled
Initial	3.1004	0	0	0
1 Hour	2.9777	8	1	0
2 Hours	2.9648	14	3	1
3 Hours	3.1591	19	16	15
4 Hours	3.1987	24	19	19
5 Hours	3.2470	25	21	20
6 Hours	3.2865	28	25	24
7 Hours	3.3199	24	25	24
8 Hours	3.2512	27	26	25

In the settling without agitation, the number of particles at the tank floor, particles with 0.0001 m/s or less velocity magnitude and the number of particles at rest were consistently the same. Given that the fluid is circulating, particles can be at the bottom of the tank but still moving and be able to resuspend, or momentarily have no velocity while being well off the tank floor and so each specific particle was checked to ensure it met both criteria to be considered settled. The velocity magnitude cutoff to be considered settled was chosen to be 0.0001 m/s, as this is slightly below the terminal settling velocity of particles in the solution. It was observed that for inlet position 1 that many particles were within 1 mm of the tank floor and had 0 y-velocity magnitude (vertical) but were slightly above the 0.0001 m/s cutoff for velocity magnitude as they were very slowly moving along the tank floor. For this specific inlet position, particles which were slightly over the velocity magnitude cutoff were also considered to be settled according to this slightly modified criterion. This was done as in real world environments a degree of roughness on the tank floor or the presence of material on the tank floor would stop these slowly moving particles. The DPM model boundary condition does not properly account

for this. The presence of a large number of particles so close to the velocity cutoff was only observed with inlet position 1.

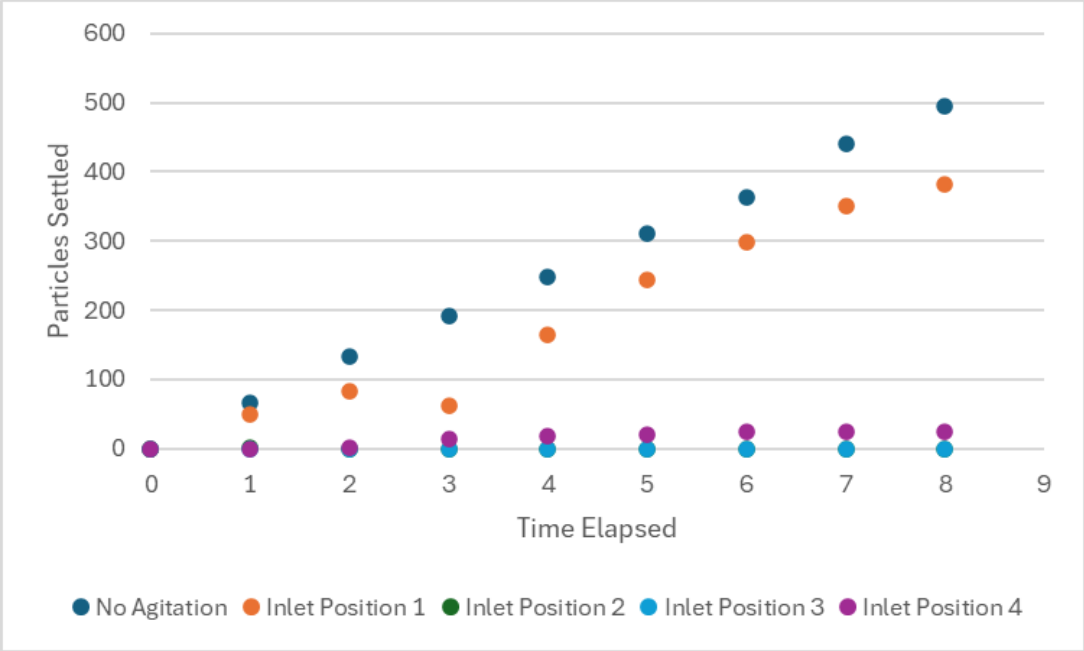

Figure 4.18. Number of particles settled with time for all inlet geometries.

Figure 4.19. Average particle height with time for all inlet geometries.

Looking at Figure 4.18, all inlet geometries have less particles settling out than the uncirculated tank. Inlet 1 (top of tank) exhibits the smallest degree of improvement compared to the tank with no agitation, having 381 instead of 494 particles settled out in 8 hours. This is less than a 25 % reduction in settling, giving the least improvement noted. The other 3 inlets modelled which enter the side wall of the tank 381 mm up all exhibited better reduction. Inlet position 4 (45 ° swirl) had 25 particles settled instead of 494, showing a 95% reduction in settled particles over 8 hours of agitation. Inlet positions 2 (straight in) and 3 (45 ° down) both completely prevented settling over 8 hours.

Another factor considered is the average particle heights over the duration of the simulation, shown in Figure 4.19. Again, all inlet positions showed an improvement over the uncirculated tank in terms of keeping the average particle height near the middle of the tank. This shows the benefit of agitation in maintaining particle suspension. Inlet position 1 (top of tank) again showed the smallest improvement compared to the tank without recirculation, with the average particle height steadily decreasing from the tank midpoint of 3 m to 1.85 m over 8 hours. The other inlet positions all maintained the average height of particles at approximately 3 m over 8 hours of recirculation, indicating that the particle dispersion is more uniform. Average particle heights did fluctuate slightly over the course of the 8 hours simulated, with inlet position 2 (straight in) showing a decrease to 2.5 m at hour 3 before recovering. This greater height deviation is less desirable and as a result, inlet positions 3 (45 ° down) and 4 (45 ° swirl) showcased the best results. Figure 4.20 shows the final height of particles after 8 hours of simulated recirculatory agitation for a visualization of the solutions.

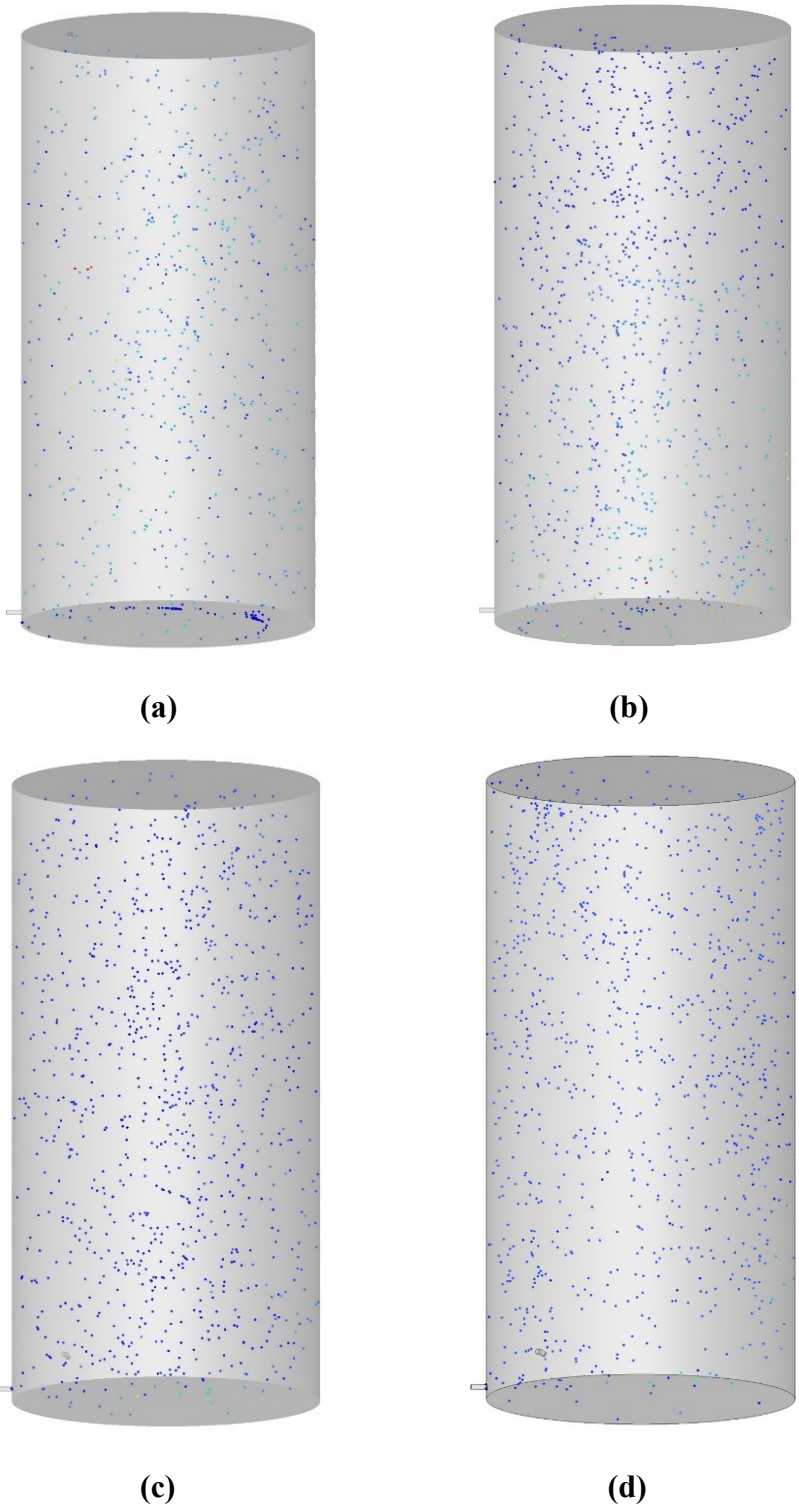

Figure 4.20. Final particle positions after 8 hours of simulation.

(a) inlet position 1; (b) inlet position 2; (c) inlet position 3; (d) inlet position 4

Inlet position 1 (top inlet) in Figure 4.20 clearly shows several particles at rest and fewer particles in the upper regions of the tank. Inlet position 2 (straight in) has no particles settled and maintains average particle height reasonably well but clearly shows areas with higher particle density near the bottom of the tank. Inlet position 3 (45 ° down) shows a good particle dispersion through the tank volume with no increased density of particles near the bottom of the tank. Inlet position 4 (45 ° swirl) appears to have a higher concentration of particles in the top portion of the tank, also has settled particles on the tank floor. The intent of inlet position 4 (45 ° swirl) was to create a swirling flow along the floor of the tank to provide better suspension, but this appears to have created dead zones on the tank floor where particles come to rest. As this is not present in inlet position 3 (45 ° down), this appears to be the superior inlet position by all metrics.

In summary, all four recirculatory designs simulated in this work are superior to uncirculated flow to prevent particles settling. The quantity of particles settling out over 8 hours was improved in all inlet position cases trialed with a flow rate of 10 GPM (0.063 kg/s). The best inlet position was found to be inlet position 3 (45 ° down), which was able to keep all particles from settling out and the average height of particles suspended uniformly over 8 hours. The worst inlet position was inlet position 1 (top inlet), which only decreased the rate of settling by 25 % while also requiring more complex installation. A system to recirculate fluid in MCA storage tanks is recommended to prevent settling during time periods where the fluid is not in use.

5.0 Conclusion

The overall objective of this study was to evaluate the causes and prevent sedimentation in the storage tanks of the wood preservative, micronized copper azole. To achieve this overall objective, the research was divided into three main components including an evaluation of how current wood treating conditions affect solution particles, the chemical composition of solution particles over 1 µm, and how adding a recirculation system to the existing storage tanks at Stella Jones may influence settling in treating solutions. Based on the completed experimental studies and computational simulations, several conclusions are made.

The first objective of this study involved investigating the effects of wood treating parameters (temperature, pressure, and vacuum) on the particle size of the stressed MCA treating solution in a pilot scale plant. Stressed samples were analyzed for copper concentration before and after passing through a 1 µm filter to determine if a significant reduction occurred compared to an unstressed baseline. The results indicated that there was no significant change in copper concentration from stressors of pressure, vacuum, and wood. However, when elevated temperatures were applied to the MCA solution, a notable change in copper concentration post-filtration was noticed, although less severe than what is observed in full scale operations at Stella-Jones facilities.

The second objective of this study was to identify the composition of particles over 1 µm that formed in stressed treating solutions. Analysis was conducted using SEM-EDS as well as XRD. The SEM-EDS analysis identified that copper containing particles could not only be larger malachite particles (a listed ingredient) as the atomic balance did not

support this. XRD analysis confirmed the presence of malachite as well as copper oxides composed the larger particles identified.

The third objective of study was to evaluate several possible inlet locations for a recirculatory piping system using CFD analysis to determine if particles could be better suspended over time. This was conducted by simulating the settling of particles for 8 hours with no recirculation, comparatively with 10 GPM of flow with 4 different inlet geometries. The results indicated that over the timespan where half of the particles would settle out in a flow with no recirculation, an inlet near the tank floor angled 45 ° downward would best prevent particle settling.

Based on the results presented in this thesis, several factors related to the sedimentation in MCA preservative storage tanks have been identified. Firstly, exposing the preservative to elevated temperatures leads to the formation of larger copper containing particles, resulting in increased sedimentation and decreased preservative efficacy. Secondly, larger particles in solution were identified to be malachite as expected, but also copper oxides indicating possible raw material inconsistencies or an unidentified reaction process, this requires future research. Lastly, according to CFD modelling the preservative particle settling issue in holding tanks can be reduced with a retrofit of a recirculatory system to the existing infrastructure at Stella-Jones.

References

Adamczyk, Klimanek, A., Białecki, R. A., Węcel, G., Kozołub, P., & Czakiert, T. (2014). Comparison of the standard Euler-Euler and hybrid Euler-Lagrange approaches for modeling particle transport in a pilot-scale circulating fluidized bed. *Particuology*, *15*(4), 129–137. https://doi.org/10.1016/j.partic.2013.06.008

American Wood Protection Association. (2022). *2022 AWPA Book of Standards*. Birmingham, Alabama.

Anderson, J. (1995). *Computational fluid dynamics : The basics with applications* (McGraw-Hill series in mechanical engineering). New York ; Montreal: McGraw-Hill.

Andrews, & O'Rourke, P. J. (1996). The multiphase particle-in-cell (MP-PIC) method for dense particulate flows. *International Journal of Multiphase Flow*, *22*(2), 379–402. https://doi.org/10.1016/0301-9322(95)00072-0

ANSYS, Inc. (2023). Ansys® Academic Research Fluent, Release 2023.1, Help System, Fluent Theory Guide, ANSYS, Inc.

Brashaw, B., & Bergman, R. (2021). Wood as a Renewable and Sustainable Resource. Wood handbook-wood as an engineering material. Forest Products Laboratory.

Biswas, R., Saha, D., & Bandyopadhyay, R. (2021). Quantifying the destructuring of a thixotropic colloidal suspension using falling ball viscometry. Physics of Fluids, 33(1).

Chhabra, & Basavaraj, M. G. (2019). *Coulson & Richardson's chemical engineering. Vol. 2a, Particulate systems and particle technology* (Chhabra & M. G. Basavaraj, Eds.; 6th edition.). Butterworth-Heinemann.

Civardi, Schubert, M., Fey, A., Wick, P., & Schwarze, F. W. M. R. (2015). Micronized Copper Wood Preservatives: Efficacy of Ion, Nano, and Bulk Copper against the Brown Rot Fungus Rhodonia placenta. *PloS One*, *10*(11), e0142578–e0142578. https://doi.org/10.1371/journal.pone.0142578

CORNER, S. (2024). Statistics Corner: Analysis of Variance. Statistics, 58(01).

Canadian Standards Association [CSA]. (2021). CAN/CSA – 080-Series 15. Wood Preservation.

Dey, S., Zeeshan Ali, S., & Padhi, E. (2019). Terminal fall velocity: The legacy of Stokes from the perspective of fluvial hydraulics. *Proceedings of the Royal Society. A, Mathematical, Physical, and Engineering Sciences, 475*(2228), 20190277.

Environment Canada. (2013). *Recommendations for the Design and Operation of Wood Preservation Facilities, 2013: Technical Recommendations Document.*

Freeman, & McIntyre, C. R. (2008). A Comprehensive Review of Copper-Based Wood Preservatives. *Forest Products Journal*, *58*(11), 6–27.

Gates-Rector, S., & Blanton, T. (2019). The Powder Diffraction File: a quality materials characterization database. *Powder Diffraction*, *34*(4), 352–360. https://doi.org/10.1017/S0885715619000812

Gerstein, B., & Zaccaria, D. (2004). Banned but not forgotten—An overview of CCA litigation past, present, and future. Environmental Claims Journal, 16(1), 17-40.

Goldstein, J. I., Newbury, D. E., Michael, J. R., Ritchie, N. W., Scott, J. H. J., & Joy, D. C. (2017). *Scanning electron microscopy and X-ray microanalysis*. springer.

Hamdan, Sebastia-Saez, D., Hamdan, M., & Arellano-Garcia, H. (2020). CFD Analysis of the Use of Desert Sand as Thermal Energy Storage Medium in a Solar Powered Fluidised Bed Harvesting Unit. In *Computer Aided Chemical Engineering* (Vol. 48, pp. 349–354). https://doi.org/10.1016/B978-0-12-823377-1.50059-8

Hibbeler. (2018). *Fluid mechanics* (Second edition.). Pearson.

Hitachi High-Tech Analytical Science. (2017). *APPLICATION NOTE-15*[Brochure]. https://hha.hitachi-hightech.com/assets/uploads/assets/uploads/documents/Brochure_LAB_X5000_for_wood_treatment.pdf (Date accessed February 20, 2024).

King, P. (2014). *Sludge control in copper chrome arsenic (CCA) wood preservatives.* [Master's Thesis, University of Melbourne]. http://hdl.handle.net/11343/50197

Klein, C., Dutrow, Barbara., Dana, J. D., & Klein, C. (2008). *The 23rd edition of the manual of mineral science : (after James D. Dana)* (23rd ed.). J. Wiley.

Morais, S., Fonseca, H. M. A. C., Oliveira, S. M. R., Oliveira, H., Gupta, V. K., Sharma, B., & de Lourdes Pereira, M. (2021). Environmental and Health Hazards of Chromated Copper Arsenate-Treated Wood: A Review. *International Journal of Environmental Research and Public Health*, *18*(11), 5518-. https://doi.org/10.3390/ijerph18115518

Muttenthaler, & Manhartsgruber, B. (2020). Euler–Lagrange CFD simulation and experiments on accumulation and resuspension of particles in hydraulic reservoirs. *Journal of the Brazilian Society of Mechanical Sciences and Engineering*, 42(4). https://doi.org/10.1007/s40430-020-02292-8

Newbury, D. E. (2004). Assessing Charging Effects on Spectral Quality for X-ray Microanalysis in Low Voltage and Variable Pressure/Environmental Scanning Electron Microscopy. *Microscopy and Microanalysis*, *10*(6), 739–744. https://doi.org/10.1017/S143192760404070X

Ochieng, A., & Onyango, M. (2010). CFD simulation of solids suspension in stirred tanks: Review. *Hemijska Industrija, 64*(5), 365-374.

Consumer Safety and Product Performance of Micronized Copper Technology Confirmed. (2009). PR Newswire Association LLC.

Rouessac, & Rouessac, A. (2007). *Chemical analysis modern instrumentation methods and techniques* (2nd ed.). John Wiley.

Saidi, Rismanian, M., Monjezi, M., Zendehbad, M., & Fatehiboroujeni, S. (2014). Comparison between Lagrangian and Eulerian approaches in predicting motion of micron-sized particles in laminar flows. Atmospheric Environment (1994), 89, 199–206. https://doi.org/10.1016/j.atmosenv.2014.01.069

Sariyerli, G., Sakarya, O., & Akcadag, U. (2018). Comparison tests for the determination of the viscosity values of reference liquids by capillary viscometers and stabinger viscometer SVM 3001. *International Journal of Metrology and Quality Engineering, 9*, 7.

Scholz, M. (2016). *Wetland for water pollution control* (Second edition.). Elsevier

Shi, & Rzehak, R. (2020). Solid-liquid flow in stirred tanks: Euler-Euler/RANS modeling. *Chemical Engineering Science*, *227*, 115875–. https://doi.org/10.1016/j.ces.2020.115875

Shultz, T., Nicholas, D. (2011). Chemical Wood Preservative Systems in North America. In Morrell, J., Brooks, K, Davis, C. (Eds). (2011). *Managing Treated Wood in the Aquatic Environment*. Forest Products Society

Tarpagkou, & Pantokratoras, A. (2013). CFD methodology for sedimentation tanks: The effect of secondary phase on fluid phase using DPM coupled calculations. *Applied Mathematical Modelling*, *37*(5), 3478–3494. https://doi.org/10.1016/j.apm.2012.08.011

Timber Specialties, "Quick Reference Chart for Production of MCA Pressure Treated Wood for Canadian Species", [Print]; Koppers, Timber Specialties, Campbellville, Ontario, Issued October 2019.

West, R. M. (2021). Best practice in statistics: Use the Welch t-test when testing the difference between two groups. Annals of clinical biochemistry, 58(4), 267-269.

287-TIM-E, MicroPro 200C-TS, [Print]; Timber Specialties, Campbellville, Ontario, Issued 2016, Revised 2019.

288-TIM-E, MicroShades Natural Brown, [Print]; Koppers, Timber Specialties, Campbellville, Ontario, Issued 2016, Revised 2021.

Appendix A: SEM-EDS Data

Table A.1. Average atomic percent data for all sub-samples.

Sample Name	Sample ID	Carbon Atomic (%)	Oxygen Atomic (%)	Copper Atomic (%)	Iron Atomic (%)
Stock Solution	TSD1-1	25.85	38.82	31.23	4.1
	TSD1-2	30.84	46.8	19.62	2.76
	TSD1-3	27.94	46.64	22.42	3.02
Temp 50°C	50C2-1	26.9	48.35	21.98	2.775
	50C2-2	28.22	51.26	17.68	2.42
	50C2-3	29.82	50.44	17.1	2.26
Temp 75°C	75C2-1	32.02	45.45	20.4	2.2
	75C2-2	27.74	50.64	19.54	2.06
	75C2-3	9.58	64.58	23.08	2.74
Stock Solution	SD2-1	30.05	46.25	20.68	3
	SD2-2	30.68	45.14	19.8	2.92
	SD2-3	32.25	46.925	17.05	2.525
Press Temp & Vac	PTV3-1	28.32	45.9	22.55	3.2
	PTV3-2	32.1	43.55	20.82	2.95
	PTV3-3	29.64	43.7	22.54	3.2
Stock Solution	SW3-1	28.48	42.3	24.98	3.54
	SW3-2	30.3	48.5	18.53	2.7
	SW3-3	30.66	47.98	18.36	2.6
Kiln Dried Wood Charge 3	KD3-1	33.08	38.16	24.7	3.58
	KD3-2	30.24	49.58	17.42	2.34
	KD3-3	26.88	46.72	22.95	3.425
Undried Wood Charge 3	UD3-1	31.52	44.96	19.74	3
	UD3-2	29.525	39.05	26.55	3.825
	UD3-3	32.95	43.1	20.05	2.875
Gormley 0.5% Work Solution	GRM.5-1	30.4	45.06	20.28	3.58
	GRM.5-2	30.88	43.22	21.06	3.78
	GRM.5-3	24.87	34.6	33.5	5.83

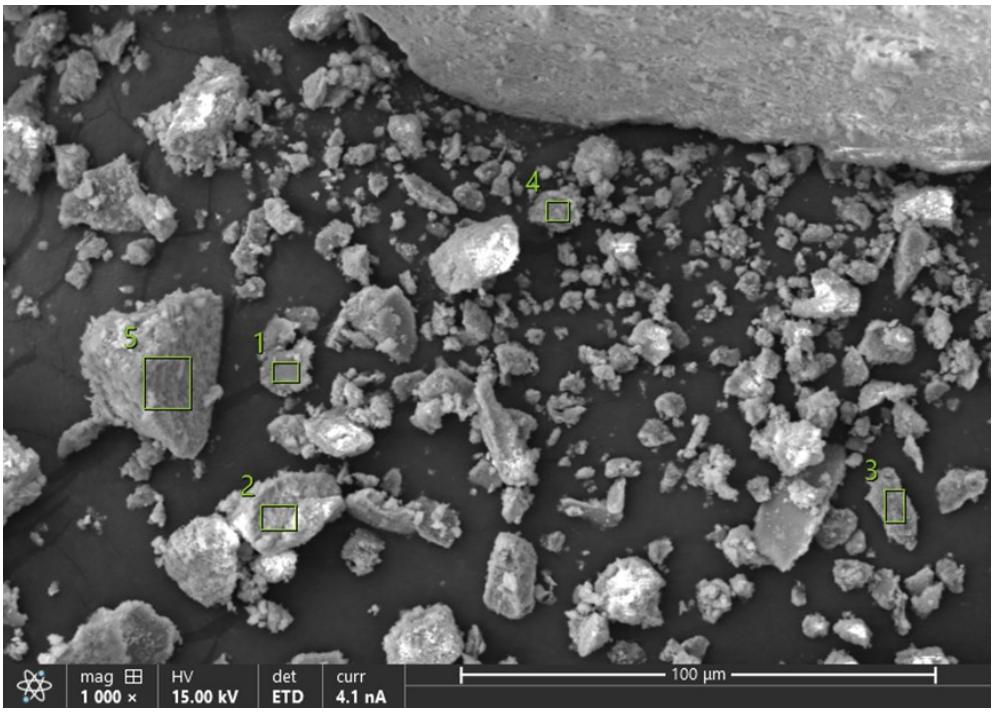

Figure A.1. SEM image capture of particles filtered from stock solution sample (TSD1) Area 1 with areas scanned using EDS analysis highlighted in numbered boxes.

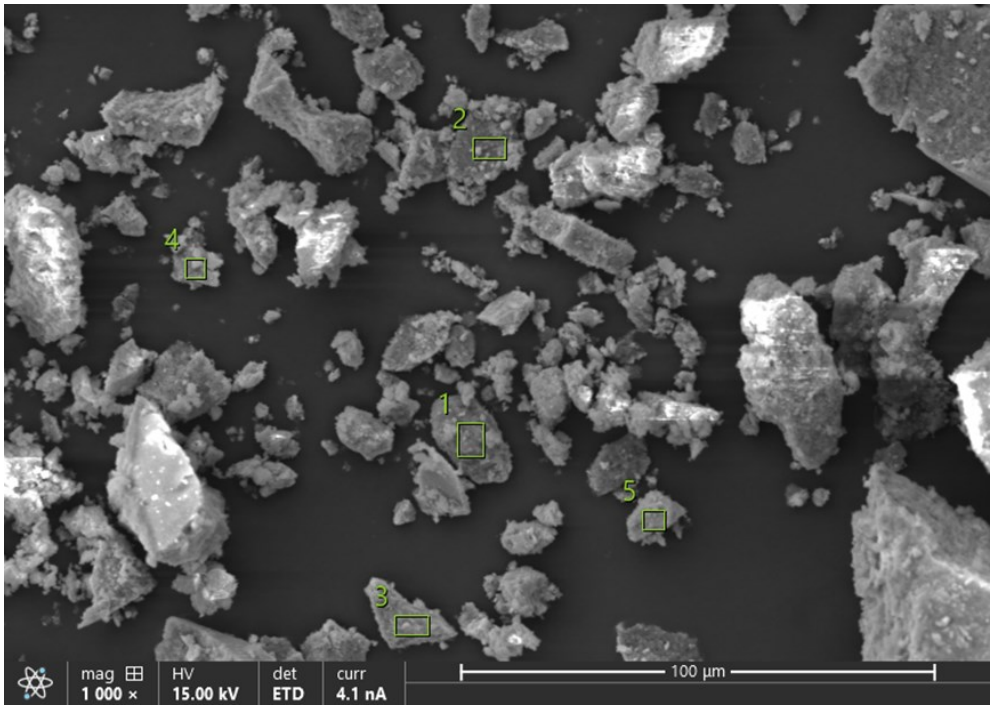

Figure A.2. SEM image capture of particles filtered from stock solution sample (TSD1) Area 2 with areas scanned using EDS analysis highlighted in numbered boxes.

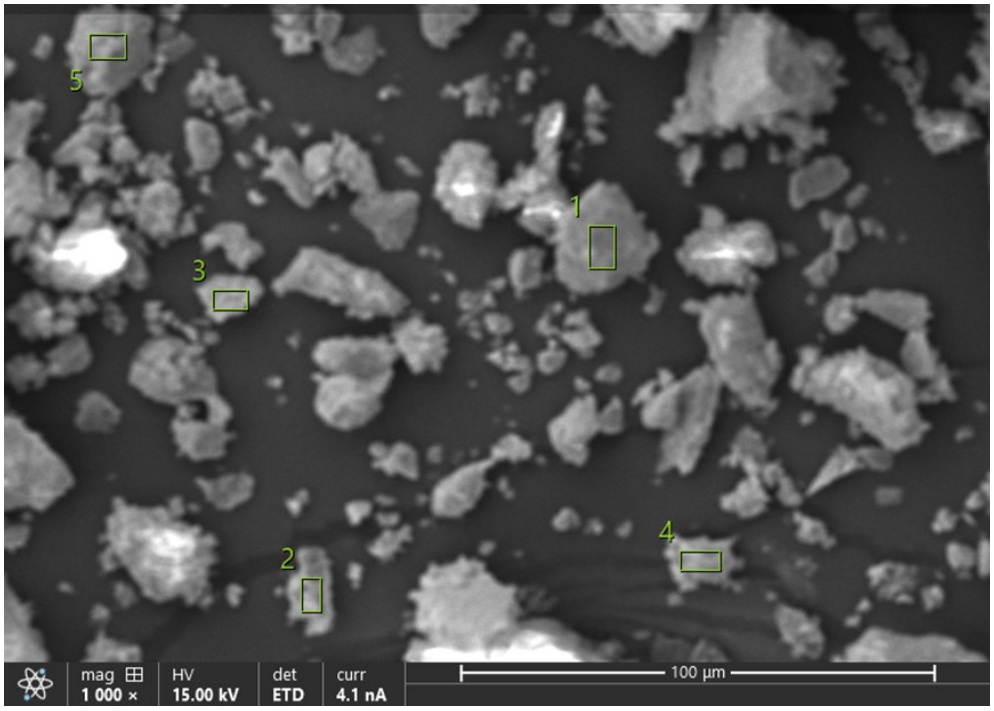

Figure A.3. SEM image capture of particles filtered from stock solution sample (TSD1) Area 3 with areas scanned using EDS analysis highlighted in numbered boxes.

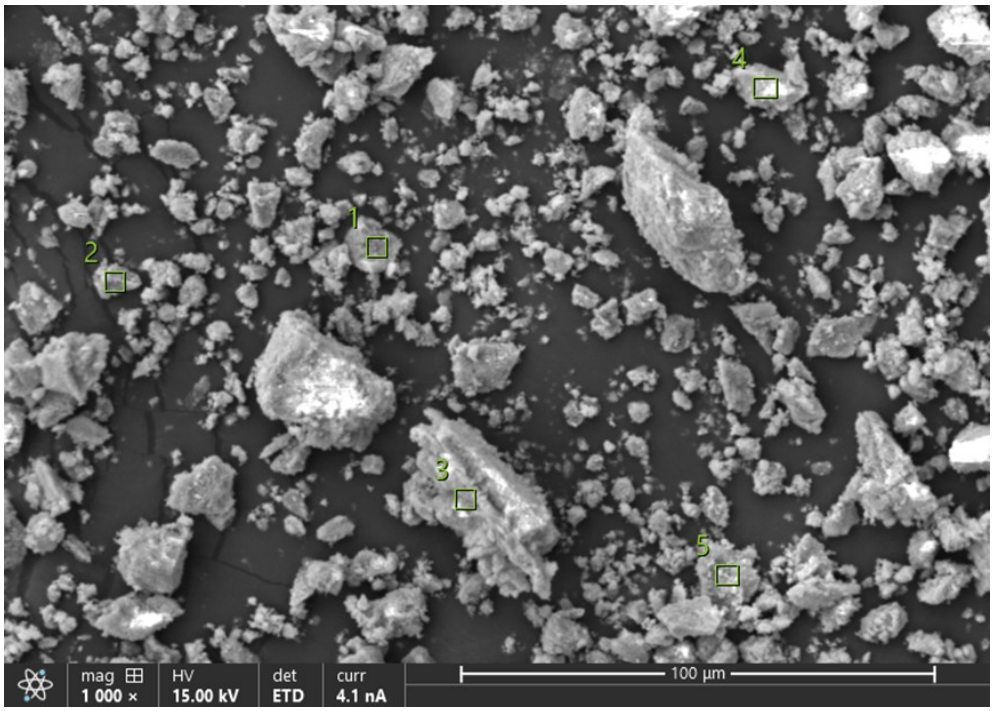

Figure A.4. SEM image capture of particles filtered from solution sample (50C2) Area 1 with areas scanned using EDS analysis highlighted in numbered boxes.

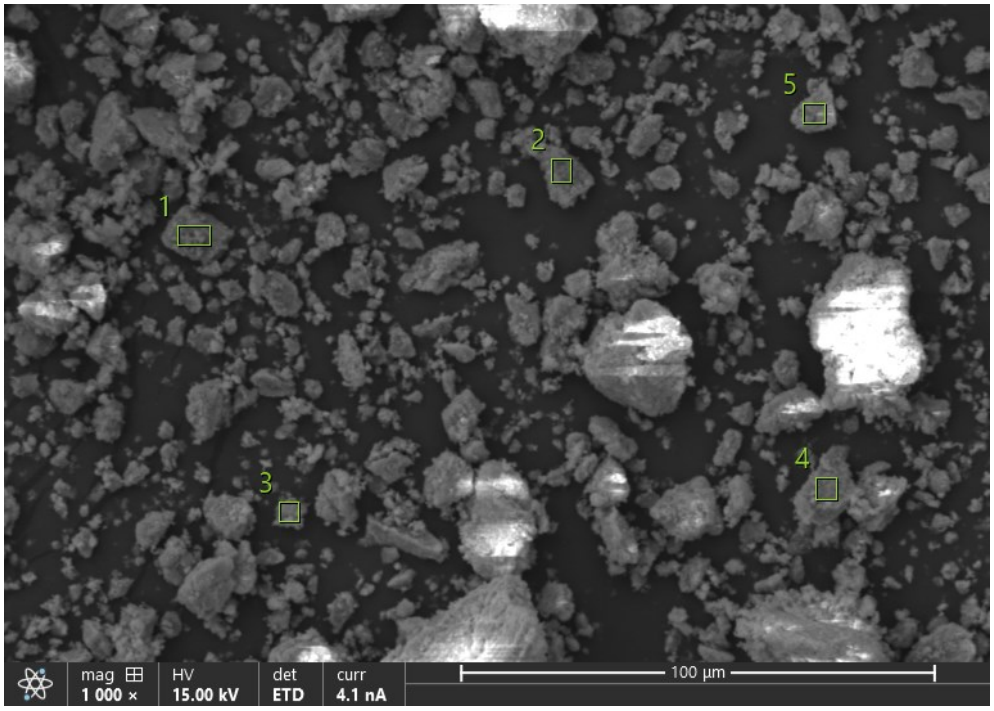

Figure A.5. SEM image capture of particles filtered from solution sample (50C2) Area 2 with areas scanned using EDS analysis highlighted in numbered boxes.

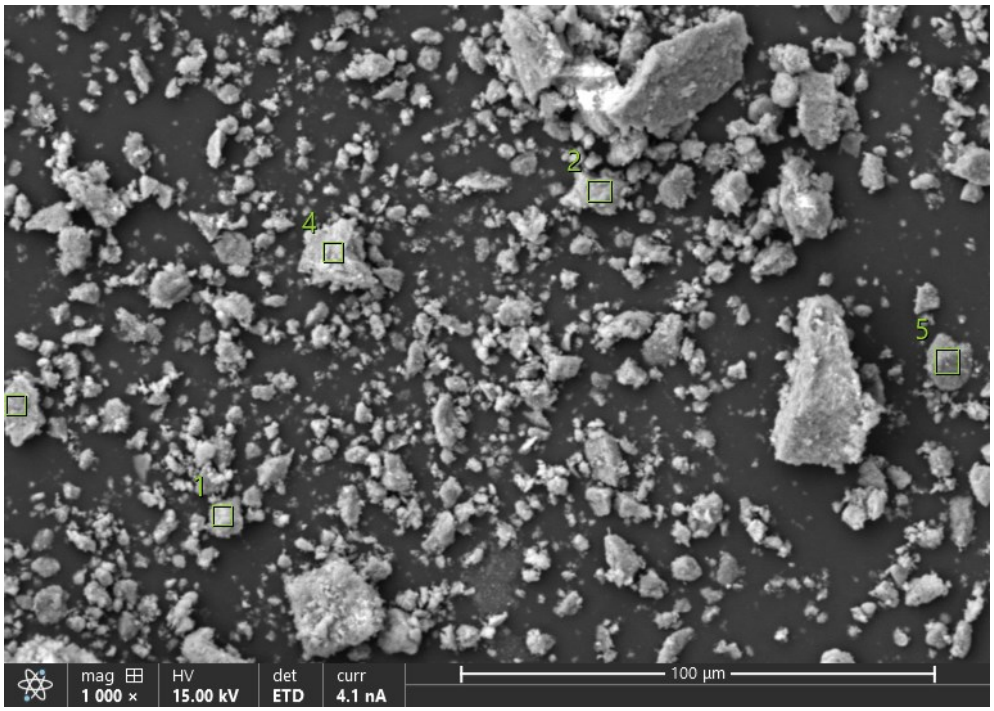

Figure A.6. SEM image capture of particles filtered from solution sample (50C2) Area 3 with areas scanned using EDS analysis highlighted in numbered boxes.

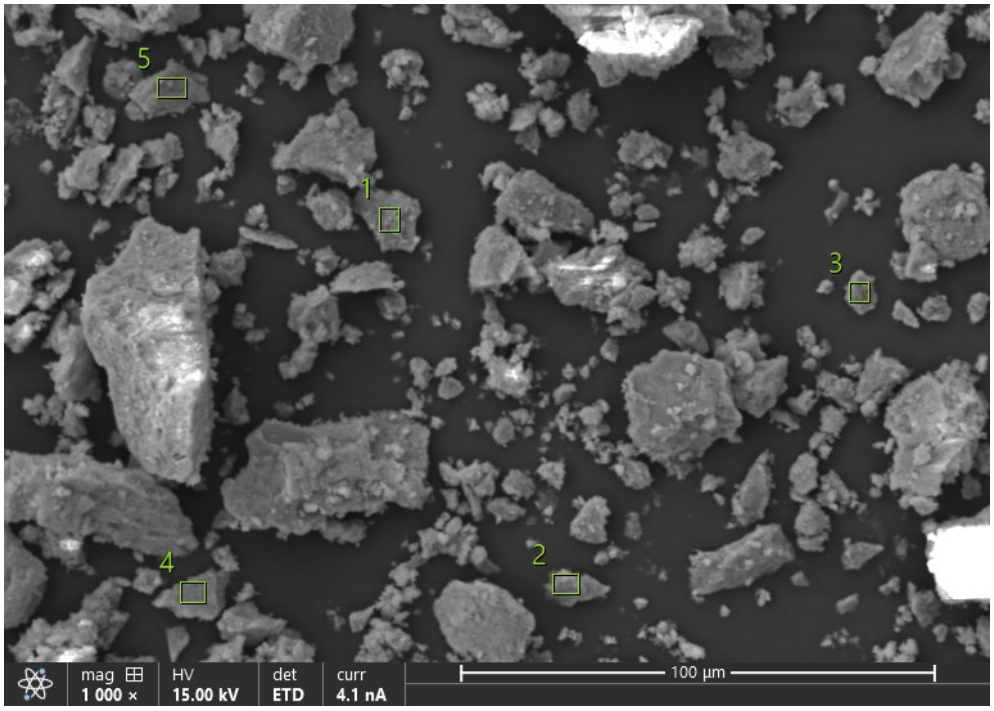

Figure A.7. SEM image capture of particles filtered from solution sample (75C2) Area 1 with areas scanned using EDS analysis highlighted in numbered boxes.

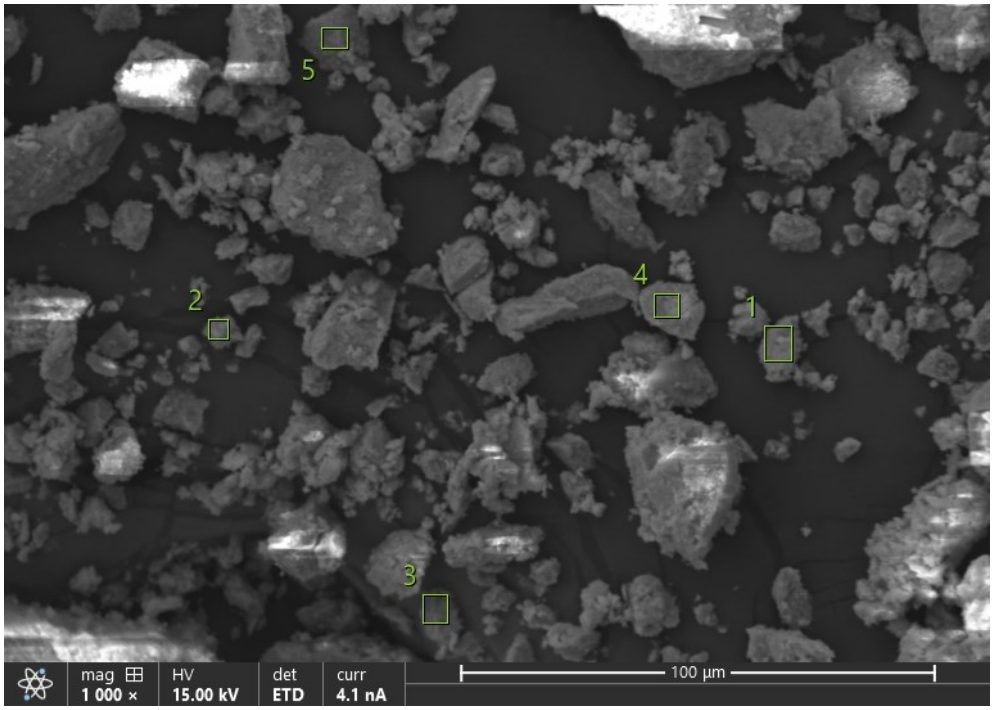

Figure A.8. SEM image capture of particles filtered from solution sample (75C2) Area 2 with areas scanned using EDS analysis highlighted in numbered boxes.

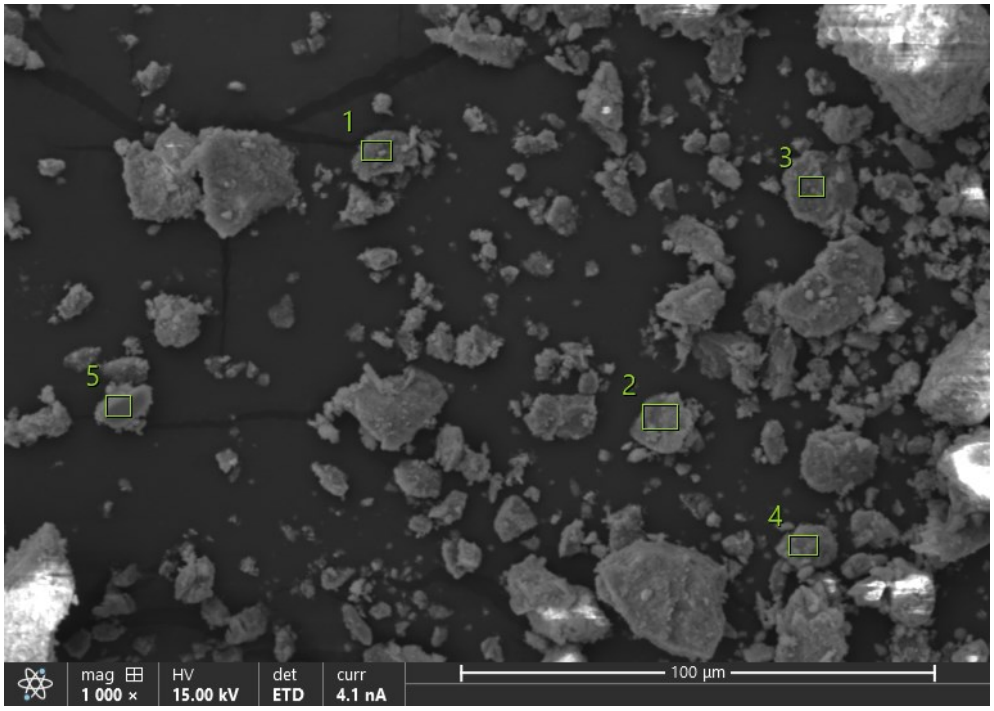

Figure A.9. SEM image capture of particles filtered from solution sample (75C2) Area 3 with areas scanned using EDS analysis highlighted in numbered boxes.

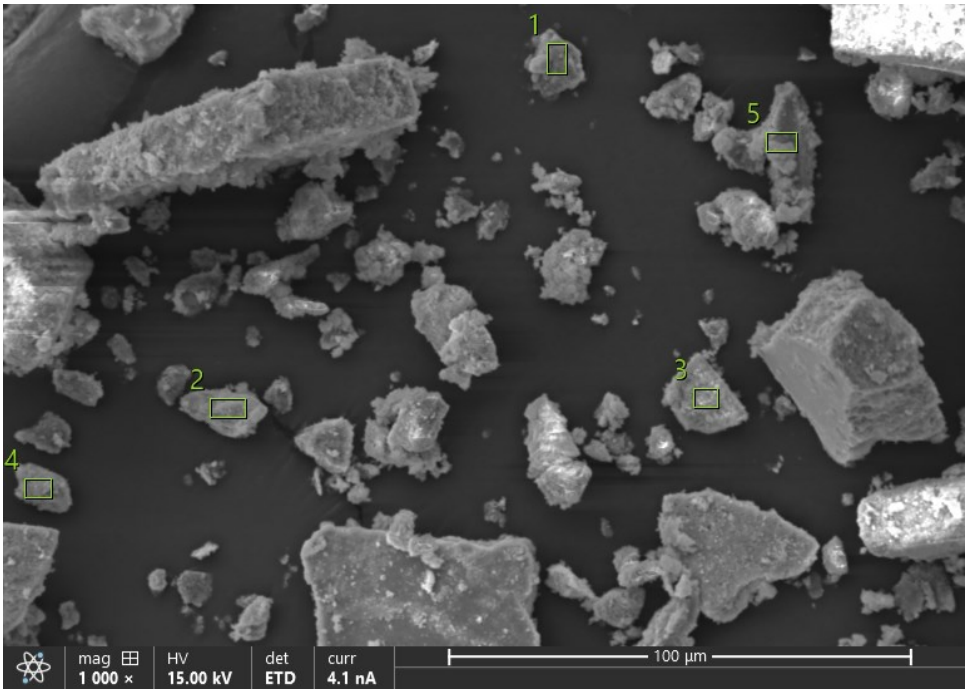

Figure A.10. SEM image capture of particles filtered from stock solution sample (SD2) Area 1 with areas scanned using EDS analysis highlighted in numbered boxes.

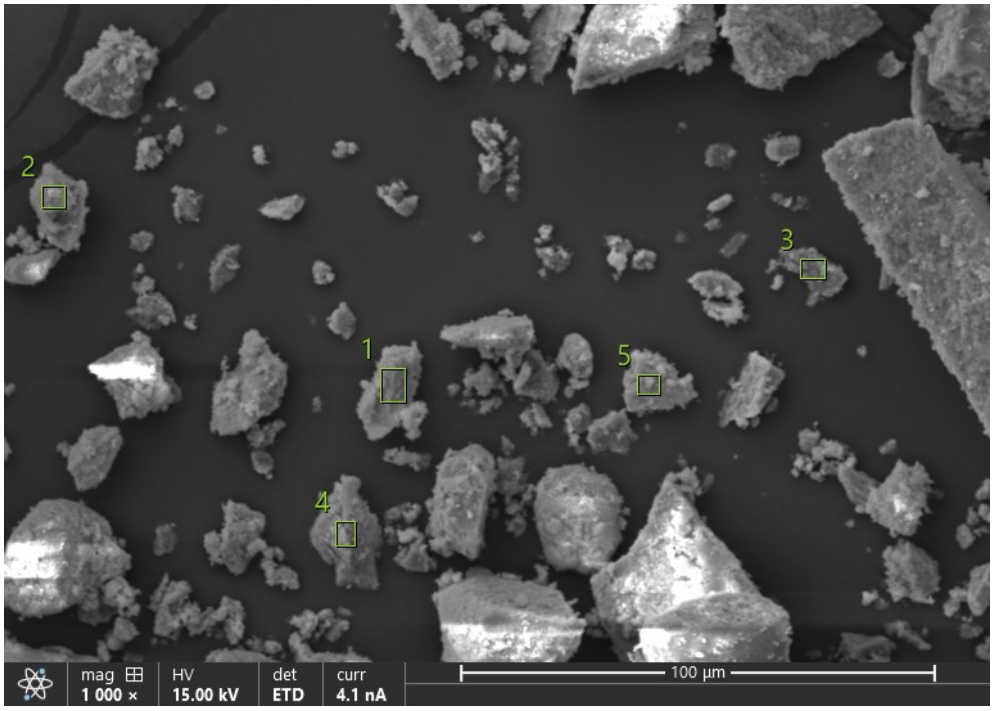

Figure A.11. SEM image capture of particles filtered from stock solution sample (SD2) Area 2 with areas scanned using EDS analysis highlighted in numbered boxes.

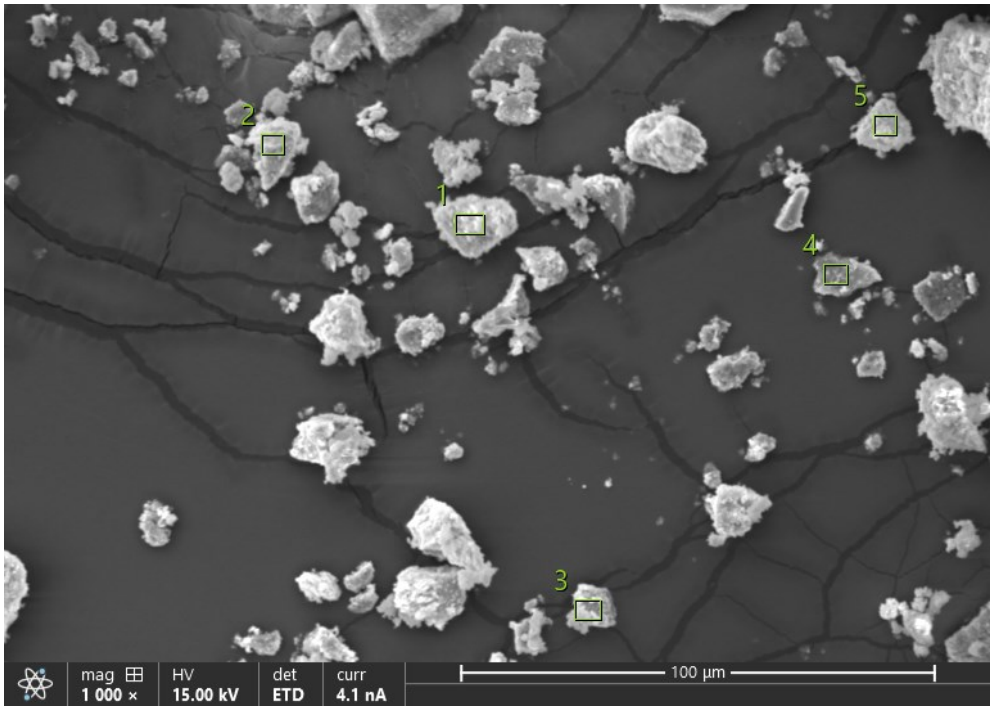

Figure A.12. SEM image capture of particles filtered from stock solution sample (SD2) Area 3 with areas scanned using EDS analysis highlighted in numbered boxes.

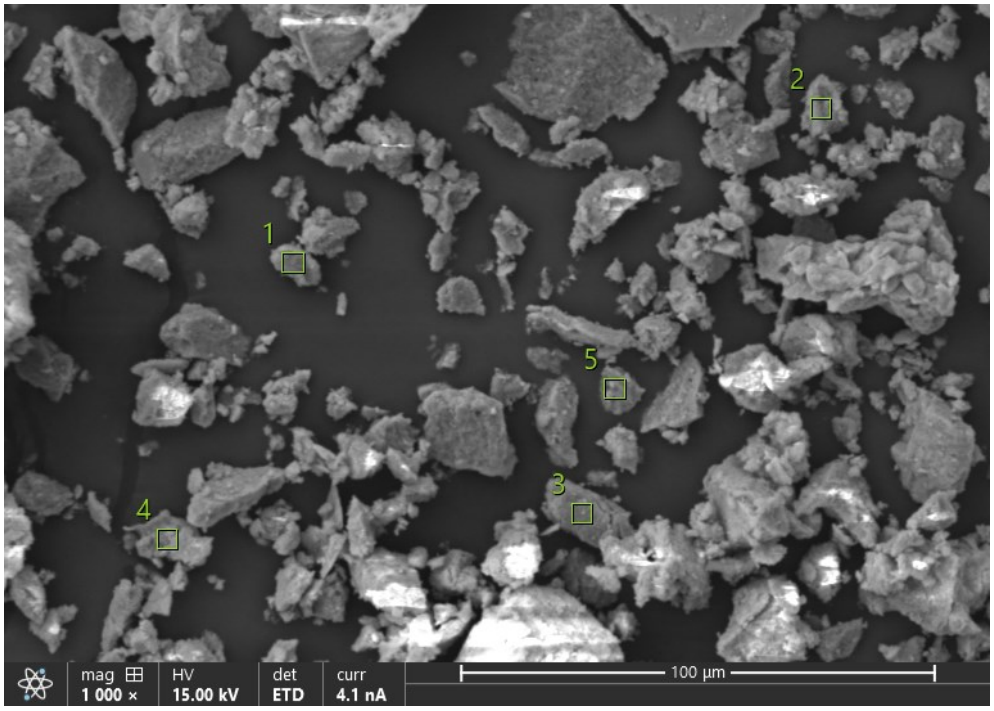

Figure A.13. SEM image capture of particles filtered from solution sample (PTV3) Area 1 with areas scanned using EDS analysis highlighted in numbered boxes.

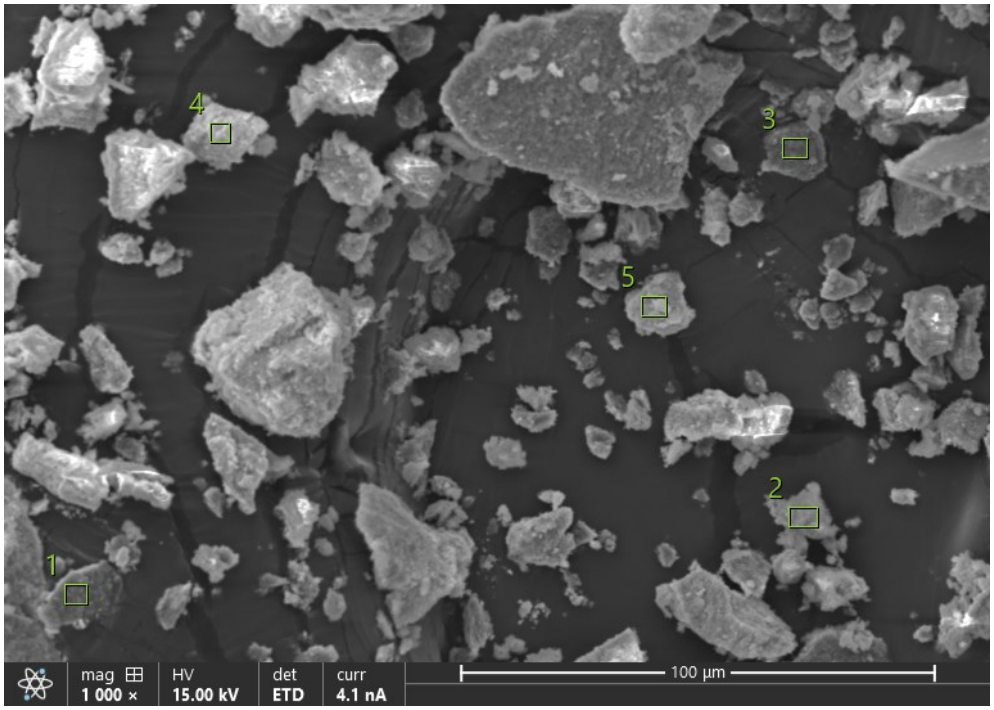

Figure A.14. SEM image capture of particles filtered from solution sample (PTV3) Area 2 with areas scanned using EDS analysis highlighted in numbered boxes.

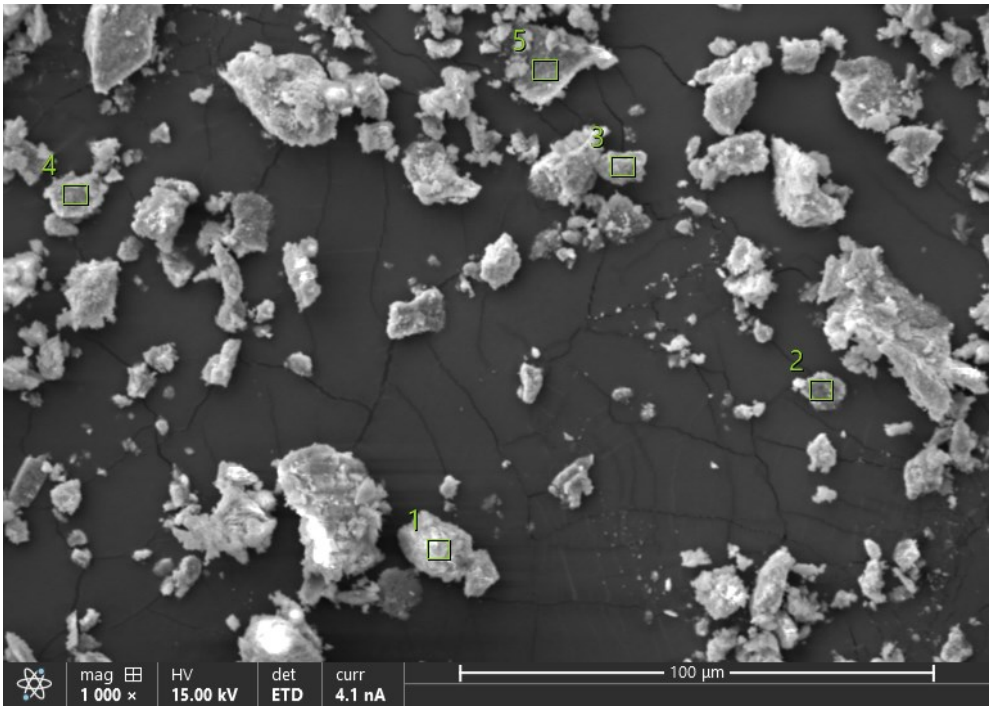

Figure A.15. SEM image capture of particles filtered from solution sample (PTV3) Area 3 with areas scanned using EDS analysis highlighted in numbered boxes.

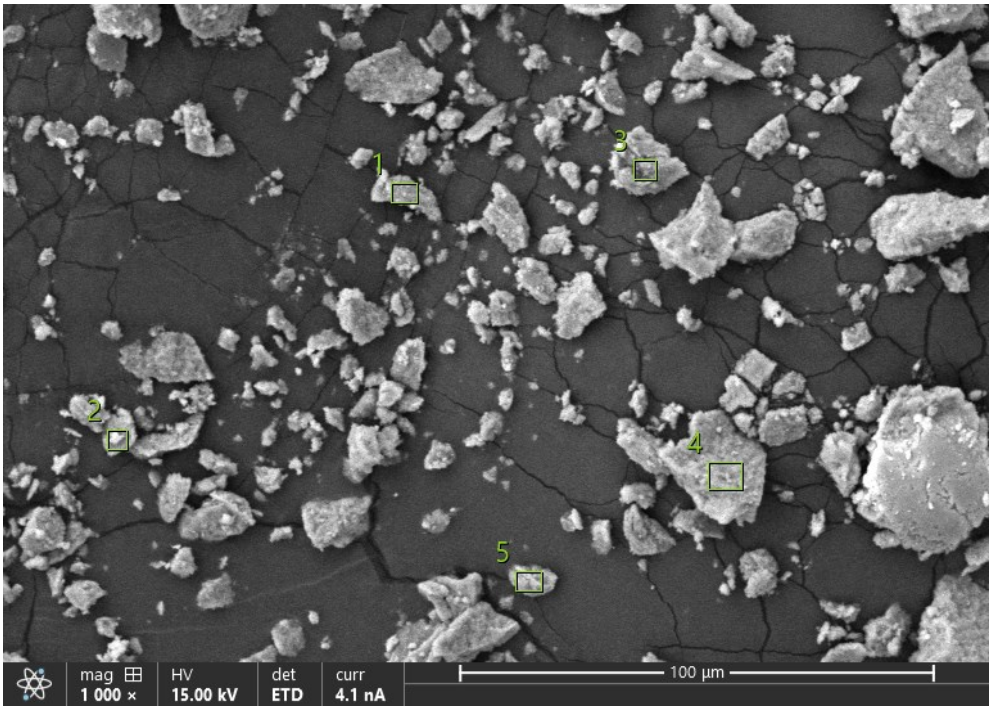

Figure A.16. SEM image capture of particles filtered from stock solution sample (SW3) Area 1 with areas scanned using EDS analysis highlighted in numbered boxes.

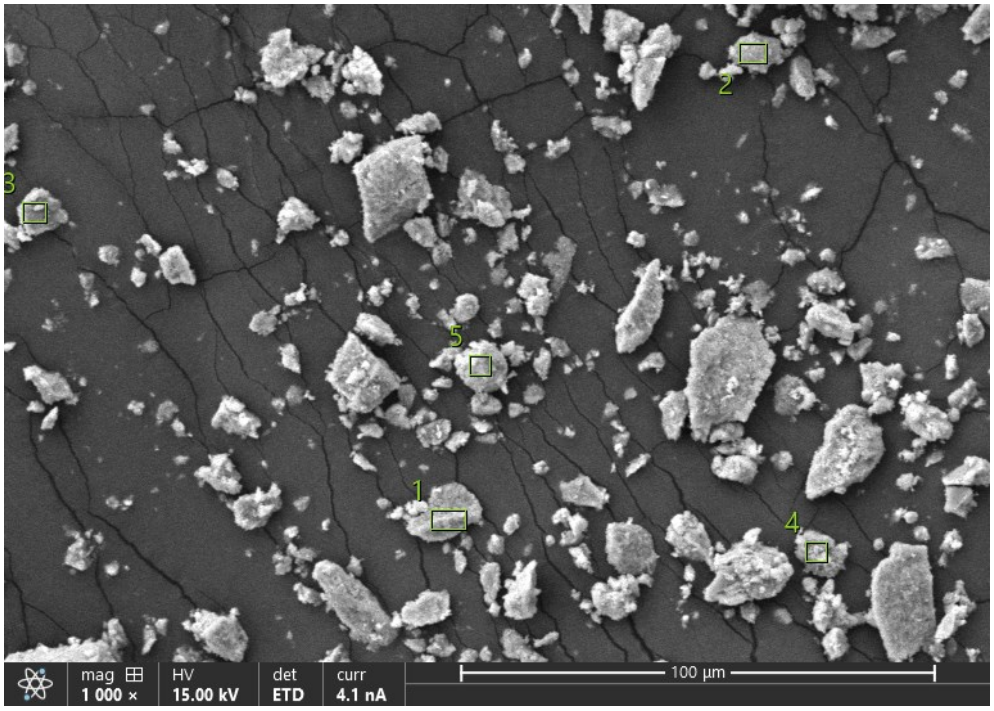

Figure A.17. SEM image capture of particles filtered from stock solution sample (SW3) Area 2 with areas scanned using EDS analysis highlighted in numbered boxes.

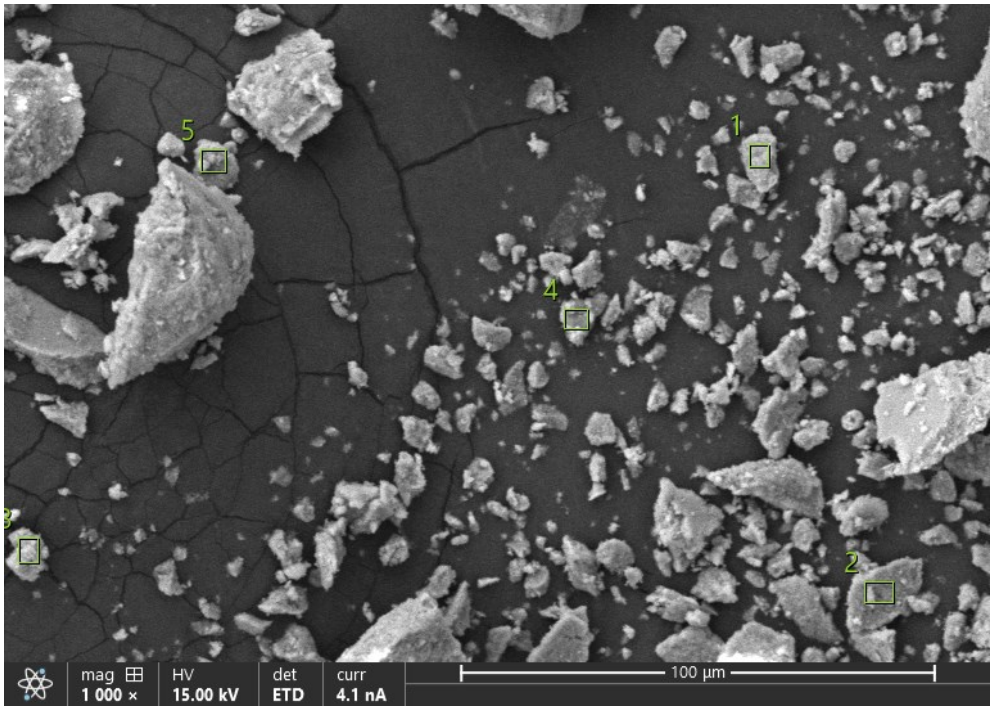

Figure A.18. SEM image capture of particles filtered from stock solution sample (SW3) Area 3 with areas scanned using EDS analysis highlighted in numbered boxes.

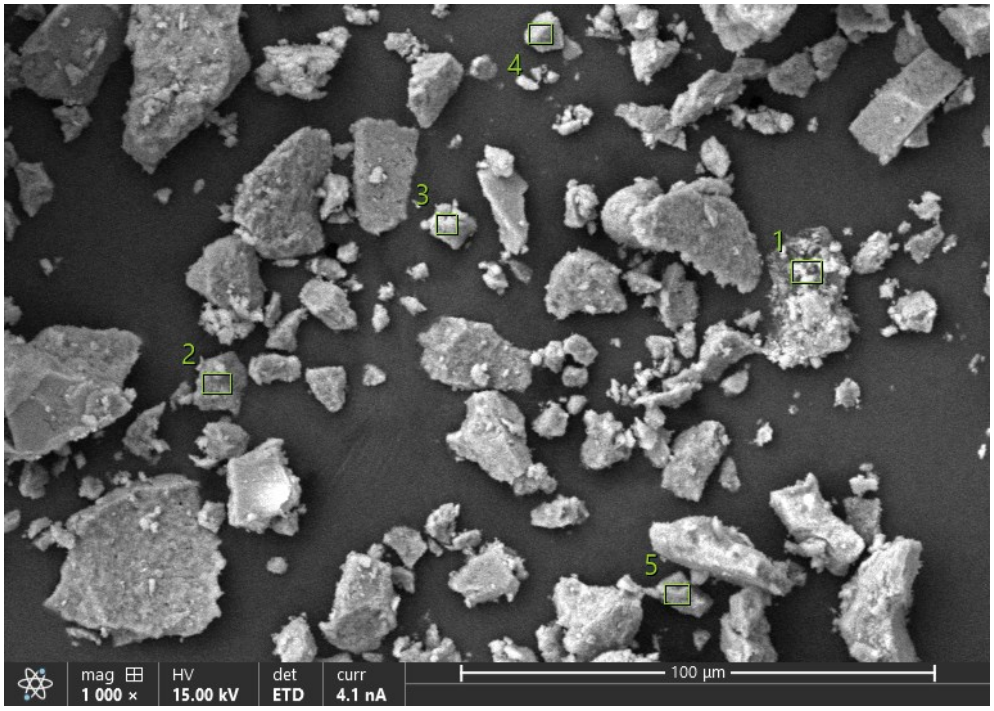

Figure A.19. SEM image capture of particles filtered from solution sample (KD3) Area 1 with areas scanned using EDS analysis highlighted in numbered boxes.

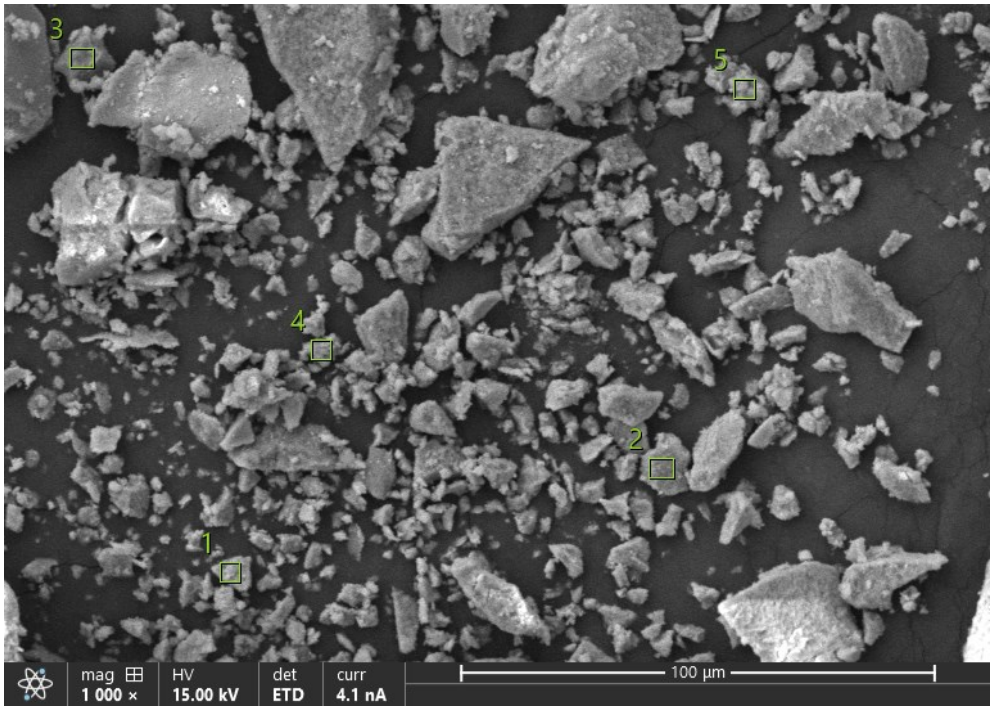

Figure A.20. SEM image capture of particles filtered from solution sample (KD3) Area 2 with areas scanned using EDS analysis highlighted in numbered boxes.

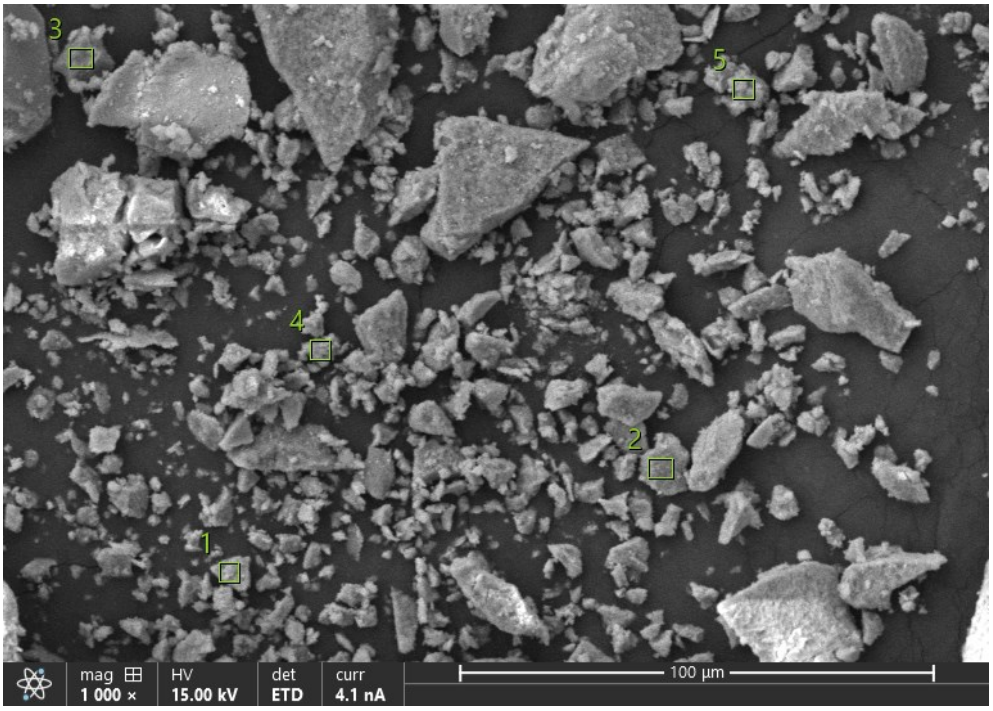

Figure A.21. SEM image capture of particles filtered from solution sample (KD3) Area 3 with areas scanned using EDS analysis highlighted in numbered boxes.

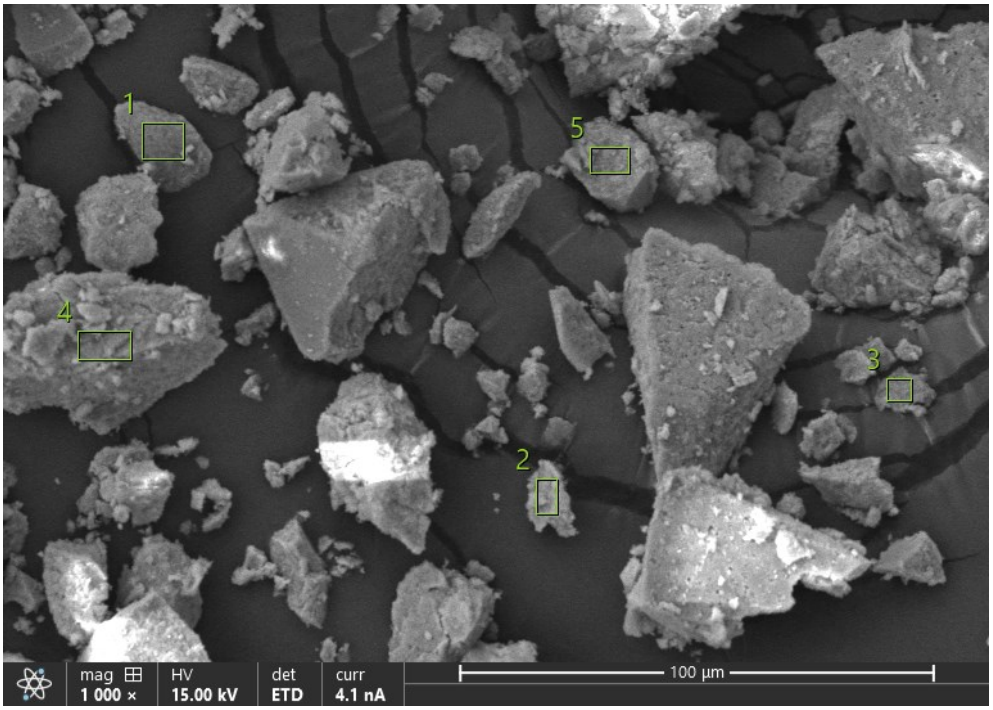

Figure A.22. SEM image capture of particles filtered from solution sample (UD3) Area 1 with areas scanned using EDS analysis highlighted in numbered boxes.

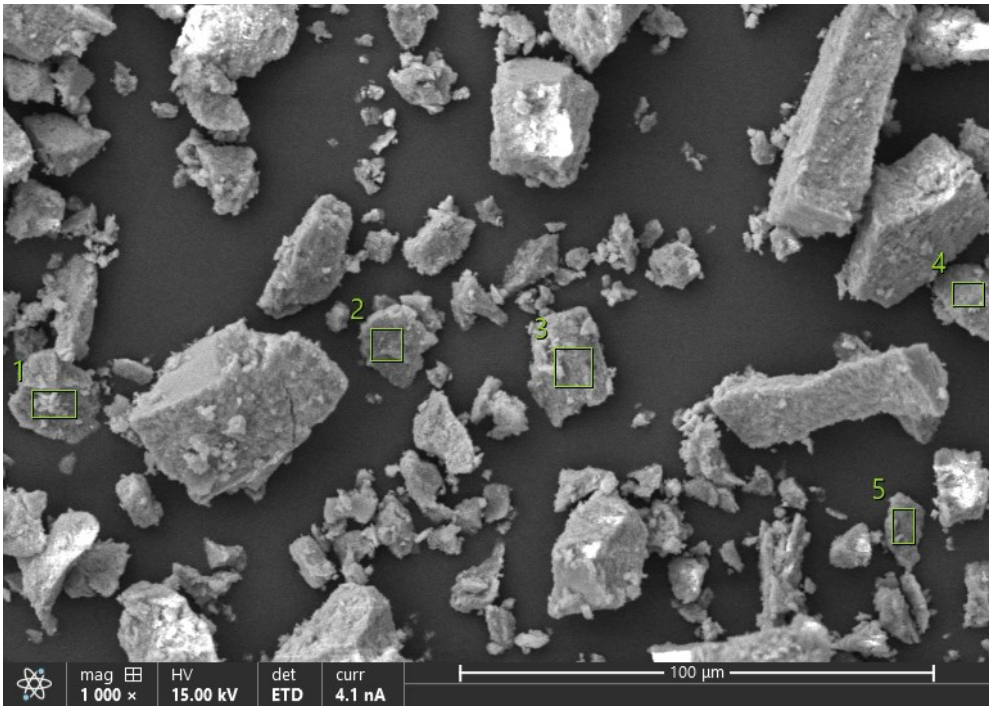

Figure A.23. SEM image capture of particles filtered from solution sample (UD3) Area 2 with areas scanned using EDS analysis highlighted in numbered boxes.

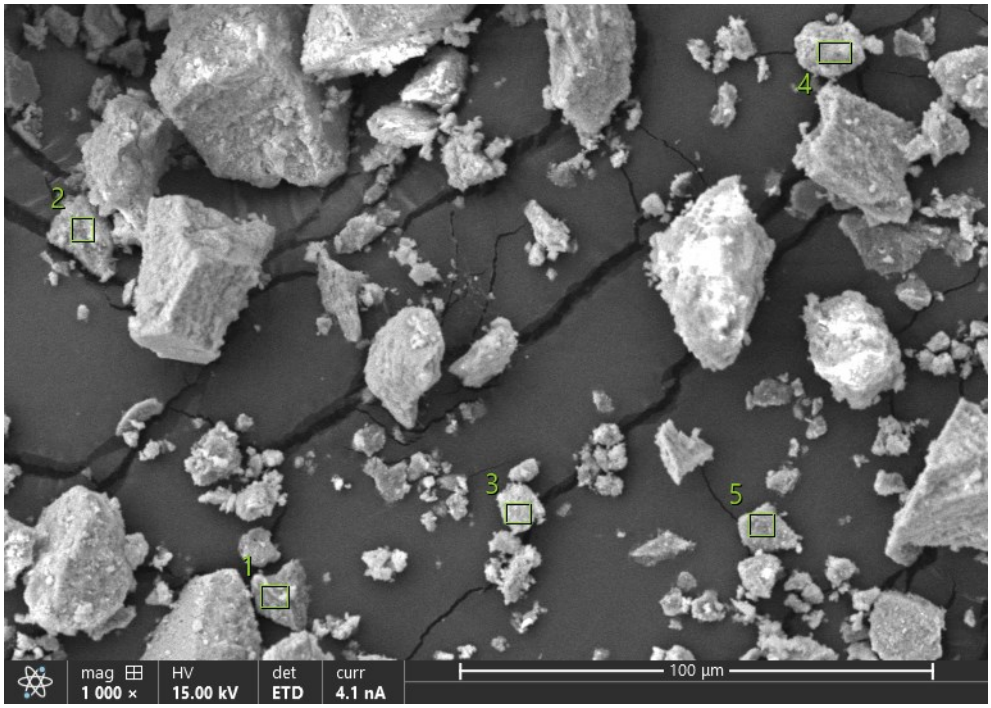

Figure A.24. SEM image capture of particles filtered from solution sample (UD3) Area 3 with areas scanned using EDS analysis highlighted in numbered boxes.

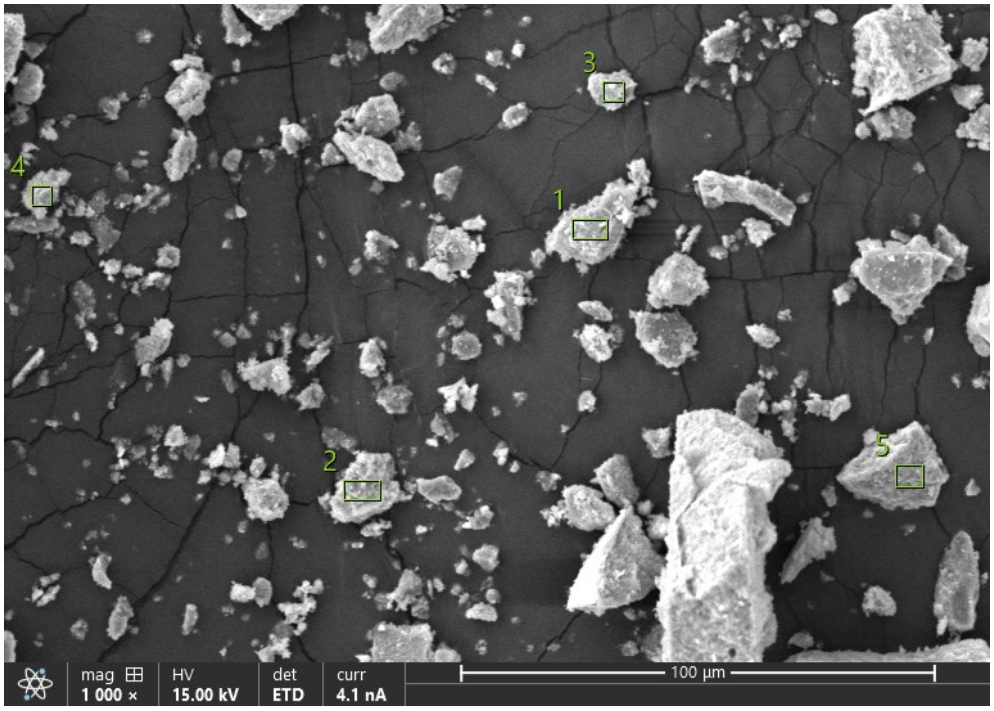

Figure A.25. SEM image capture of particles filtered from solution sample (GRM.5) Area 1 with areas scanned using EDS analysis highlighted in numbered boxes.

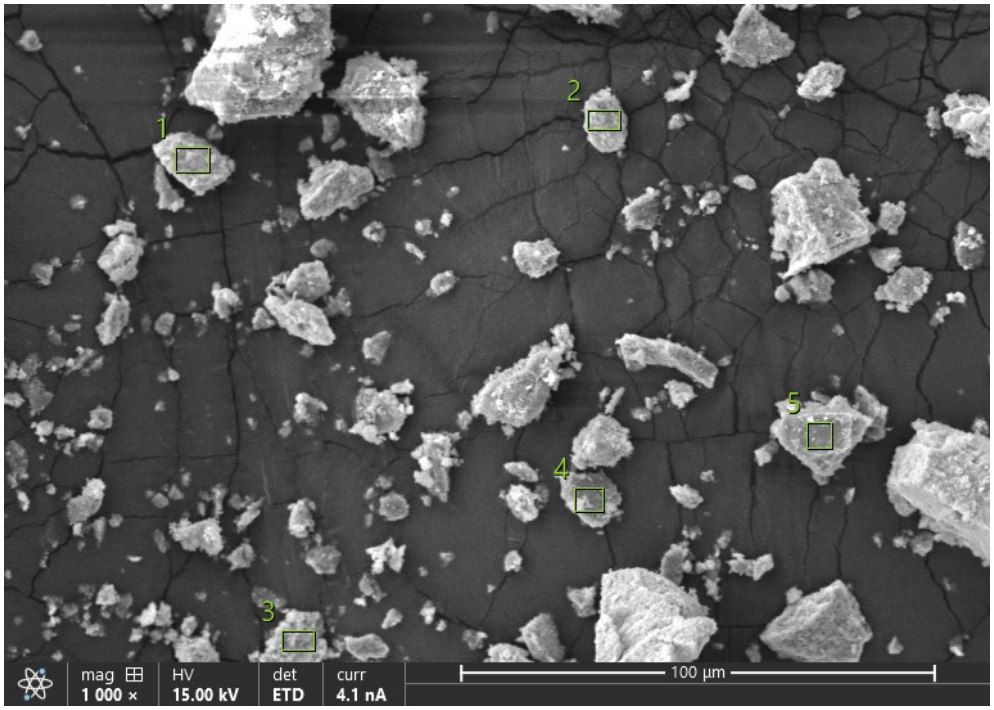

Figure A.26. SEM image capture of particles filtered from solution sample (GRM.5) Area 2 with areas scanned using EDS analysis highlighted in numbered boxes.

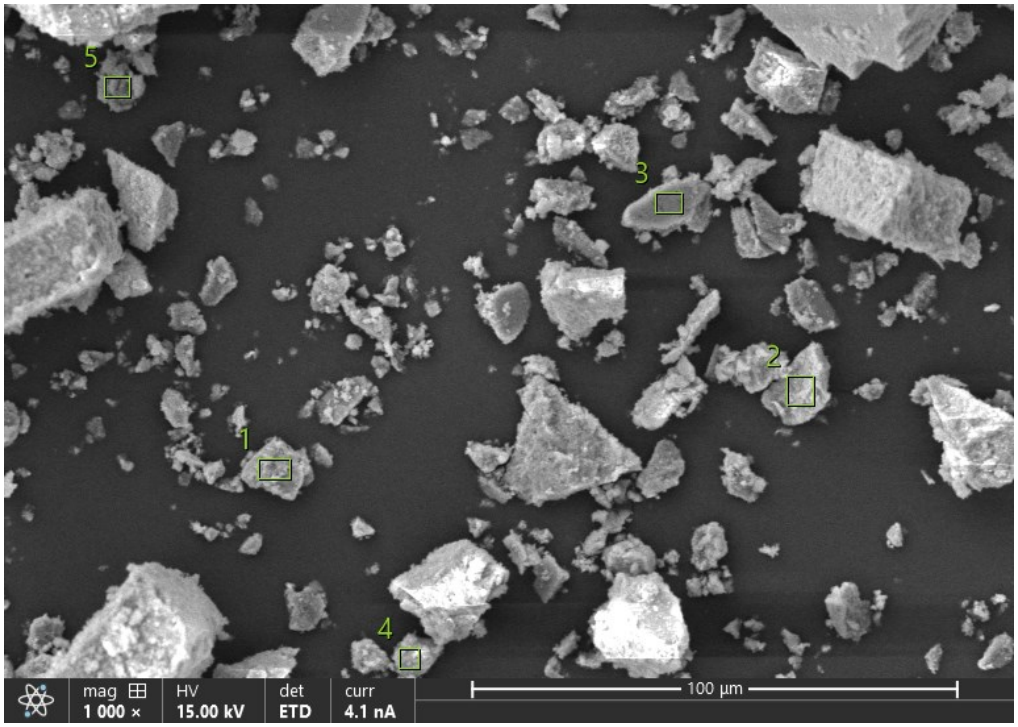

Figure A.27. SEM image capture of particles filtered from solution sample (GRM.5) Area 3 with areas scanned using EDS analysis highlighted in numbered boxes.

Appendix B: X-Ray Diffraction

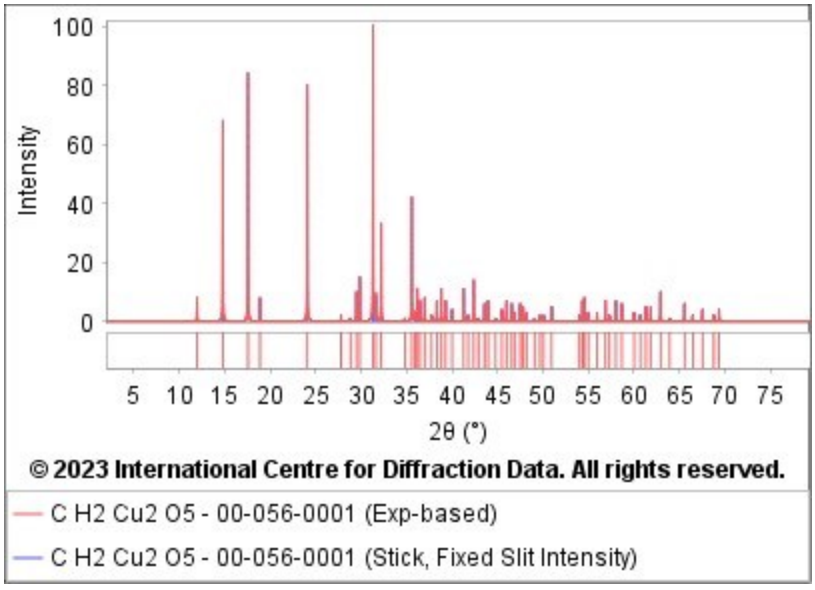

Figure B.1. Malachite ($Cu_2CO_3(OH)_2$) characteristic diffraction pattern PDF 00-056-001 (Gates-Rector & Blanton, 2019)

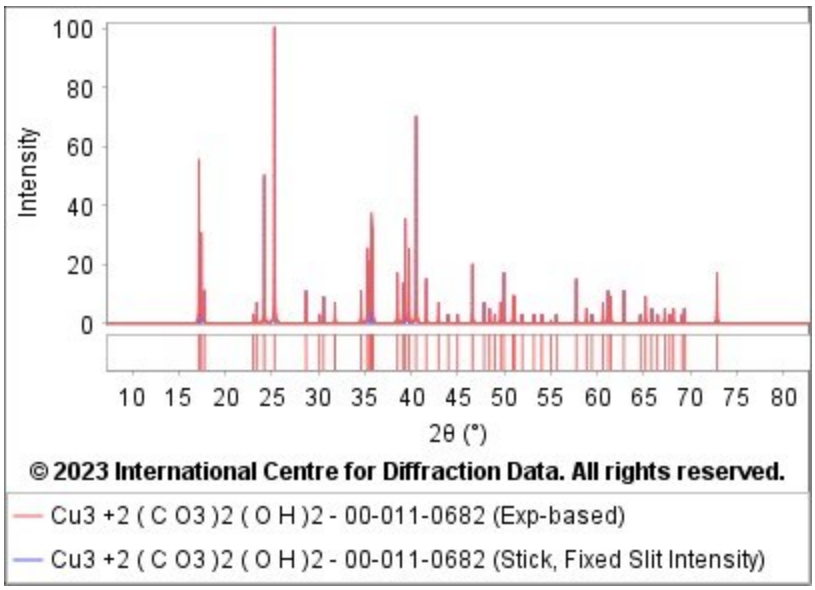

Figure B.2. Azurite ($Cu_3(CO3)_2(OH)_2$) characteristic diffraction pattern PDF 00-011-0682 (Gates-Rector & Blanton, 2019)

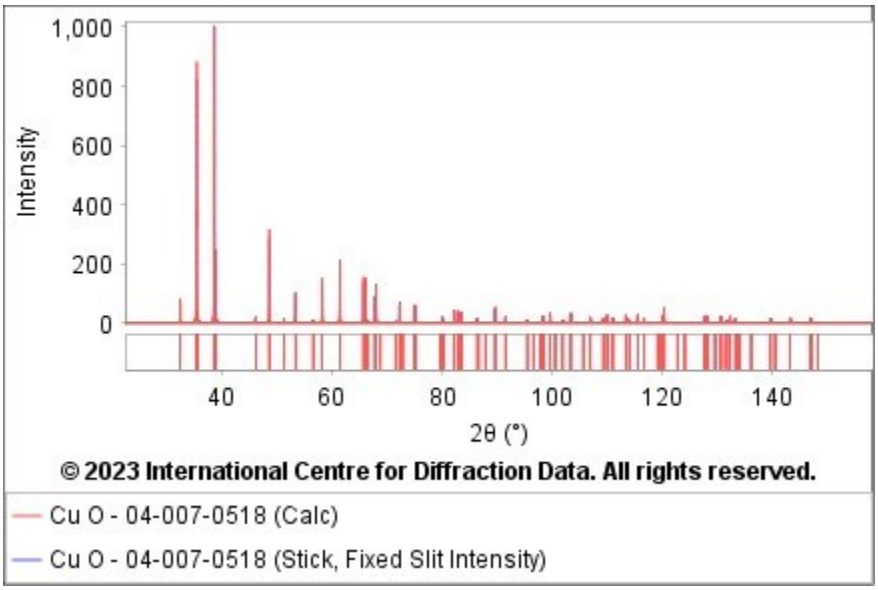

Figure B.3. Tenorite (CuO) characteristic diffraction pattern PDF 00-047-0518 (Gates-Rector & Blanton, 2019)

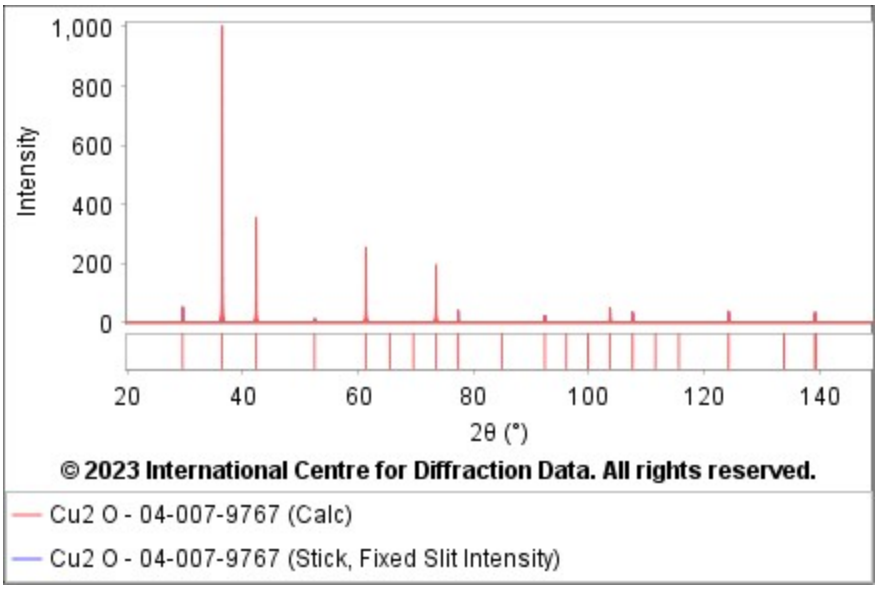

Figure B.4. Cuprite (Cu_2O) characteristic diffraction pattern PDF 04-007-9767 (Gates-Rector & Blanton, 2019)

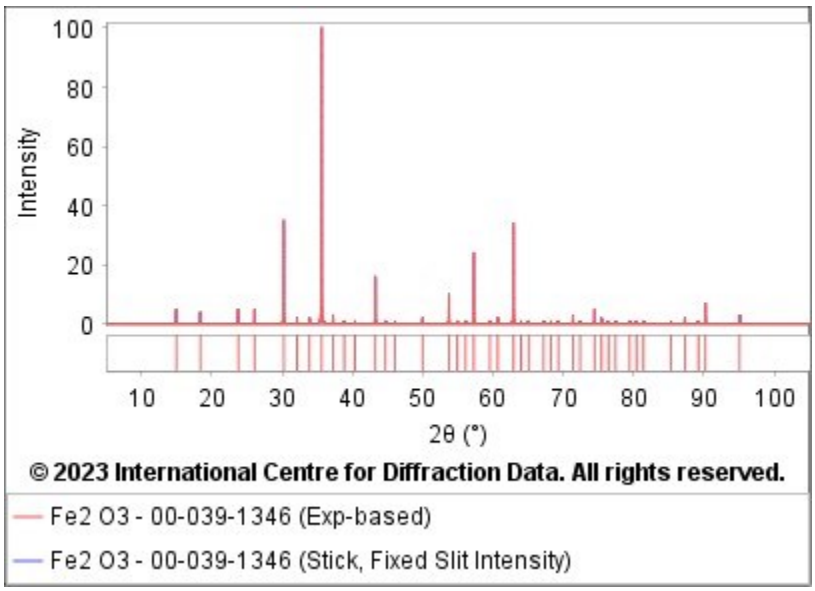

Figure B.5. Maghemite (Fe_2O_3) characteristic diffraction pattern PDF 00-039-1346 (Gates-Rector & Blanton, 2019)

Appendix C: CFD Simulations

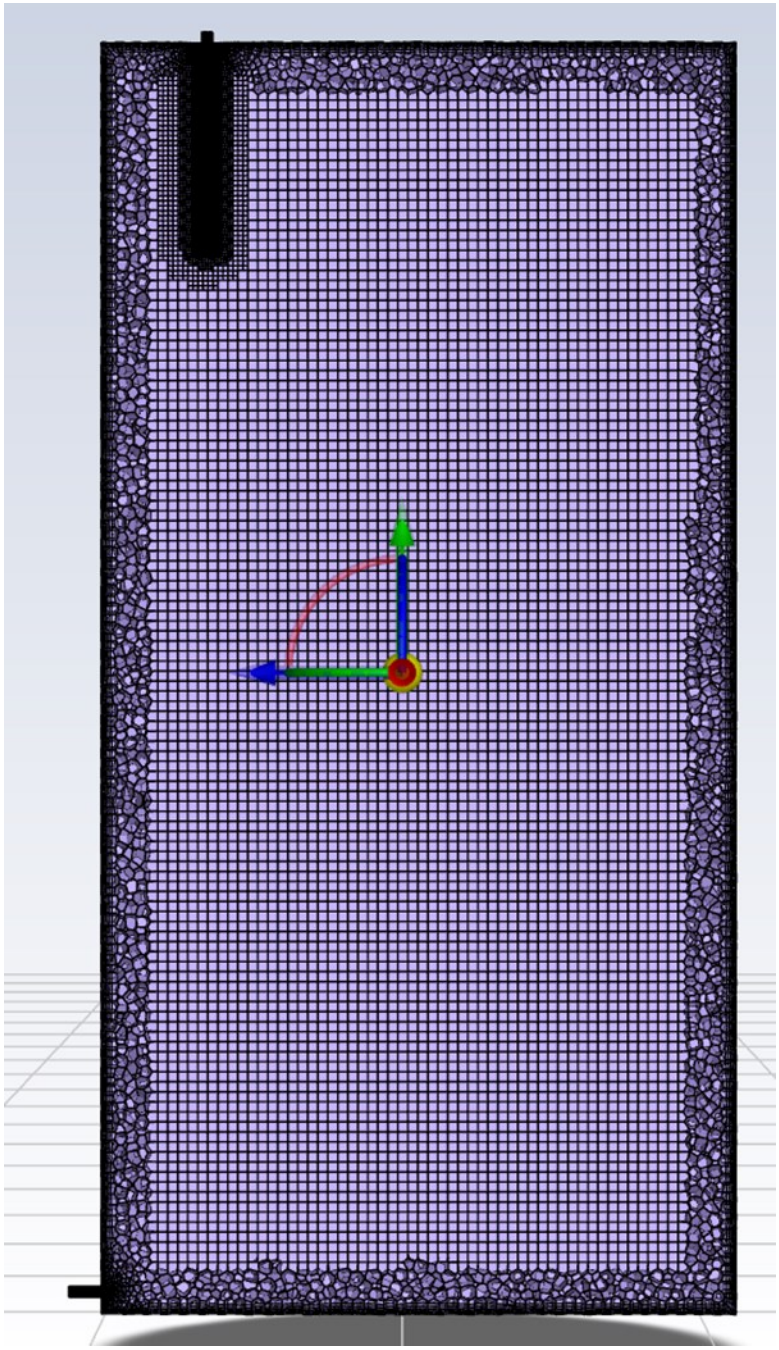

Figure C.1. Cross section of inlet position 1 mesh to show internal structure and mesh detail.